

**INTEGRATION OF COMPOSITE PART DESIGN AND PROCESSING  
SIMULATION IN LIQUID COMPOSITE MOLDING**

by

Jiayin Wang

A dissertation submitted to the Faculty of the University of Delaware in partial fulfillment of the requirements for the degree of Doctor of Philosophy in Mechanical Engineering

Summer 2017

© 2017 Jiayin Wang  
All Rights Reserved

**INTEGRATION OF COMPOSITE PART DESIGN AND PROCESSING  
SIMULATION IN LIQUID COMPOSITE MOLDING**

by

Jiayin Wang

Approved: \_\_\_\_\_  
Ajay K. Prasad, Ph.D.  
Chair of the Department of Mechanical Engineering

Approved: \_\_\_\_\_  
Babatunde A. Ogunnaike, Ph.D.  
Dean of the College of Engineering

Approved: \_\_\_\_\_  
Ann L. Ardis, Ph.D.  
Senior Vice Provost for Graduate and Professional Education

I certify that I have read this dissertation and that in my opinion it meets the academic and professional standard required by the University as a dissertation for the degree of Doctor of Philosophy.

Signed:

---

Suresh G. Advani, Ph.D.  
Professor in charge of dissertation

I certify that I have read this dissertation and that in my opinion it meets the academic and professional standard required by the University as a dissertation for the degree of Doctor of Philosophy.

Signed:

---

Pavel Simacek, Ph.D.  
Member of dissertation committee

I certify that I have read this dissertation and that in my opinion it meets the academic and professional standard required by the University as a dissertation for the degree of Doctor of Philosophy.

Signed:

---

Shridhar Yarlagadda, Ph.D.  
Member of dissertation committee

I certify that I have read this dissertation and that in my opinion it meets the academic and professional standard required by the University as a dissertation for the degree of Doctor of Philosophy.

Signed:

---

Michael Keefe, Ph.D.  
Member of dissertation committee

## ACKNOWLEDGMENTS

My first and most important acknowledgement is to my advisor, Dr. Suresh G. Advani for his valuable assistance and guidance with my graduate work. Apart from his outstanding academic background in composites that have imparted upon me how to perform as a scientist and communicate effectively within the research community, moreover, his great personality of treating students with both high standards and patience has impacted me in all aspects far beyond the research.

Next, I would like to acknowledge LIMS “Guru” in the group, Dr. Pavel Simacek. His impeccable precise logical thinking guarantees that every piece of work we generated meets for the strict standards. Talking with him is always inspiring. Also thanks to Dr. Simacek to agree to serve on my dissertation committee.

I acknowledge and give thanks to the following professors who also have agreed to serve on my dissertation committee: Dr. Shridhar Yarlagadda, Dr. Michael Keefe.

I acknowledge and give thanks to the following current and former students and researchers from the group that supported me to completion: Erik Andres, Jeffery Lugo, Richard Readdy, Dr. John Gangloff, Dr. Hatice Sas, Thomas Cender, Dr. Hang Yu, Hong Yu and Mike Yeager.

I acknowledge and give thanks to all the students from the “Pit” (CCM graduate student office), Preston McDaniel, Sandeep Tamakar, Albraa Jabar, Hao Liu, Chris Scott, Hongbo Dai, Danning Zhang, Minyong Yun, for all the good discussion and memorable moments.

I acknowledge and give thanks to the support staff of University of Delaware – Department of Mechanical Engineering and Center for Composite Materials and thank them for all the years of assistance and support: Ann Connor, Lisa Katzmire, Letitia Toto, Corinne Hammed, Robin Mack, Penny O’Donnell, Therese Stratton, and Megan Hancock.

I acknowledge and give thanks to the financial support from the Army Research Laboratory and the Defense Advanced Research Projects Agency under Cooperative Agreement Number W911NF-13-2-0027, Defense Advanced Research Projects Agency under Grant FA8650-11-C-7132.

This work is dedicated to my family and friends for the love and support all along this journey.

## TABLE OF CONTENTS

LIST OF TABLES .....	xi
LIST OF FIGURES .....	xii
ABSTRACT .....	xxi
 Chapter	
1 INTRODUCTION .....	1
1.1 Liquid Composite Molding (LCM) Processes .....	1
1.2 Part design for composites manufactured using LCM processes .....	3
1.3 Dissertation overview .....	8
2 USE OF CENTROIDAL VORONOI DIAGRAM TO FIND OPTIMAL GATE LOCATIONS TO MINIMIZE MOLD FILLING TIME IN RESIN TRANSFER MOLDING.....	11
2.1 Introduction .....	11
2.2 Previous Work .....	13
2.3 Objective.....	14
2.4 Injection model and fill time functional definition for single gate injection .....	14
2.4.1 Discretized correlations between fill time and distance to the gate .....	15
2.4.2 Geodesic distance definitions for the spatial surface .....	18
2.4.3 First and second moments with respect to injection gate for spatial surfaces.....	19
2.4.4 Fill time cost functional definition for single gate injection .....	22
2.5 Voronoi Diagram (VD) and Centroidal Voronoi Diagram (CVD) for multiple gate injection locations.....	22
2.5.1 VD and CVD of the surface and fill time functional definition for multiple injection gates .....	24
2.5.2 Alternative way to calculate the flow centroid on spatial surfaces .....	27
2.5.3 Lloyd’s algorithm .....	29

2.6	Case studies .....	32
2.6.1	Simple Square.....	32
2.6.2	Orthotic leg geometry using isotropic material .....	36
2.6.2.1	Minimum number of gates optimization for the fast cure resin injection .....	37
2.6.2.2	Comparison of two-gate injection optimization using exhaustive search and Genetic Algorithm.....	40
2.6.2.3	Comparison of three-gate injection optimization using Genetic Algorithm .....	42
2.6.3	Chassis.....	43
2.7	Summary.....	46
3	USE OF MEDIAL AXIS TO FIND OPTIMAL CHANNEL DESIGNS TO REDUCE MOLD FILLING TIME N RESIN TRANSFER MOLDING .....	47
3.1	Introduction .....	47
3.1.1	Resin Transfer Molding (RTM) process using line injection.....	47
3.1.2	Previous work .....	50
3.2	Medial Axis definition based on the fill time.....	52
3.3	Optimal injection channel from fill time based medial axis.....	56
3.3.1	Fill time based Medial Axis topology generation .....	56
3.4	Medial Axis correction for non-homogeneous preform.....	58
3.4.1	Different resin arrival times between two points on the part surface.....	58
3.4.2	Updating the injection line location .....	62
3.5	Case studies .....	65
3.5.1	Chassis containing highly anisotropic permeability fabrics .....	66
3.5.2	Orthotic device with various material configurations .....	68
3.5.2.1	Fabric with isotropic material permeability .....	69
3.5.2.2	Fabric containing non-homogeneous section .....	71
3.5.3	Humvee hood containing geometrical flow disturbances .....	75

3.6	Summary.....	77
4	PROCESS AND MATERIAL VARIABILITY IN LCM PROCESSES.....	79
4.1	Introduction .....	79
4.1.1	Flow pattern variability and flow disturbances .....	80
4.1.2	Coupling part design and process analysis .....	83
4.2	Methodology for Automating Effects of Variability in Mold Filling Process.....	84
4.2.1	Approach and Procedure .....	84
4.2.2	Logistics and implementation.....	85
4.2.2.1	CAD environment and mold filling simulation tools ...	85
4.2.2.2	Creation of the base geometry .....	86
4.2.3	Infusion line or injection gate plan.....	88
4.2.4	Detection of disturbance regions and generation of possible scenarios .....	90
4.2.4.1	Topology analysis and identification of disturbances channels .....	90
4.2.4.2	Assigning race-tracking properties to the channels.....	93
4.2.4.3	Automatic generation of possible scenarios .....	94
4.2.5	Mold filling simulations .....	95
4.2.6	Analysis of simulation results .....	97
4.2.6.1	Vent map generation.....	97
4.2.6.2	Success rate for a specific infusion plan.....	99
4.2.6.3	Feedback to designer .....	100
4.3	Case studies .....	101
4.3.1	Chassis.....	101
4.3.1.1	Disturbances recognition .....	101
4.3.1.2	RTM-light process.....	102
4.3.1.3	VARTM process.....	107
4.3.1.4	RTM process .....	109
4.3.2	Trailer using the VARTM processes.....	111

4.4	Summary.....	114
5	<b>FAST MOLD FILLING SIMULATION BASED ON THE GEODESIC DISTANCE CALCULATION ALGORITHM FOR LCM .....</b>	<b>116</b>
5.1	Introduction .....	116
5.2	Previous work.....	117
5.3	Distance based method for mold filling pattern prediction and its piecewise simplification on FE meshes.....	118
5.3.1	One-dimensional distance time model .....	118
5.3.2	Implementation of the one-dimensional flow model on spatial surfaces .....	122
5.3.3	Treatment of permeability variations and the race-tracking channels .....	126
5.3.4	Substitution of distance based flow pattern prediction for robust processing parameters' design.....	127
5.4	Case studies .....	127
5.4.1	Box .....	128
5.4.2	Drop fairing .....	129
5.4.3	Humvee hood.....	130
5.4.4	Vent location optimization for trailer with many race-tracking possibilities along the edges .....	132
5.5	Summary.....	132
6	<b>MULTI-TIER STRATEGY TO INTEGRATE COMPUTER AIDED DESIGN AND PROCESSING SIMULATION MODULES .....</b>	<b>134</b>
6.1	Introduction .....	134
6.2	Multidisciplinary wind blade design and analysis.....	134
6.2.1	Introduction .....	134
6.2.2	Design Process as applied to Wind Blade Design.....	136
6.2.3	Approach .....	140
6.2.3.1	Tier 1: Initial feasibility analysis .....	142
6.2.3.2	Tier 2: Analysis for a fixed dimension. ....	146
6.2.3.3	Tier 3: Cross-section model introduction.....	150
6.2.4	Summary.....	152

6.3	Multi-tier integration of processing simulation with CAD software SimXpert .....	152
6.3.1	Level 0: Initial feasibility analysis .....	154
6.3.2	Level 1: Comparison and Selection of Processing Method(S) and feature recognition .....	155
6.3.3	Level 2 – Analysis of sensitivity to disturbances .....	157
6.3.3.1	Assigning race-tracking properties .....	157
6.3.3.2	Generation of scenario space .....	158
6.3.3.3	Vent plan analysis .....	159
6.3.3.4	Integrate design-manufacturability iteration .....	160
6.3.4	Case studies .....	161
6.3.5	Summary .....	163
7	CONCLUSIONS, CONTRIBUTIONS, AND FUTURE WORK .....	165
7.1	Contributions and Conclusions .....	165
7.2	Future Work .....	168
	REFERENCES .....	170
Appendix		
A	LIQUID INJECTION MOLDING SIMULATION (LIMS) .....	177
A.1	Introduction .....	177
A.2	Processing Parameters specification .....	178
A.3	Package API .....	179
B	REPRINT PERMISSION LETTERS .....	181
B.1	“Use Of Centroidal Voronoi Diagram To Find Optimal Gate Locations To Minimize Mold Filling Time In Resin Transfer Molding” .....	181
B.2	“Use Of Medial Axis To Find Optimal Channel Designs To Reduce Mold Filling Time In Resin Transfer Molding” .....	188

## **LIST OF TABLES**

Table 2-1: Two-gate injection optimization comparison using different methods ..... 42

## LIST OF FIGURES

Figure 1-1: Fiber reinforcement polymer composite schematic .....	1
Figure 1-2: Schematic of common Liquid Composite Molding (LCM) processes RTM (rigid mold), VARTM (one sided mold, atmospheric pressure to infuse the resin) and RTM light (one sided mold with compliant second surface) .....	3
Figure 1-3: Flowchart of composite part design and processing integration framework .....	5
Figure 2-1: One-dimensional flow model with mesh.....	16
Figure 2-2: 1D model is further generalized for weighted geodesic distance and weighted fill time for node $n$ over a spatial surface .....	19
Figure 2-3: Control volume assignment for each node in FE/CV approach [26– 28].....	20
Figure 2-4: Voronoi Diagram of a square surface using (a) Euclidian distance; and using (b) the distance defined in equation (2.7) .....	23
Figure 2-5: Flow pattern for a square part surface when resin is introduced from four injection gates, and four Voronoi Diagrams are generated based on the fill time results.....	25
Figure 2-6: Comparison between regular VD (left) and CVD (right) of the square surface with two injection gates .....	27
Figure 2-7: Search for the centroid of a Voronoi Diagram through running LIMS for homogeneous part: (a) Voronoi Diagram generation for three-gate injection of an orthotic foot (b) flow centroid found for $V1$ by running infusion simulation by setting infusion lines on the region boundary ....	28
Figure 2-8: Search for the centroid of a Voronoi Diagram for non-homogeneous part: (a) low permeability section at the heel due to preform compaction; (b) centroid found for Voronoi Diagram $V1$ . .....	29

Figure 2-9: Flow chart that optimizes the location of k gates using Lloyd's algorithm .....	30
Figure 2-10: Use of Lloyd's algorithm to find the optimal four-gate injection plan for a square part. ....	31
Figure 2-11: Different initial four-gate configurations for the square converge to the same optimal gate locations.....	33
Figure 2-12: An example of four-gate location optimization process converging to the local optimum for the square geometry in which each gate is on the centroid of the its VD whereas the fill time (4700s) is not close to the optimum value as shown in figure 2.11.....	34
Figure 2-13: Three-gate optimization for the square with anisotropic fabrics: (a) optimal gate locations for 0° laminates after 6 iterations (24 simulations $K1 = 2K2$ ); (b) optimal gate locations for -45° laminates after 5 iterations (20 simulations $K1 = 2K2$ ); (c) optimal gate locations for 0° laminates after 4 iterations (16 simulations $K1 = 10K2$ ); (d) optimal gate locations for -45° laminates after 4 iterations (16 simulations $K1 = 10K2$ ) .....	36
Figure 2-14: Orthotic part design and optimal one-gate injection fill time result.....	38
Figure 2-15: Two-gate location optimization for the orthotic leg.....	39
Figure 2-16: Three-gate location optimization for the orthotic leg which satisfies the resin gel time restrictions.....	40
Figure 2-17: Two-gate injection optimization results comparison when using (a): exhaustive search on the coarse mesh with 210 nodes, (b): Genetic Algorithm after 190 simulations, and (c): CVD method after 12 simulations.....	41
Figure 2-18: Three-gate injection optimization results comparison when using (a): Genetic Algorithm after 230 simulations, and (b) CVD method after 28 simulations.....	43
Figure 2-19: Two gate optimization for a chassis: (a) part geometry with homogeneous isotropic permeability, (b) optimal two-gate results after 15 simulations, (c) part geometry with low permeability region, (d) optimal two-gate results after 18 simulations.....	44

Figure 2-20: Two gate location optimization for the chassis with flow disturbance (high permeability) region shown in (a), and (b) VDs calculation in iteration 5, and (c) inaccurate centroid found for V1 because of the extra flow front meeting point.....	45
Figure 3-1: Channels used in RTM processes to reduce mold filling times by creating a resin distribution network: (a) sandwich structures where channels are machined on the core material, and (b) channels are pre-printed on the inside surface of the mold wall .....	49
Figure 3-2: Medial Axis definition based on distance for an “L” shape part.....	51
Figure 3-3: Example of the requirement of a node within the domain to be the fill time based Medial Axis: Point A is on the medial axis because two locations on the boundary returns identical minimum fill times; whereas Point B is not on the Medial Axis because only one location on the boundary returns the minimum fill time.....	53
Figure 3-4: Voronoi Diagram of the part geometry from the control points on the part boundary.....	55
Figure 3-5: Generating the integrated fill time map (a) select N control points on the boundary (b) Record minimum resin arrival time at each interior node from a N flow simulations conducted with each control point on the boundary set as the gate (c) generate minimum fill time map from contours of minimum fill times .....	57
Figure 3-6: A non-homogeneous 1D example that has higher permeability in the left half than in the right half.....	58
Figure 3-7: Medial axis calculation based on the resin arrival at various locations injected from left and right end respectively.....	60
Figure 3-8: Fill time plot from each point in between the two boundary points to the boundary, and the optimal location returns a fill time that is 47% of the initial medial axis fill time shown in Figure 3-7.....	61
Figure 3-9: Flow pattern when setting the injection channel on the initial medial axis.....	62
Figure 3-10: Flow contour with the initial medial axis as the injection channel, and the methodology to move the medial axis to the new location. ....	64

Figure 3-11: Initial medial axis and the arrival at the final injection channel design after four iterations with resin flow patterns when injected from this optimized injection line. ....	65
Figure 3-12: Chassis geometry and material permeability specifications.....	66
Figure 3-13: Part domain is divided into a Voronoi Diagram based on a set of simulation results from the boundary(left)nodes to select the medial axis which will be the injection channel (right). ....	67
Figure 3-14: Flow pattern when resin is introduced from the injection channel along the medial axis with location of the two vents. ....	67
Figure 3-15: Flow pattern if the injection line is selected to be along the (a) geometric symmetry axis, and (b) geometry symmetry axis rotated according to the material permeability principal directions. Fill time in this case is more than twice for case (a) and nearly five time for case (b) .....	68
Figure 3-16: A personalized orthotic device with injection pressure and resin gel time constraints.....	69
Figure 3-17: Medial axis calculated from the integrated fill time map.....	70
Figure 3-18: Flow pattern with injection line on the medial axis for the orthotic device using isotropic material.....	71
Figure 3-19: Orthotic device with non-homogeneous fabric configuration that contains a low permeable section along the surface edge of the part.....	72
Figure 3-20: Integrated fill time map for the initial medial axis for the orthotic device containing non-homogeneous permeability section as shown in Figure 3-19. ....	72
Figure 3-21: Flow pattern if the injection line is placed along the initial medial axis.	74
Figure 3-22: Final injection line/vents design and flow pattern after four iterations to move the initial medial axis to final optimal position that reduces the fill time by 10% .....	74
Figure 3-23: Humvee hood geometry and fabric permeability specification with “racetracking” channel located on one internal edge .....	76

Figure 3-24: Initial medial axis location and flow pattern when selecting it as the injection line, based on which, the injection line moving direction is determined .....	76
Figure 3-25: Flow pattern for the final injection line design and venting plan. Convergence was achieved in three iterations. The filling time reduced by 46% as compared to the initial medial axis as the injection line .....	77
Figure 4-1: Potential race-tracking regions along (a) outer edge; (b) bifurcation lines; (c) tapered regions; (d) sharp corners .....	82
Figure 4-2: Preform permeability is interpreted from PCOMP card and material library information .....	88
Figure 4-3: Automatic selection of infusion location depends on the type of process and the geometry of the part. ....	90
Figure 4-4: Automatic feature recognition of potential race-tracking channels .....	92
Figure 4-5: An example race-tracking strength with probabilities .....	94
Figure 4-6: Scenario space generation for three potential race-tracking strengths along five edges of a simple sidewall.....	95
Figure 4-7: Each scenario filling simulation flow chart.....	96
Figure 4-8: Each mold filling scenario is executed twice to find (a) fill time and (b) last region to fill.....	97
Figure 4-9: The mold filling results from each scenario from the scenario space are weighted with the respective probabilities to generate a vent map denoting the probability of placing a vent at that location for successful filling. In this example, four vents along the four corners ensure that one would be able to fill the mold for any scenarios from the entire scenario space.....	99
Figure 4-10: (a) Chassis CAD model (b) FE mesh for mold filling simulations .....	101
Figure 4-11: (a) Potential race-tracking channels identified (b) Assigned race-tracking distribution along outer edges and along folds.....	102

Figure 4-12: Scenario space generation for RTM-light process: (a) potential race-tracking channels identified; (b) race-tracking strength distribution on folds; (c) scenario space generated with equal probability for each scenario.....	103
Figure 4-13: Resin flow contours for chassis. Injection is from outer boundaries using RTM Light process .....	104
Figure 4-14: Unfilled regions as predicted by LIMS for all 16 scenarios with the RTM Light process.....	105
Figure 4-15: Feedbacks and recommendations: (a) vent locations; (b) fill time histogram; (c) successful yield vs. number of vents .....	106
Figure 4-16: Simulation results for (a) Fill Pattern and (b) Fill Factor when race-tracking effect is not taken into account for RTM-light process.....	107
Figure 4-17: Simulation cycle and results for the chassis with VARTM process (a) Infusion line and potential race-tracking channels; (b) Mold filling simulation to find fill times and unfilled regions for all 1024 scenarios; (c) Vent map; (d) Fill time histogram .....	108
Figure 4-18: Flow front development comparison between the cases when (a) race-tracking effect is not present (b) race-tracking effect is introduced along all of the edges and folds .....	109
Figure 4-19: Mold filling simulation for the chassis using the RTM process: (a) Injection gate location and potential race-tracking channels identified; (b) Fill time and unfilled regions results for some of the scenarios in the scenario space; (c) Vent map and vent locations; (d) Successful yield vs. number of vents; (e) Fill time histogram. ....	110
Figure 4-20: (a) Filling pattern and (b) Unfilled regions in the absence of racetracking when the injection gate is located in the center .....	111
Figure 4-21: Ten race-tracking channels are detected for the trailer along the folds.	112
Figure 4-22: Scenario expansion for the trailer and vent map generation using LIMS. ....	113
Figure 4-23: Four vents are predicted if only running LIMS for one scenario without considering potential racetracking disturbances along the folding lines, and defect areas are flagged .....	114

Figure 5-1: One-dimensional flow model (above) and its mesh (below) .....	118
Figure 5-2: Fill time calculation for one-dimensional flow: (a) no distribution media; and (b) with distribution media. ....	121
Figure 5-3: Channel simplification for 2D quadrilateral elements .....	123
Figure 5-4: Comparison between distance based fill pattern estimation (left) and LIMS result (right) .....	125
Figure 5-5: Calculation time comparison between distance-based simulation and LIMS simulation with increasing number of nodes. Distance-based flow pattern converges to the LIMS results as shown in Figure 5-4.....	126
Figure 5-6: Flow pattern comparison between distance-based method and LIMS when 4 race-tracking channels are present at the plate cutout .....	127
Figure 5-7: Box with preform permeability variations along the edges .....	128
Figure 5-8: Simulation results comparison between distance-based simulation (left) results and LIMS results (right), and possible locations of flow entrapment are flagged where vents should be placed .....	129
Figure 5-9: Flow pattern simulation results for a double-curved drop fairing using distance-based method (left) and LIMS (right).....	130
Figure 5-10: Surface geometry and preform permeability distribution for a humvee hood.....	131
Figure 5-11: RTM simulation results comparison for the humvee hood: (a) non-dimensional fill time results using distance-based method; (b) non-dimensional fill time results returned by LIMS, and possible location of flow entrapment is flagged towards the end of the hood along z axis.....	131
Figure 5-12: Vent map generated using distance based results. The flow front pattern is similar to the one predicted by LIMS (Figure 4-22), and the difference (distance between the vent locations returned by two methods respectively) is smaller than the size of the vents.....	132
Figure 6-1: Five necessary simulation modules for wind blade design: Aerodynamic analysis, structural analysis, laminate design, manufacturing analysis, and cost analysis.....	137

Figure 6-2: Sequential resin infusion to manufacture a composite blade using three infusion lines. Injection lines 2 and 3 are opened when the resin arrives there. ....	139
Figure 6-3: Separation of design variables and materials into three tiers with increasing fidelity and decreasing uncertainty for manufacturing analysis .....	141
Figure 6-4: Refinement of Design through three-tier strategy manufacturing analysis .....	142
Figure 6-5: Preliminary design parameters based on wind blade capacity with the largest imprecision .....	144
Figure 6-6: (a) Tier 1: Blade geometric approximation at the cross section with largest chord length; (b) 1D flow simplification using sequential injection combining the geometric approximation parameters and material properties. ....	145
Figure 6-7: Tier 1 input and output (tool infusion analysis package is developed in this work and is combined along with other packaged developed by cooperating teams to generate approximate infusion times and financial cost) .....	146
Figure 6-8: Wind blade geometry specification from aerodynamic analysis and laminate material specification for stress analysis .....	148
Figure 6-9: Tier 2 material specification for infusion analysis .....	149
Figure 6-10: LIMS tier 2 output for (a) blade top skin and (b) blade bottom skin, which are infused separately in the manufacturing process simulation.	150
Figure 6-11: Tier 3 laminate specification .....	151
Figure 6-12: Cross section model schematics. ....	151
Figure 6-13: Three levels of composite manufacturability analysis .....	153
Figure 6-14: Flow chart of Level 0 feasibility estimation based on part geometry dimensions for a preliminary facility requirement check.....	154
Figure 6-15: Automatic feature recognition of potential race-tracking channels .....	156
Figure 6-16: Discretized race-tracking strength probability distribution for (a) outer edge, (b) folding lines and (c) bifurcation lines .....	158

Figure 6-17: (a) Potential race-tracking channels identified around folding lines for a trailer; (b) Scenario space generated with probability distribution in Figure 6-16 .....	159
Figure 6-18: Venting plan for the trailer using the RTM process. (a) detect CAD part with 10 race-tracking channels (b) generate vents for each scenario in the list and weight the nodes set as vent with scenario probability (c) superimpose the venting nodes for all scenarios and generate final venting plan. ....	160
Figure 6-19: Integration of manufacturability analysis packages with CAE software SimXpert .....	161
Figure 6-20: Three levels of manufacturability analysis for the trailer.....	163
Figure A-1: Important processing parameters' specification in LIMSUI: (a) single node as resin inlet (b) 1d elements connected with resin inlet node as infusion line (c) high permeable 2d elements as distribution mesh (d) 1d elements to represent racetracking channel.....	179

## **ABSTRACT**

Liquid Composite Molding (LCM) processes encompass a large family of composite processing methods that use a pressure difference to drive a liquid resin into a mold to saturate all the empty spaces between fibers of a stationary preform. The success in such net shape manufacturing processes is strongly correlated with the part geometry and design. Coupling LCM processing simulation tools with part design could make the manufacturing of composites more efficient. The aim of this dissertation is to present models, methodologies and frameworks to integrate the composite process simulation within the composite part design cycle.

To bridge the gap between the composite process simulations with the part design, one needs to first automate the processing parameters' selection and optimization in mold filling simulation packages. Various effective optimizers are developed to find the optimal injection/infusion scheme so that the results returned by the mold filling simulation packages can guide the part design process.

Next, approaches are developed to improve the LCM simulation workflows by combining stochastic models and frameworks with the simulation engine to address possible variability in the process. Such improved simulation methodologies will provide useful feedback to the designer on how to reduce variability in the manufacturing process within the design workspace.

To increase the efficiency of the design-simulation iteration cycle, a fast distance based model is developed to replace time intensive finite element based LCM simulation which makes it possible to provide qualitatively accurate information about

the process to part designers in a very short period of time for them to modify the design to accommodate robust processing. This tool is shown to be useful in the initial stages of design when large number of permutations are inevitable.

The methodology and integration framework is exercised to provide general design coupled with simulations solutions for manufacturing of net shaped composite parts and demonstrated with an application that couples the design with optimized process models that account for variability to achieve specific objective such as in wind blade design and manufacturing.

# Chapter 1

## INTRODUCTION

### 1.1 Liquid Composite Molding (LCM) Processes

Composite materials are manufactured by combining two or more distinct materials with significantly different physical properties, usually in the form of a reinforcement phase surrounded by matrix phase (Figure 1-1). The resulting composites will retain each component's outstanding properties, exhibiting superior performances tailored for desired engineering applications compared to conventional materials, which make them very desirable for various components in industries such as transportation and infrastructure mainly driven by their much lighter weight, high strength-to-weight ratio and corrosion resistant property. However, these advantages need to overcome the obstacles of more expensive materials and their complex behavior and variability during manufacturing.

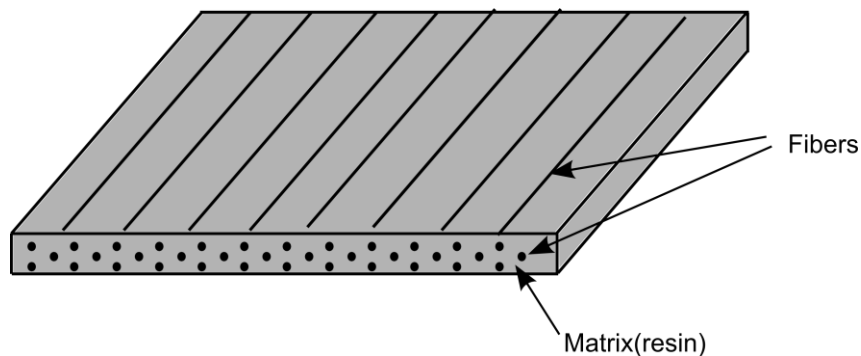


Figure 1-1: Fiber reinforcement polymer composite schematic

According to Advani and Sozer [1], one of the most important composite processing method that has been widely used in the manufacturing of fiber-reinforced polymer composites is called Liquid Composite Molding (LCM) process. It encompasses a family of processing methods that use a pressure difference to drive the resin into the mold to saturate all the empty spaces between fibers of a stationary dry fiber preform with polymer resin. In LCM dry fiber preform, which serves as the reinforcement and is mostly woven or stitched textiles, is first placed within a mold cavity. Next the mold is closed and sealed using normal force or pressure draping the reinforcement into the desired net shape of the mold. Catalyzed resin is then introduced into the mold through openings called gates in the mold walls until all the empty spaces between the fibers of the preform are filled with the resin. Once the resin oozes out of the vent opening in the mold, the injection is discontinued. Once the resin cures and solidifies, the mold is opened and the part is de-molded. The two main processes that belong to LCM family of processes are Resin Transfer Molding (RTM), which uses a rigid mold in which highly pressurized resin can be injected and Vacuum Assisted Resin Transfer Molding (VARTM) which uses one-sided mold, vacuum bag and atmospheric pressure as the driving force. There are other techniques such as RTM Light which uses a compliant mold (Figure 1-2). LCM is widely used because it allows one to manufacture complex net-shaped parts with good structural properties and class “A” surface finish in a single step. Depending on the LCM variant, large parts can be produced [1].

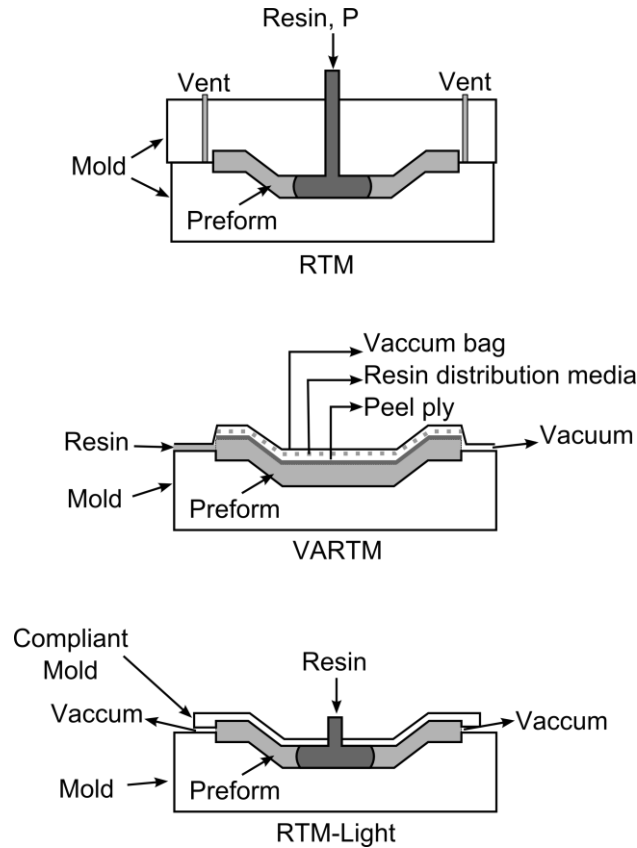


Figure 1-2: Schematic of common Liquid Composite Molding (LCM) processes RTM (rigid mold), VARTM (one sided mold, atmospheric pressure to infuse the resin) and RTM light (one sided mold with compliant second surface)

## 1.2 Part design for composites manufactured using LCM processes

The normal work flow to produce a part is to have the designer design the part with material selection and layout considering the functional requirements and then pass the design to a manufacturing engineer to manufacture the composite part. It is possible that multiple designs are possible to meet the functional requirements but the designer has no other constraints so he or she may pick one of the designs of the multiple ones that may be possible. Providing the constraint of ease of manufacturing through mold filling simulations to the designer will allow the designer to down select

a design that meets the functional requirements and is easy to manufacture. The designer builds the geometric design usually in a Computer Aided Design (CAD) environment, such as CATIA, Pro Engineering, Solidworks, SimXpert, etc. To meet the part's functional demands, modern CAD software packages usually integrate various finite element based stress analysis tools within the workbench to aid the designer in creating qualified drawings for part production. This integration has proved to be quite beneficial in constructing the functional design by being guided by low cost computer simulations. Hence one can also integrate LCM mold filling resin flow simulations within the CAD environment for composite part design guidance to increase the manufacturing success rate.

Over the last two decades, many LCM simulation tools based on control volume and finite element models have been developed to model the mold filling process [6–23]. Reasonably accurate flow pattern and pressure profile within the mold during the LCM processing cycle can be predicted once the material property (including fabric permeability and resin viscosity) along with the processing parameters are specified. Processing constraints (such as vent locations on the mold) can then be determined based on the predicted mold filling pattern. As an example of such tools, a well-tested Finite Element/Control Volume (FE/CV) package known as “Liquid Injection Molding Simulation” (LIMS) developed at University of Delaware [6,26,27] is used as the main LCM mold filling simulation engine for this research to create filling pattern during LCM processing. LIMS can simulate 3D flow but as LCM is most commonly used to manufacture net shape shell structures, it is reasonable to mesh the part geometry with 2-D shell elements

However, even provided with these well-defined LCM simulation tools, the composite part designer, who is not a processing expert, still cannot use such packages effectively to generate geometries that satisfy manufacturing constraints in terms of LCM processing workflows. Even though stress analysis packages have aided the designer to produce drawings that address physical and mechanical requirements, these are not sufficient to guarantee successful manufacturing of the part. Processing constraints during LCM processes are strongly correlated with the part geometry and material design and need to be included within this cycle (Figure 1-3). Therefore, composite processing analysis that accounts for process and material variability must also be integrated within the design cycle to generate drawings that meet the functional requirements and provide robust process design to fabricate the mold in which the fiber preforms can be placed to manufacture the composite part successfully and with ease.

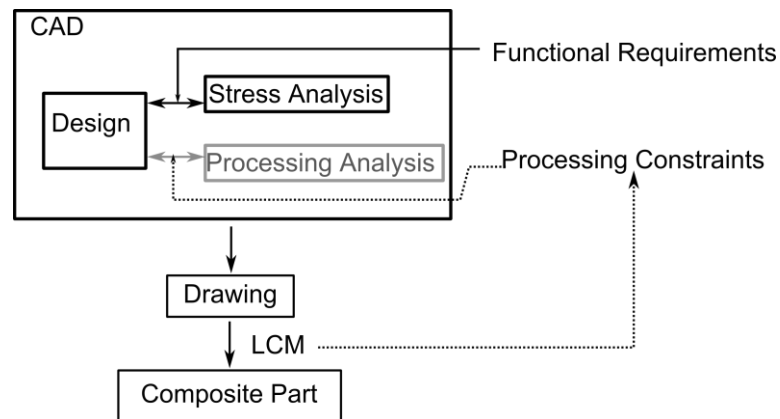


Figure 1-3: Flowchart of composite part design and processing integration framework

Several goals are expected out of this design-mold filling simulation cycle for composites that integrate LCM processing simulation packages within a CAD environment. First, part geometry that is created to meet the functional demand also has to guarantee a high yield of manufacturing with minimum cost possible using LCM processes, which calls for development of and inclusion of optimization approaches (usually with the objective of reducing process time) in this cycle. Second, LCM processing parameters have to be determined to ensure all the empty regions in between the fibers are saturated with resin, leaving no micro or macro voids that can degrade the quantity of the final composite part significantly despite material and process variability. This requires generation of robust processing parameters from the process simulation cycle. Third, the material parameters and effects that are directly correlated with manufacturing but not being determined from physical and mechanical requirements have to be also integrated within the design cycle. Finally, the integrated tool has to be automated as much as possible for easy use and fully benefit to the designer, or the software user, to optimize his or her drawings.

However, these goals cannot be easily achieved using the same integration framework for traditional design-stress analysis by simply adding the aforementioned LCM processing simulation tools on top of the CAD interfaces. Comparing with traditional metal material design-stress analysis integration, several challenges need to be overcome to build the connection between the composite part designing, LCM processes simulation, and passing drawing and designs to the manufacturing floor for production. First, defining a set of optimized processing parameters that are necessary to initiate the LCM simulations is usually not within the part designer's expertise. If the designer (or the software user) does not have sufficient composite processing

experience, less ideal simulation results returned from the simulation packages may not imply a faulty design, but may be simply a result from poorly defined processing parameters. Second, some features in the part drawing may introduce disturbances or process variations which could result in lower manufacturing yield and slow down the production process. These geometric features are often not in the way of satisfying functional requirements and can be altered and addressed in LCM simulations.

However, failing to consider such deviations in the LCM simulation results will return back the designer inaccurate processing information. Third, the inherent complexity of the composite processing simulations has to be well aligned with natural design flows. Going through all the details and scenarios in the processing simulation is not always necessary, such as during the early design stage. A one-for-all integration framework is not the optimal solution for the design analysis cycle for composites, and usually serves as a deterrent to the designer from using the tool at the initial stage.

This dissertation aims at addressing these challenges to by building a robust integration between the composite part design and processing simulations. Models and algorithms are developed to optimize processing parameters for different LCM variations. Strategic frameworks are defined to fit these models in the integration cycle to reflect the material and process variations encountered during the manufacturing processes. The integration framework not only provides feedback to the designer for geometry refinement effectively, it also delivers the optimized processing parameters downstream to process engineers to increase part manufacturability. Meanwhile, models and approaches are well defined and validated so that the tool can address general cases with complicated geometries and material specifications.

### **1.3 Dissertation overview**

To achieve the goals mentioned above, Chapter 2 and 3 develop a series of optimization methods to automate and speed up optimization of processing parameters. In Chapter 2 an effective iterative method is implemented for multiple-gate injection optimization in Resin Transfer Molding (RTM) processes. Minimum number of gates and the gate locations for minimal fill time are quickly generated based on the concept of Centroidal Voronoi Diagram (CVD) of the mold surface. In Resin Transfer Molding (RTM) processes, pre-designed channels branching out like runners from the injection port can be used for faster resin distribution and impregnation as compared to traditional single gate injection to reduce the mold filling time. To search for the optimal channel design for minimum fill time, a methodology is developed in Chapter 3 to search for the topology of such channels. Both models can handle general design cases, when fabricating composite parts that contain complexities in both the geometric features such as compound curvatures and corners and in material properties such as non-homogeneous and highly anisotropic fiber preform permeability.

After introducing the two advanced optimization methods with the objective of reducing fill time and increasing manufacturing yield, Chapter 4 introduces how process and material variability can cause stochastic behavior in LCM processes. Methodologies and algorithms are developed to examine the designed part geometry and material layups for ease of manufacturing with feasible infusion schemes by accounting for the inherent variability of the material and preform layup during the infusion processes. To accomplish this, the integrated tool has to automatically identify possible regions that are likely to introduce variability in resin flow, such as race-tracking channels near corners, edges and inserts, which will cause dramatically

different resin flow patterns and could result in voids. These possible scenarios are then simulated and evaluated to formulate an injection and venting scheme that is sufficiently robust to manufacture a part without any voids despite these variations.

Chapter 5 focuses on the application aspect of the integration by exploring faster simulation approximations in lieu of using the finite element based LCM simulation packages to provide answers to the designer in real time. A discretized one-dimensional flow model is developed to predict the fill time based on the distance resin travels. Combined with Dijkstra's algorithm, this model is then implemented on spatial surface meshes to calculate fill time for each node and generate flow development patterns. The computational model developed can predict the mold filling pattern for complex parts and address variable permeability or changing thickness of the fiber preform, and can capture the disturbed flow behavior along any difficult geometric features at a fraction of the computational cost.

Next chapter 6 presents two examples of software packages that are developed to integrate the design and the optimized LCM simulations to demonstrate its usefulness for composite wind blade design & analysis, and an Artificial Vehicle Manufacturing (AVM) simulation software for composites. Both software packages will be applied to composite part design-manufacturing cycle using LCM processes. Two different methodologies are developed and implemented in these two packages when integrating multi-disciplinary analysis modules with CAD software. Both mimic the practical design flow by separating analysis into multiple levels with increasing simulation accuracy and less uncertainty in the definition of design parameters. Therefore, the intuitive strategy will be more natural for the designer to use and make progressive decisions.

Finally, in chapter 7 original contributions from this dissertation are summarized and discussed. Also future paths for improving the integration between CAD and mold filling simulation in Liquid Composite Molding (LCM) processes are suggested.

## Chapter 2

### USE OF CENTROIDAL VORONOI DIAGRAM TO FIND OPTIMAL GATE LOCATIONS TO MINIMIZE MOLD FILLING TIME IN RESIN TRANSFER MOLDING

#### 2.1 Introduction

This Chapter introduces an effective optimizer to generate injection/venting plan for multiple gate injection schemes in Resin Transfer Molding (RTM) processes. In RTM, resin must fill all the empty regions between the fibers to produce a composite with no voids or defects. Voids or dry fiber regions are usually a result of resin not saturating the part before the resin gels. This may be due to resin reaching the vent prematurely before covering all the fibers, or a simple outcome of the infusion taking too long (resin gelling before it reaches the vent). The latter would be avoided if the mold filling time is less than the resin gel time limit. To avoid this, one must provide strategic infusion and venting locations and sufficient driving pressure. An effective method for reducing fill time is to use multiple injection gates[2–5]. The gates may be opened either sequentially during the resin impregnation stage, or simultaneously to reduce the fill time[2]. The designer can assign proper single gate location for a part with obvious symmetry, when using isotropic homogeneous fabrics, however, this task of finding the optimal gate location becomes much more complicated for designers when multiple gates are needed, and/or part geometry and fabric used is complicated. Hence there is a need to develop an automated

methodology to generate optimal multiple injection gate schemes with the mold filling simulation software to provide guidance to the designer.

The ever-reducing computational times (it takes less than one minute to run one simulation with LIMS on a mesh with 5000 nodes- details about the LIMS software which is a finite element control volume approach to mold filling using flow through porous media physics is given in Appendix A) for a typical 1x1x1 foot part for the composite orthotic leg application, and the current levels of modeling automation suggest that one can let the computer simulation generate all possible infusion scenarios and declare the most optimal gate location which will fill the mold in least amount of time. As the location of a gate is specified by a single node in the FE mesh, the problem is de-facto discrete and the number of simulations required to find one optimal gate is limited to number of nodes in the mesh. For a coarse mesh, say with 5000 nodes, one would need to execute 5000 simulations to find a single gate location that will provide the minimum time to fill the mold. Each simulation may take about a minute on a modern workstation, resulting in the best gate for minimum fill time in few hours.

However, this exhaustive search or brute force method is not practical when multiple gate locations are required to reduce fill time further. For example for two gates, one would need  $1.25 \times 10^7$  ( $5000 \times 4999 / 2$ ) simulations to execute which will take months to complete. For N gates, the number of simulations to be executed on a 5000 node mesh will be  $C_{5000}^N$ . Thus, using the brute force method to find the best locations for more than one gate from all possible gate-location permutations is inefficient and impractical. Hence the need for an efficient optimization method which can find the most optimal multiple gate locations without resorting to millions of

simulations. The objective of this chapter is to construct models to calculate geodesic distances that account for part non-homogeneities, material variability and anisotropies. Then, the fill time cost functional is formulated and correlated with the modified geodesic distance model. Using this model, effective algorithms are further developed to reduce the computational times for multiple gate location optimization, and vent locations can then be easily determined from the mold flow simulation results.

## **2.2 Previous Work**

Previously, many local and global search techniques have been attempted to optimize gate location using mold filling simulations to replace exhaustive search methods [6–15]. Gradient-based methods (such as Quasi-Newton method) [11] have been used to optimize the gate locations for RTM. However, there is a danger that the searching process can converge to a local optimum[7]. Therefore, Genetic Algorithm (GA) and Artificial Neural Networks that are less prone to be trapped in a local optimum have been implemented to optimize gate locations in RTM to minimize cycle time [6,8–10,12–14]. However, the complexity in formulating performance index requires one to evaluate a large number of generations before it converges, and renders these method less effective to handle complicated geometries and anisotropic material property variation. To improve the searching effectiveness, another meta-heuristic optimization method known as Branch and Bound Search (BBS) has been implemented to search for the optimum injection gate locations [7]. Compared with GA, BBS requires lower number of permutations to be evaluated. However, it is not clear how one can use this method to optimize multiple gate injections.

### **2.3 Objective**

In this work, we introduce modified Centroidal Voronoi Diagrams (CVD) [16] to search for the optimal multiple gate locations in RTM and demonstrate its utility for a variety of case studies with complex mold geometries. A one-dimensional model for mold flow is first developed and used to define the weighted geodesic distance and weighted fill time and their relations to each node on the mesh [17,18]. Next, this model is implemented on the spatial surfaces of the designed shell-like composite parts to formulate a convex functional for fill time cost. Searching for the minimum of this functional is therefore used as the objective functional to determine optimal gate locations. Next, the surface is re-interpreted using Voronoi Diagram [16] generated from the nodes that are set as gates on the mesh. Centroidal Voronoi Diagram (CVD), which is a specific type of VD of the surface, is proved to be the optimal solution that can minimize the cost functional [16]. However, this specific type of diagram of the surface is not readily available, and Lloyd's algorithm [19,20] which is an iterative algorithm can be employed to search the CVD of the surface that minimizes the cost functional. The gate nodes identified in CVD are the optimal gate locations which will minimize the fill time. Finally, the efficiency and accuracy of CVD method is demonstrated by comparing the results with those returned by Exhaustive Search and Genetic Algorithm methods.

### **2.4 Injection model and fill time functional definition for single gate injection**

Many models have been developed to correlate the fill time for each point on the part surface with its distance to the injection gate[12,13,18,21,22]. On flat surfaces, resin flow was assumed as the combination of radial flow on the surface and channel flow along the boundaries and resin time is formulated in terms of the

Euclidian distance to the injection gate [21]. This model is further extended to polyhedral spaces[22]. However, material anisotropy and variability and more generalized complicated geometries were not accounted for in this approximate model. Therefore, another continuous one-dimensional model has been formulated to relate the fill time for each point with its distance to the injection gate based on Darcy's Law as shown in equation (2.1) [17].

$$\int_0^t \frac{p_{in}}{\eta} dt = \int_0^{L(t)} h(\psi) \cdot \phi(\psi) \cdot \left( \int_0^\psi \frac{dx}{K_{xx}(x)h(x)} \right) d\psi \quad (2.1)$$

in which  $p_{in}$  is the injection pressure,  $\eta$  is resin viscosity, and  $h, \phi, K_{xx}$  are preform thickness, porosity and permeability in the x direction respectively. Permeability variation in through thickness direction [23–25] is neglected and the porous domain is considered to be single scale. This model can be used to calculate fill time for each point on the surface based on its distance to the injection gate for 1D flow. In this paper, this model is discretized over 1D FE mesh, and further expanded to address spatial surface mesh of a complex domain based on the geodesic distance to the injection gate[13,18].

#### 2.4.1 Discretized correlations between fill time and distance to the gate

First, equation (2.1) is discretized over the piecewise 1D FE mesh, which is shown in Figure 2-1. For an arbitrary node  $i$  on the mesh, resin travels from node 0 to node  $i$  sequentially. Fill time for node  $i$ , can then be calculated by integrating equation (1) from injection gate node 0 to node  $i$ , as is shown in equation (2.2):

$$t_i = \sum_{j=1}^i \Delta t_j = \frac{\eta}{P_{in}} \sum_{j=1}^i \Delta x_j h_j \phi_j \left[ \sum_{k=1}^{j-1} \left( \frac{\Delta x_k}{K_k h_k} \right) + \frac{\Delta x_j}{2K_j h_j} \right], i = 1, 2 \dots N \quad (2.2)$$

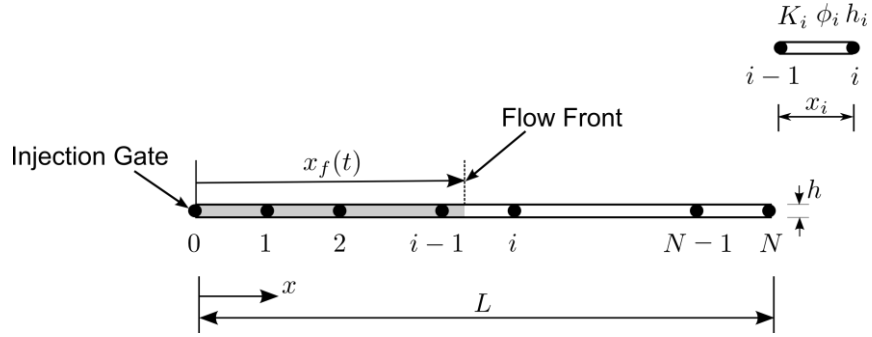


Figure 2-1: One-dimensional flow model with mesh

The fill time,  $t_f$  of a 1D part of length  $L$  can be written as:

$$t_f = \frac{\bar{\phi} \eta L^2}{2 \bar{K} P_{in}} \quad (2.3)$$

where permeability  $\bar{K}$ , thickness  $\bar{h}$ , and porosity  $\bar{\phi}$ , are the average material properties of the preform.

The variables in equation (2.2) are non-dimensionalized by

$$x^* = \frac{x}{L}, h^* = \frac{h}{L}, t^* = \frac{t}{t_f}, K^* = \frac{K}{K_c}, \phi^* = \frac{\phi}{\bar{\phi}} \quad (2.4)$$

Thus, the non-dimensional form of equation (2.2) becomes:

$$\begin{aligned}
t_i^* &= \sum_{j=1}^i \Delta t_j^* = 2 \sum_{j=1}^i \Delta x_j^* h_j^* \phi_j^* \left[ \sum_{k=1}^{j-1} \left( \frac{\Delta x_k^*}{K_k^* h_k^*} \right) + \frac{\Delta x_j^*}{2K_j^* h_j^*} \right] \\
&= 2 \sum_{j=1}^i K_j^* \phi_j^* h_j^{*2} \cdot \frac{\Delta x_j^*}{K_j^* h_j^*} \left[ \sum_{k=1}^{j-1} \left( \frac{\Delta x_k^*}{K_k^* h_k^*} \right) + \frac{\Delta x_j^*}{2K_j^* h_j^*} \right], i = 1, 2 \dots N
\end{aligned} \tag{2.5}$$

Equation (2.5) includes the piecewise defined material variability over the mesh, and the elemental lengths are weighted by material permeability and thickness in the same pattern. Then we define the weighted fill time and weighted length for each element as:

$$\begin{aligned}
\widetilde{\Delta t}_j^* &:= \frac{\Delta t_j^*}{K_j^* \phi_j^* h_j^{*2}} \\
\widetilde{\Delta x}_j^* &:= \frac{\Delta x_j^*}{K_j^* h_j^*}
\end{aligned} \tag{2.6}$$

and also define weighted fill time and weighted distance to the injection gate for each node as:

$$\begin{aligned}
\widetilde{t}_i^* &:= \sum_{j=1}^i \widetilde{\Delta t}_j^* \\
\widetilde{x}_i^* &:= \sum_{j=1}^i \widetilde{\Delta x}_j^*
\end{aligned} \tag{2.7}$$

Equation (2.5) can then be recast as:

$$\begin{aligned}
\widetilde{t}_i^* &= \sum_{j=1}^i \widetilde{\Delta t}_j^* = 2 \sum_{j=1}^i \widetilde{\Delta x}_j^* \sum_{k=1}^{j-1} \widetilde{\Delta x}_k^* + \sum_{j=1}^i \widetilde{\Delta x}_j^* = \left( \sum_{j=1}^i \widetilde{\Delta x}_j^* \right)^2 \\
&= \widetilde{x}_i^{*2}
\end{aligned} \tag{2.8}$$

This non-dimensional analysis provides a simple expression to relate each node's weighted fill time and its weighted distance to the injection gate.

#### **2.4.2 Geodesic distance definitions for the spatial surface**

For simplification, equation (2.6) – (2.8) are then implemented on spatial surfaces of any complex geometry by considering the surface mesh as a graph. Within each element, weighted resin travel time and length are defined using equation (2.6). The geodesic paths from the injection gate to any other nodes on the surface are calculated, and 1D resin flow is assumed along this path [18]. Thus, the distance between node  $i$  on the part surface and the injection gate is the geodesic distance weighted by the material properties, and the weighted fill time for node  $i$  can be calculated using equation (2.8). This allows one to define the first and second moments of the mesh with respect to the injection gate, and a cost functional can be formulated to calculate the cost in terms of time to fill the part. The objective of gate location optimization process is to minimize this fill time cost functional.

The weighted fill time and geodesic distance definition in equation (2.6) and equation (2.7) are then implemented on spatial surfaces. As is shown in Figure 2-2, resin is assumed to be travelling along the geodesic path which connects the injection gate with the current node  $n$ , and the weighted fill time and distance defined in equation (2.6) and equation (2.7) are used on each element on the resin travel path. Summation of all the  $\widetilde{\Delta x}_i$  and  $\widetilde{\Delta t}_i$  along the resin travel path will give the weighted geodesic distance connecting node  $n$  and the injection gate and the weighted fill time of node  $n$ . Equation (2.8) is therefore further used to relate the weighted geodesic distance and weighted fill time for spatial surfaces.

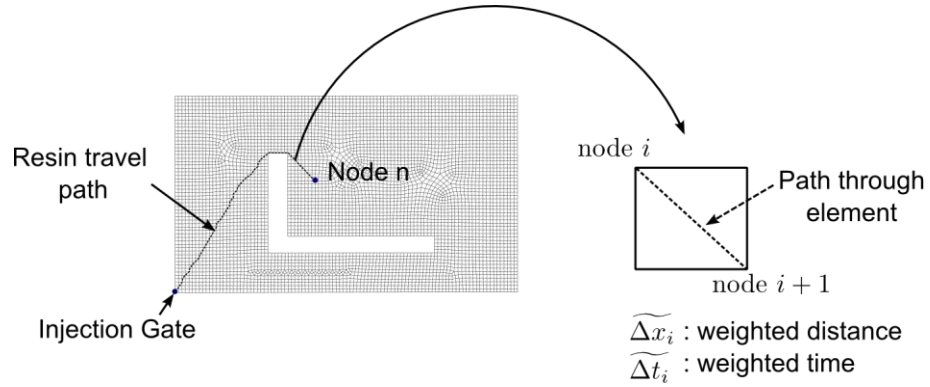


Figure 2-2: 1D model is further generalized for weighted geodesic distance and weighted fill time for node  $n$  over a spatial surface

### 2.4.3 First and second moments with respect to injection gate for spatial surfaces

Based on the Control Volume definition (Figure 2-3) in Finite Element/Control Volume (FE/CV) solution schemes [1,2,13,14] which has been used in mold filling simulation software LIMS, the weight function for each node is defined as:

$$w_n = \frac{V_n}{V_{mesh}} \quad (2.9)$$

in which  $V_n$  is the control volume assigned for the node, and  $V_{mesh}$  is the entire mesh volume. Obviously, the weight function satisfies:

$$\sum_{n=all\ nodes} w_n = 1 \quad (2.10)$$

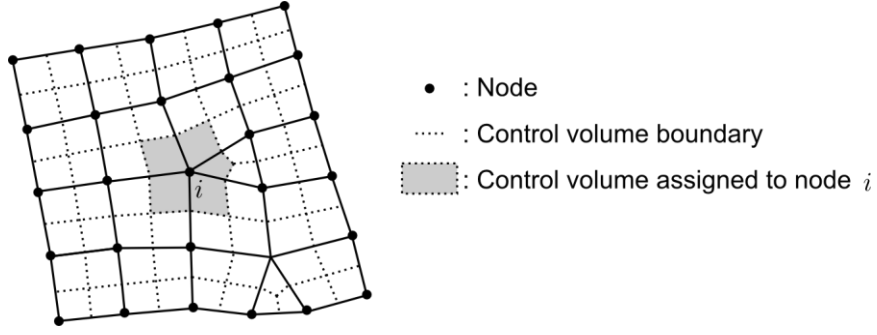


Figure 2-3: Control volume assignment for each node in FE/CV approach [26–28].

Using the distance defined in equation (2.7), the first order of moment with respect to the injection gate can be written as

$$\mathbf{M} = \sum_{n=\text{all nodes}} w_n \tilde{\chi}_{g \rightarrow n}^* \frac{\mathbf{r}_n - \mathbf{r}_g}{|\mathbf{r}_n - \mathbf{r}_g|} \quad (2.11)$$

in which  $w_n$  is the weight function for node  $n$ , and  $\tilde{\chi}_{g \rightarrow n}^*$  is the weighted geodesic distance from injection gate to node  $n$  using the distance definition in equation (2.7). For simplification, the coordinates of each node in the mesh are used to describe their position and calculate the direction vector for each node to the injection gate which is  $\mathbf{r}_n - \mathbf{r}_g$  in equation (2.11). The flow centroid can be defined by setting  $\mathbf{M} = 0$ , which yields the coordinates of the centroid:

$$\begin{aligned} \mathbf{r}_c &= (c_x, c_y, c_z) \\ &= \left( \sum_{n=\text{all nodes}} w_n \tilde{\chi}_{g \rightarrow n}^* \mathbf{r}_n \right) / \left( \sum_{n=\text{all nodes}} w_n \tilde{\chi}_{g \rightarrow n}^* \right) \end{aligned} \quad (2.12)$$

In equation (2.12), the geodesic distance from the injection gate to node  $n$ ,  $\tilde{\chi}_{g \rightarrow n}^*$ , is calculated using equation (2.8). However, to avoid the calculation of geodesic paths, weighted fill time  $\tilde{t}^*$  in equation (2.8) is substituted by the nodal fill

time  $t$  calculated by the flow simulation software, LIMS. Next, second moment tensor in global Cartesian Coordinates is defined as:

$$[I] = \begin{bmatrix} I_{xx} & I_{xy} & I_{xz} \\ I_{xy} & I_{yy} & I_{yz} \\ I_{xz} & I_{yz} & I_{zz} \end{bmatrix} \quad (2.13)$$

Each component can be written as:

$$\begin{aligned} I_{xx} &= \sum_{n=\text{all nodes}} \frac{w_n t_n}{|\mathbf{r}_n - \mathbf{r}_c|^2} [(y_n - y_c)^2 + (z_n - z_c)^2] \\ I_{yy} &= \sum_{n=\text{all nodes}} \frac{w_n t_n}{|\mathbf{r}_n - \mathbf{r}_c|^2} [(x_n - x_c)^2 + (z_n - z_c)^2] \\ I_{zz} &= \sum_{n=\text{all nodes}} \frac{w_n t_n}{|\mathbf{r}_n - \mathbf{r}_c|^2} [(x_n - x_c)^2 + (y_n - y_c)^2] \\ I_{xy} &= - \sum_{n=\text{all nodes}} \frac{w_n t_n}{|\mathbf{r}_n - \mathbf{r}_c|^2} [(x_n - x_c)(y_n - y_c)] \\ I_{xz} &= - \sum_{n=\text{all nodes}} \frac{w_n t_n}{|\mathbf{r}_n - \mathbf{r}_c|^2} [(x_n - x_c)(z_n - z_c)] \\ I_{yz} &= - \sum_{n=\text{all nodes}} \frac{w_n t_n}{|\mathbf{r}_n - \mathbf{r}_c|^2} [(y_n - y_c)(z_n - z_c)] \end{aligned} \quad (2.14)$$

in which  $t_n$  is the nodal fill time calculated by LIMS, and  $\mathbf{r}_n = (x_n, y_n, z_n)$ ,  $\mathbf{r}_c = (x_c, y_c, z_c)$  are coordinates for node  $n$  and the centroid node respectively. The eigenvalues and eigenvectors of  $[I]$  can provide the three principal axes of second moment and their norms. When the centroid defined in equation (2.12) is not on the surface, it can be projected onto the surface following the directions of the principal axes of second moment.

#### 2.4.4 Fill time cost functional definition for single gate injection

Next, the objective functional to minimize is defined in terms of the mold filling time for single gate injection cases. Instead of using the largest fill time as the optimized function, a fill time cost functional which includes the material permeability and thickness is defined as follows:

$$F(g) := \sum_{n=\text{all nodes}} w_n \tilde{t}_{g \rightarrow n}^* / 2 = \sum_{n=\text{all nodes}} w_n \tilde{x}_{g \rightarrow n}^{*2} / 2 \quad (2.15)$$

in which  $g$  is the node that is set as the gate,  $w_n$  is the weight function for each node. In equation (2.15), equation (2.8) is used to change the fill time functional ( $F(g) \sim \tilde{t}^*$ ) into the second order distance functional ( $F(g) \sim \tilde{x}^{*2}$ ). This functional is convex over the surface [16], and therefore, the minimum of this functional is reached when setting the gradient of  $F$  equal to  $\mathbf{0}$ , which can be written as:

$$\nabla F = \sum_{n=\text{all nodes}} w_n \tilde{x}_{g \rightarrow n} \frac{\mathbf{r}_n - \mathbf{r}_g}{|\mathbf{r}_n - \mathbf{r}_g|} = \mathbf{0} \quad (2.16)$$

Obviously, the centroid location defined in equation (2.12) is the single gate solution for equation (2.16). The optimal single gate solution is therefore to set the gate at the centroid. If the centroid location given by equation (2.12) does not lie on the surface, the centroid will be projected onto the surface along the principal axes of second moment calculated in equation (2.14).

#### 2.5 Voronoi Diagram (VD) and Centroidal Voronoi Diagram (CVD) for multiple gate injection locations

After the relation between fill time and geodesic distance model is formulated in section 3, Voronoi diagram can be defined by a finite set of locations on the surface

to separate the part surface into subdomains. Each subdomain is associated with one location and consists of all points that are closer to that location than to any other of the preselected locations. The distance used can either be the Euclidian distance (Figure 2-4(a)), or it can be generalized to a convex function of the distance (Figure 2-4(b)).

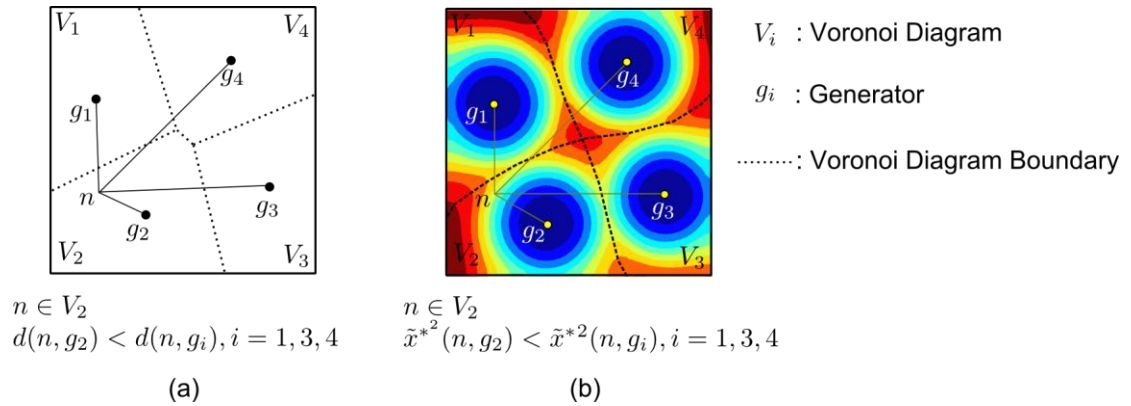


Figure 2-4: Voronoi Diagram of a square surface using (a) Euclidian distance; and using (b) the distance defined in equation (2.7)

When multiple gates are required for the injection, the part surface can be segregated into regions according to the weighted geodesic distance to these gates. A generalized Voronoi Diagram (VD) of the part surface is first defined based on the weighted distance defined in equation (2.6) and equation (2.7). Fill time functional defined in equation (2.15) for single gate injection is further generalized for multiple gate injection cases. The optimization objective for single gate to minimize the fill time cost is thus transformed into finding the optimal Voronoi Diagram of the part surface such that the fill time functional is minimum. Next, a special VD called as Centroidal Voronoi Diagram (CVD) of the part surface is defined based on the

weighted fill time and weighted geodesic distance definition. It has been proven that the nodes set as generators for CVDs is the optimal solution for minimizing the fill time cost functional. Finally, an iterative algorithm, Lloyd's Algorithm, is used to search for the CVDs of part surfaces, which will give the optimal multiple gate locations' configuration that returns the minimum fill time cost [19].

### 2.5.1 VD and CVD of the surface and fill time functional definition for multiple injection gates

For a part with a total number of  $k$  gates:  $\{g_i\}_{i=1}^k$  the meshed surface of the part is separated into  $k$  regions:  $\{V_i\}_{i=1}^k$ , each of which is called a Voronoi Diagram (VD) of the part and is associated with each gate accordingly. Each node contained in a specific VD  $V_i$  corresponding to the gate  $g_i$  satisfies the following equation:

$$V_i = \left\{ n \in \Omega \mid \tilde{x}^*_{g_i \rightarrow n} < \tilde{x}^*_{g_j \rightarrow n} \text{ for } j = 1, \dots, k, j \neq i \right\} \quad (2.17)$$

In equation (2.17),  $\Omega$  is the set for all the nodes in the mesh, and  $\tilde{x}^*_{g_i \rightarrow n}$  is the geodesic distance from gate  $g_i$  to node  $n$ , which is defined in equation (2.7). Because equation (2.8) describes a simple monotonous (quadratic) relations between (non-negative) weighted fill time  $\tilde{t}^*$  and geodesic distance  $\tilde{x}^*$ , the separation of the surface into regions based on the distance to the injection gates defined in equation (2.17) can be replaced with the following rule:

$$V_i = \left\{ n \in \Omega \mid \tilde{t}^*_{g_i \rightarrow n} < \tilde{t}^*_{g_j \rightarrow n} \text{ for } j = 1, \dots, k, j \neq i \right\} \quad (2.18)$$

The weighted fill time can be calculated from mold filling simulation using LIMS which provides the fill time for each node. Flow pattern contour can be plotted based on the fill time results, and the surface is separated into sub-regions based on the resin traces from each injection gate. An example of separating a square surface into four sub-regions based on the flow pattern using four-gate injection plan is shown in Figure 2-5.

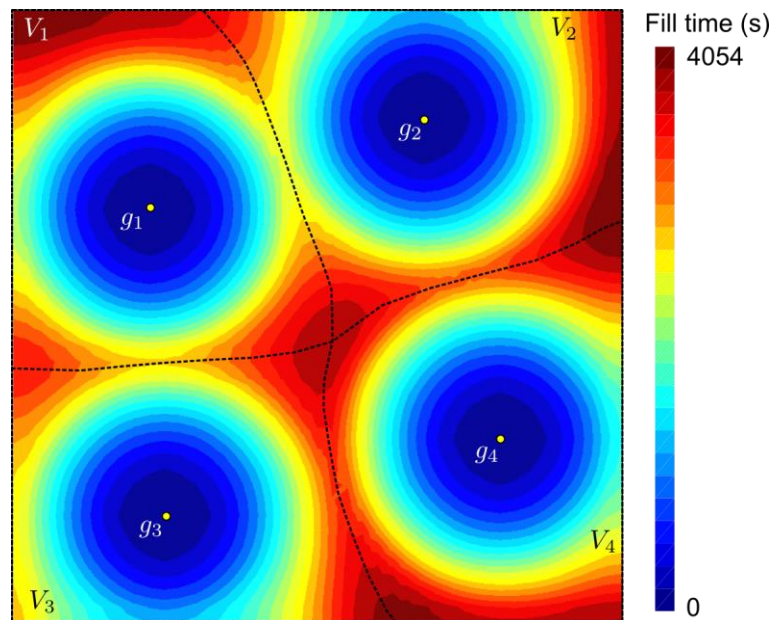


Figure 2-5: Flow pattern for a square part surface when resin is introduced from four injection gates, and four Voronoi Diagrams are generated based on the fill time results.

Next, the fill time cost functional defined in equation (2.15) for single gate injection is further generalized for the injection scheme with a number of  $k(k > 1)$  gates  $\{g_i\}_{i=1}^k$ , which is as follows:

$$F(\{V_i\}_{i=1}^k, \{g_i\}_{i=1}^k) = \sum_{i=1}^k \sum_{n \in \{V_i\}} w_n \tilde{t}_{g_i \rightarrow n}^* \quad (2.19)$$

Next, the centroid for each Voronoi region  $V_i$  associated with gate  $g_i$  can be defined by:

$$\mathbf{M}_i = \sum_{n \in \{V_i\}} w_n \tilde{x}_{g_i \rightarrow n}^* \frac{\mathbf{r}_n - \mathbf{r}_{g_i}}{|\mathbf{r}_n - \mathbf{r}_{g_i}|} = 0 \quad (2.20)$$

$$\mathbf{r}_{ci} = (c_{xi}, c_{yi}, c_{zi}) = \left( \sum_{n \in \{V_i\}} w_n \tilde{x}_{g \rightarrow n}^* \mathbf{r}_n \right) / \left( \sum_{n \in \{V_i\}} w_n \tilde{x}_{g \rightarrow n}^* \right)$$

For simplicity, the weighted geodesic distance from gate  $g_i$  to node  $n$ ,  $\tilde{x}_{g_i \rightarrow n}^*$ , in equation (2.20) can be calculated from equation (2.8), in which the weighted fill time is substituted by the fill time returned by LIMS. If the centroid location calculated from equation (2.20) is not on the surface, it is projected onto the surface based on the three principal axes of second moment of the sub-region according to the centroid  $\mathbf{M}_i$  using equation (2.14) over the sub-region.

Each multiple-gate pattern corresponds to a specific Voronoi Diagram of the surface. There exists a special Voronoi Diagram of the surface which is called Centroidal Voronoi Diagram (CVD). In CVD, the centroid of each sub-region coincides with the generator (gate) of that region (Figure 2-6). It has been proven that under CVD, the fill time cost functional defined in equation (2.19) reaches minimum, and therefore it provides the optimal multiple gate locations for the part [19]. Vent locations are then placed where the resin arrives last and where flow front merge based on the flow pattern return by LIMS in the last iteration. However, for some complicated geometries, one may not be able to place a vent at suggested locations.

Besides, because the mathematical model is based on geodesic distance, the geometry of each Voronoi Diagram is required to be convex in geometry so that the CVD represents the optimal results. Also, CVD is usually not readily available and algorithms have been developed to search for a CVD of the surface.

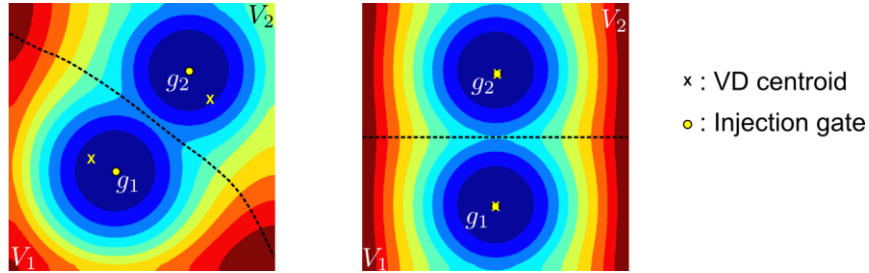


Figure 2-6: Comparison between regular VD (left) and CVD (right) of the square surface with two injection gates

### 2.5.2 Alternative way to calculate the flow centroid on spatial surfaces

To relax the convex shape requirement condition for each Voronoi Diagram, instead of using equation (2.20) to calculate the flow centroid for each Voronoi Diagram, we proposed an effective yet accurate method to locate the flow centroid through running LIMS by setting infusion lines on the outer boundary of each VD. To find the centroid for a specific Voronoi Diagram  $V_i$ , the boundary nodes of  $V_i$  are first selected as infusion line, as shown in Figure 2-7 (a). All the nodes not contained by  $V_i$  are set as filled. Next, LIMS is executed to calculate the flow pattern, and the last node to fill is then set as the centroid (Figure 2-7 (b)). This method executes one LIMS simulation to find the centroid for each Voronoi Diagram. This approach is numerically efficient and convenient as compared to calculating the geodesic distances using equation (2.20). An added advantage of using LIMS simulation is that it can be

used to find centroid for VDs that contain non-homogeneous permeability regions. For example in Figure 2-8(a), the compaction around the heel section of the orthotic foot results in low permeability region. The centroid found for the Voronoi Diagram  $V_1$ , which is the same with  $V_1$  in Figure 2-7, is moved up as shown in Figure 2-8(b). Using this method to find centroid for each Voronoi Diagram no longer requires that each Voronoi be geometrically convex. However, a much relaxed constraint that the flow pattern returned from each LIMS simulation has to be convex still needs to be guaranteed to achieve an accurate gate location optimization procedure.

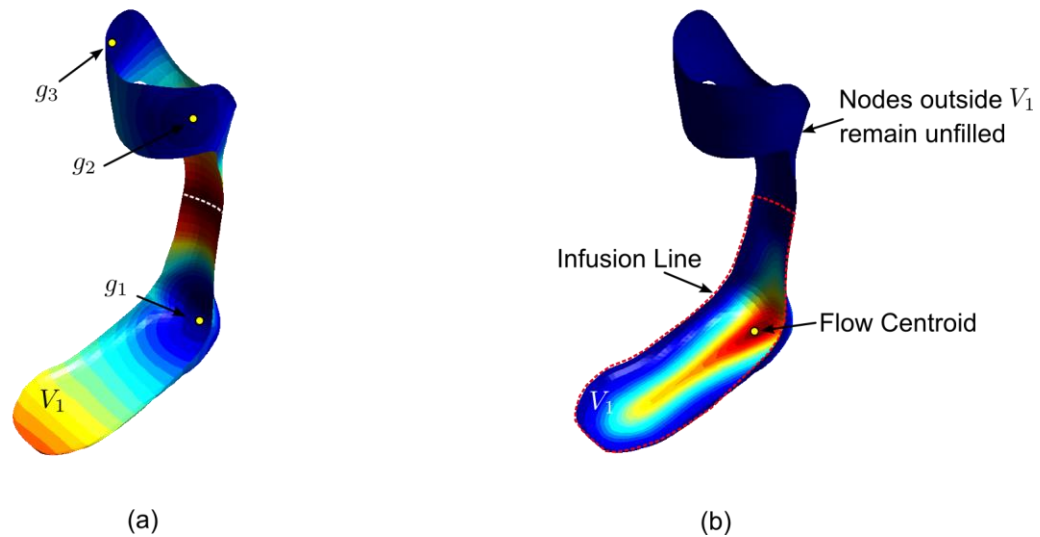


Figure 2-7: Search for the centroid of a Voronoi Diagram through running LIMS for homogeneous part: (a) Voronoi Diagram generation for three-gate injection of an orthotic foot (b) flow centroid found for  $V_1$  by running infusion simulation by setting infusion lines on the region boundary

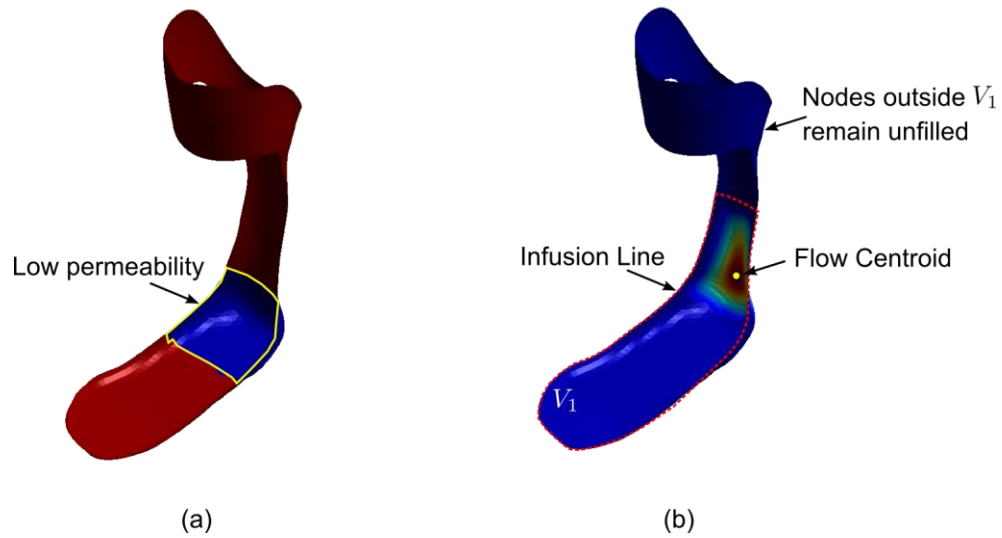


Figure 2-8: Search for the centroid of a Voronoi Diagram for non-homogeneous part: (a) low permeability section at the heel due to preform compaction; (b) centroid found for Voronoi Diagram  $V_1$ .

### 2.5.3 Lloyd's algorithm

A well-constructed iterative algorithm, Lloyd's method, is used as the search algorithm to find the CVDs for a surface. It has been proven that Lloyd's algorithm will converge to the final optimal configuration in limited number of iterations [19,20]. Lloyd's algorithm is then combined with LIMS to accommodate multiple gate location optimization during mold filling. If the number of gates selected was  $k$ , the  $k$ -gates optimization in RTM is carried out using the modified Lloyd's algorithm as shown in Figure 2-9.

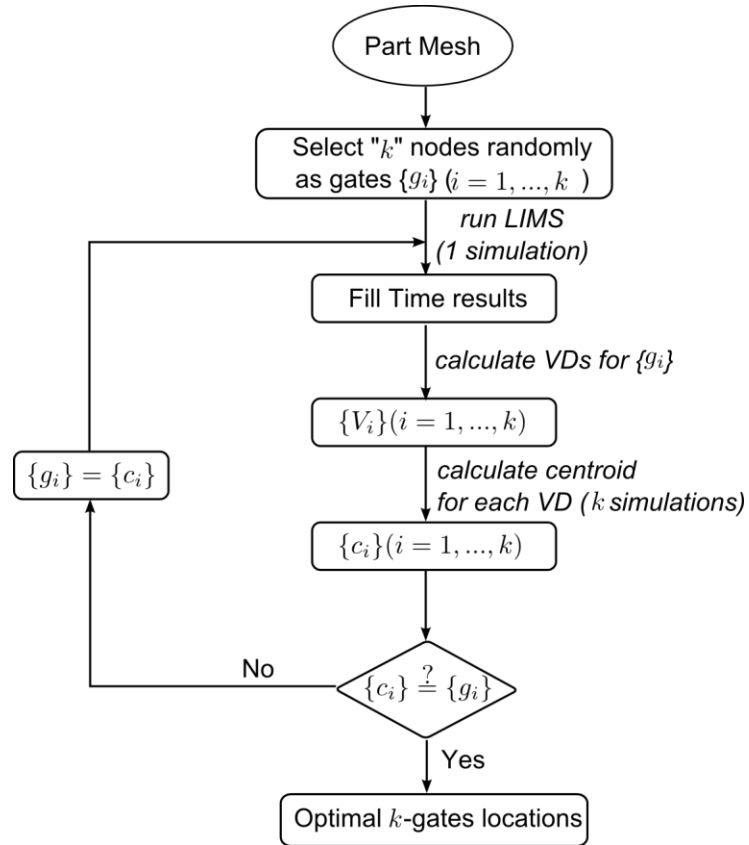


Figure 2-9: Flow chart that optimizes the location of  $k$  gates using Lloyd's algorithm

For the  $k$ -gates optimization problem ( $k > 1$ ) shown in Figure 2-9, one LIMS simulation is used to calculate each Voronoi Diagram region of the part surface, and " $k$ " simulation results are used to provide the centroid for each VD using the method introduced in section 2.4.2. Therefore the total number of simulations to find CVD of the part surface using modified Lloyd's algorithm is thus equal to  $(number\ of\ iterations) \times (k + 1)$ . In this paper, CVD method is specifically referred as this searching method that employs modified Lloyd's algorithm in conjunction with LIMS to find the optimal  $k$ - injection locations (gates) in RTM.

Iteration can be stopped at the converged iteration, or at the iteration in which the fill time drops below the max fill time that is allowed. An example that uses the modified Lloyd's algorithm to find the optimal four-gate injection plan for a square part is shown in Figure 2-10.

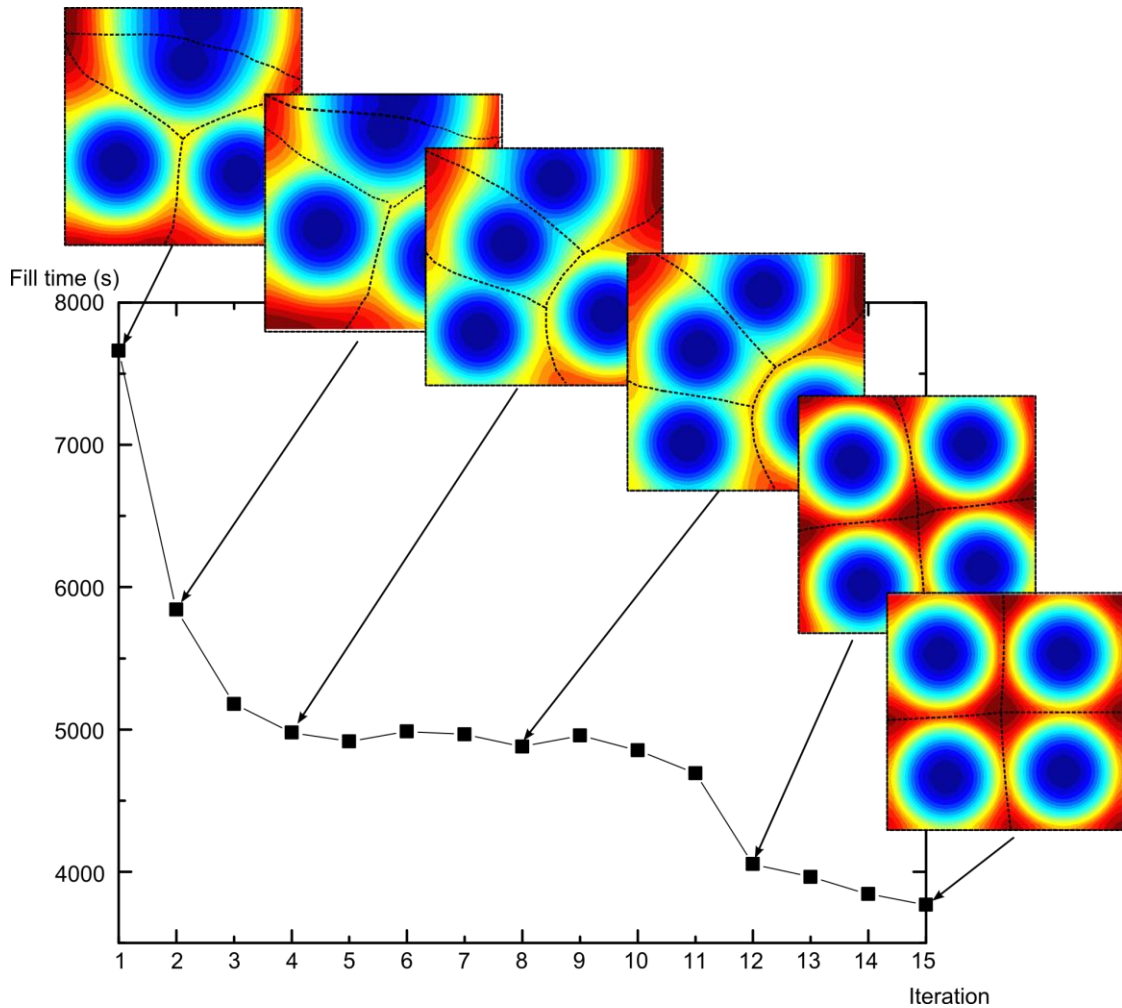


Figure 2-10: Use of Lloyd's algorithm to find the optimal four-gate injection plan for a square part.

Comparing to the exhaustive method which quickly gets out of hand when number of gates are greater than two, Lloyd's algorithm can greatly reduce the number of scenarios to be executed in LIMS.

## **2.6 Case studies**

In this section, case studies are shown to exemplify the implementation of CVD method for multiple gate injection optimization. Examples chosen represent a wide range of composite parts that have manufacturing complexity in both geometry and material properties.

### **2.6.1 Simple Square**

For comparisons, three sets of different initial four-gate locations are randomly selected for the square surface which uses isotropic and homogeneous fabric with permeability equal to  $K = 1.0 \times 10^{-11} m^2$ . As shown in Figure 2-11, all of the initial configurations converge to the final optimal gate within limited number of iterations, and the error of the results (distance between each of the four gates) are within two elemental lengths.

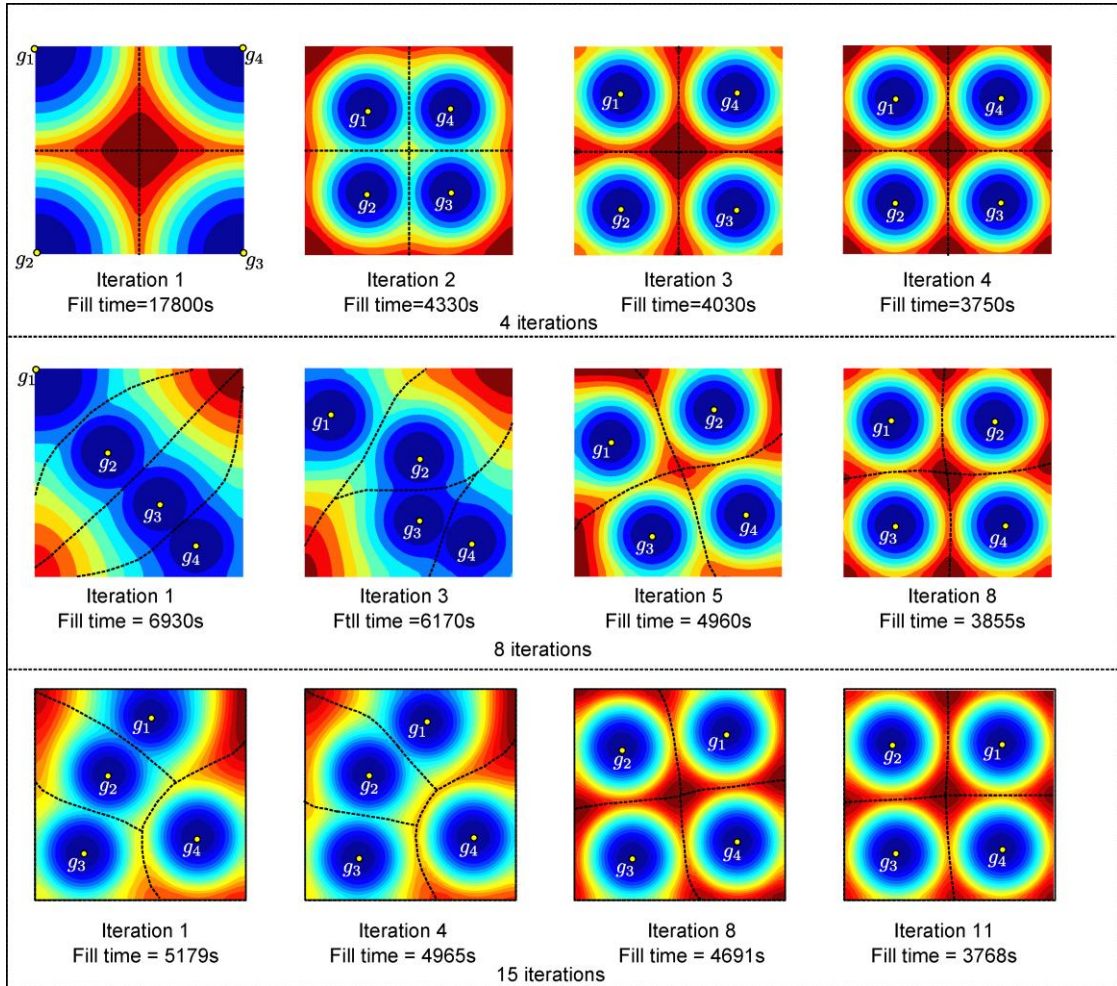


Figure 2-11: Different initial four-gate configurations for the square converge to the same optimal gate locations.

The Lloyd's algorithm may lead to local optimum instead of the global minimum of the fill time functional. An example of the iteration getting stuck at a local optimum for the square surface is shown in Figure 2-12. However, because each set of iteration requires limited number of simulations, this problem can be avoided by selecting different sets of initial gate configurations without adding significant computational effort.

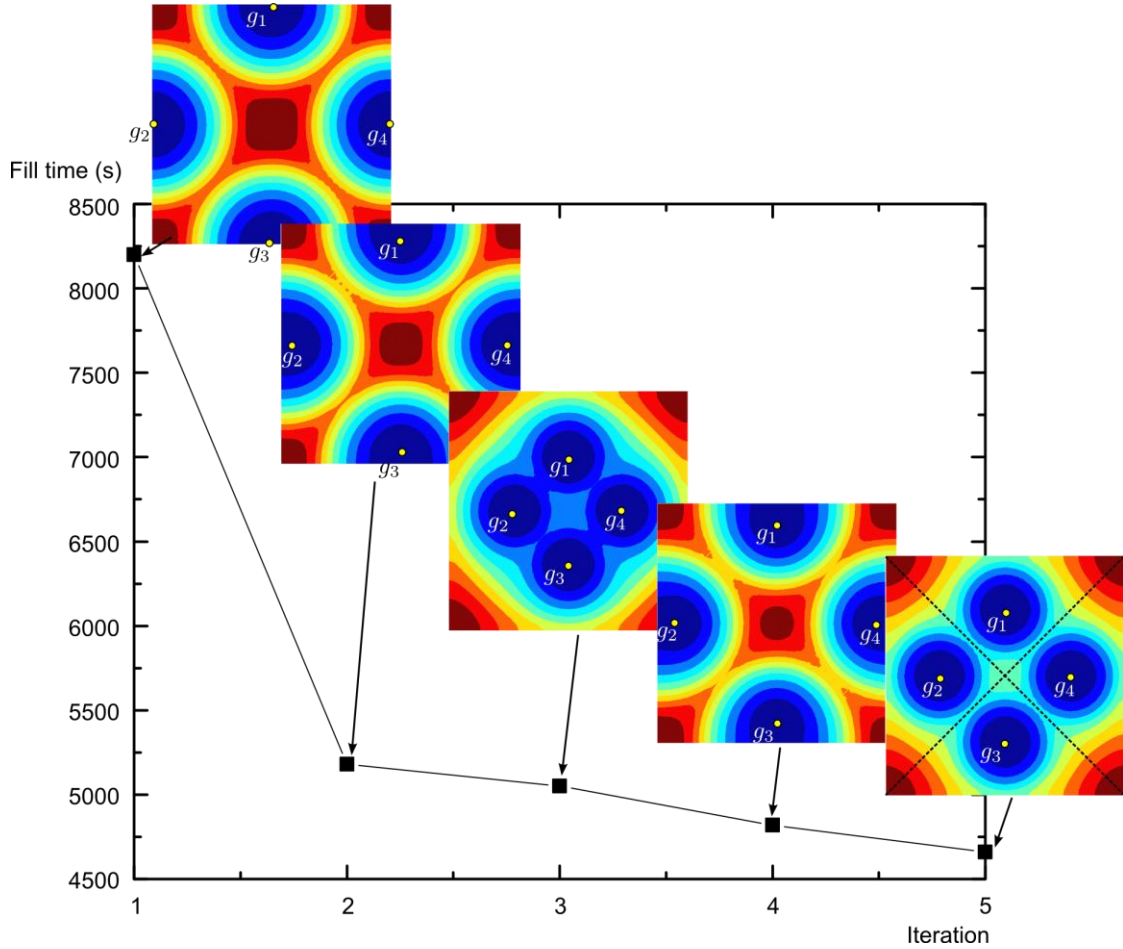


Figure 2-12: An example of four-gate location optimization process converging to the local optimum for the square geometry in which each gate is on the centroid of the its VD whereas the fill time (4700s) is not close to the optimum value as shown in figure 2.11.

The Lloyd's algorithm is then used for three-gate location optimization when anisotropic fabric is used or if the local permeability are modified due to the draping process [29]. The fabric permeability in the two principal directions are assigned as  $K_1 = 2.0 \times 10^{-11}m^2$  and  $K_2 = 1.0 \times 10^{-11}m^2$ , respectively. Optimal three-gate locations are shown in Figure 2-13(a) for the  $0^\circ$  laminate after 6 iterations and 24

simulations and the minimum fill time is 2125 s. Figure 2-13(b) shows the optimal three-gate locations for  $-45^\circ$  laminates, and returns a minimum fill time of 2271s after 5 iterations and 20 simulations. Then CVD method is implemented to find the optimal gate locations when higher anisotropies ( $K_1 = 10K_2$ ) are present (Figure 2-13 (c), (d)). It can be shown that the optimal gate locations change with the laminate directions, and the CVD method converges and can well capture the flow behavior of anisotropic fabrics.

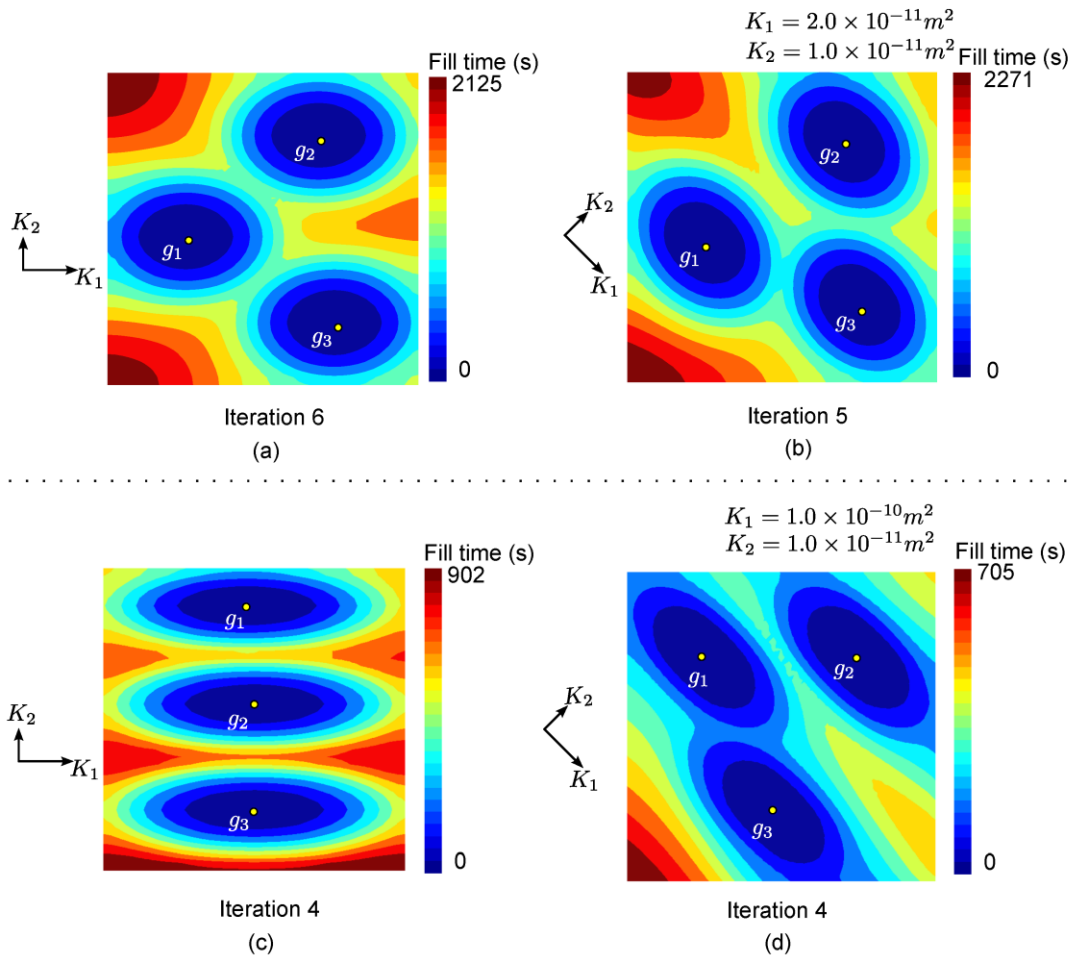


Figure 2-13: Three-gate optimization for the square with anisotropic fabrics: (a) optimal gate locations for  $0^\circ$  laminates after 6 iterations (24 simulations  $K_1 = 2K_2$ ); (b) optimal gate locations for  $-45^\circ$  laminates after 5 iterations (20 simulations  $K_1 = 2K_2$ ); (c) optimal gate locations for  $0^\circ$  laminates after 4 iterations (16 simulations  $K_1 = 10K_2$ ); (d) optimal gate locations for  $-45^\circ$  laminates after 4 iterations (16 simulations  $K_1 = 10K_2$ )

## 2.6.2 Orthotic leg geometry using isotropic material

The fabric material used is isotropic with permeability  $K = 1.92 \times 10^{-11} \text{m}^2$ . The gate locations optimization, for a personalized orthotic leg device (~15 inches tall) which has complex geometrical features, is important as the mold filling

needs to be completed in less than 20 minutes. This is because the mold is injected with fast-cure resin systems and the mold filling process needs to be complete before the resin starts to gel and increase the resin viscosity exponentially restricting resin movement. Also, this becomes a bigger challenge as the injection pressure is limited to one atmosphere as the mold material is not designed to bear higher pressures without resulting in dimensional changes. Therefore the number of minimum injection gates and their locations have to be optimized so that the fill time is minimum and satisfies the cycle time requirement. Next, the CVD method is compared with Genetic Algorithm results and exhaustive search method.

#### **2.6.2.1 Minimum number of gates optimization for the fast cure resin injection**

As is shown in Figure 2-14, the centroid of the part is first calculated and projected onto the part surface and is set as the injection gate, which will give the shortest single gate injection plan. However, the shortest single gate fill time is 4468s which far exceeds the resin gel time of 1200s. Next, the CVD method is used to find optimal two-gate injection plan for this orthotic leg (Figure 2-15). In 4 iterations, the optimal two-gate injection plan is found and the shortest cycle time using two gates is 1506s, which is still more than resin gelation initiation time of 1200s. Next, three-gate injection plan is explored using the CVD method and a shortest fill time of 918s is reached (Figure 2-16), which is much below the gelation time and is completed by executing a total of 28 simulations. In comparison, the brute force for this part mesh which contains 4684 nodes is impossible because of the large number of simulations ( $C_{4684}^1 + C_{4684}^2 + C_{4684}^3 = 1.71 \times 10^{10}$ ) needed.

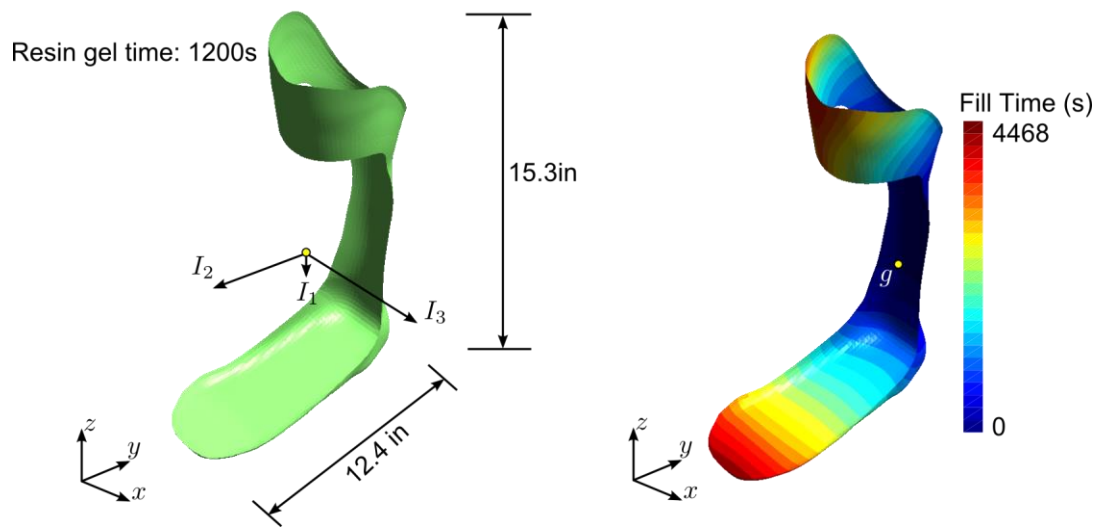


Figure 2-14: Orthotic part design and optimal one-gate injection fill time result

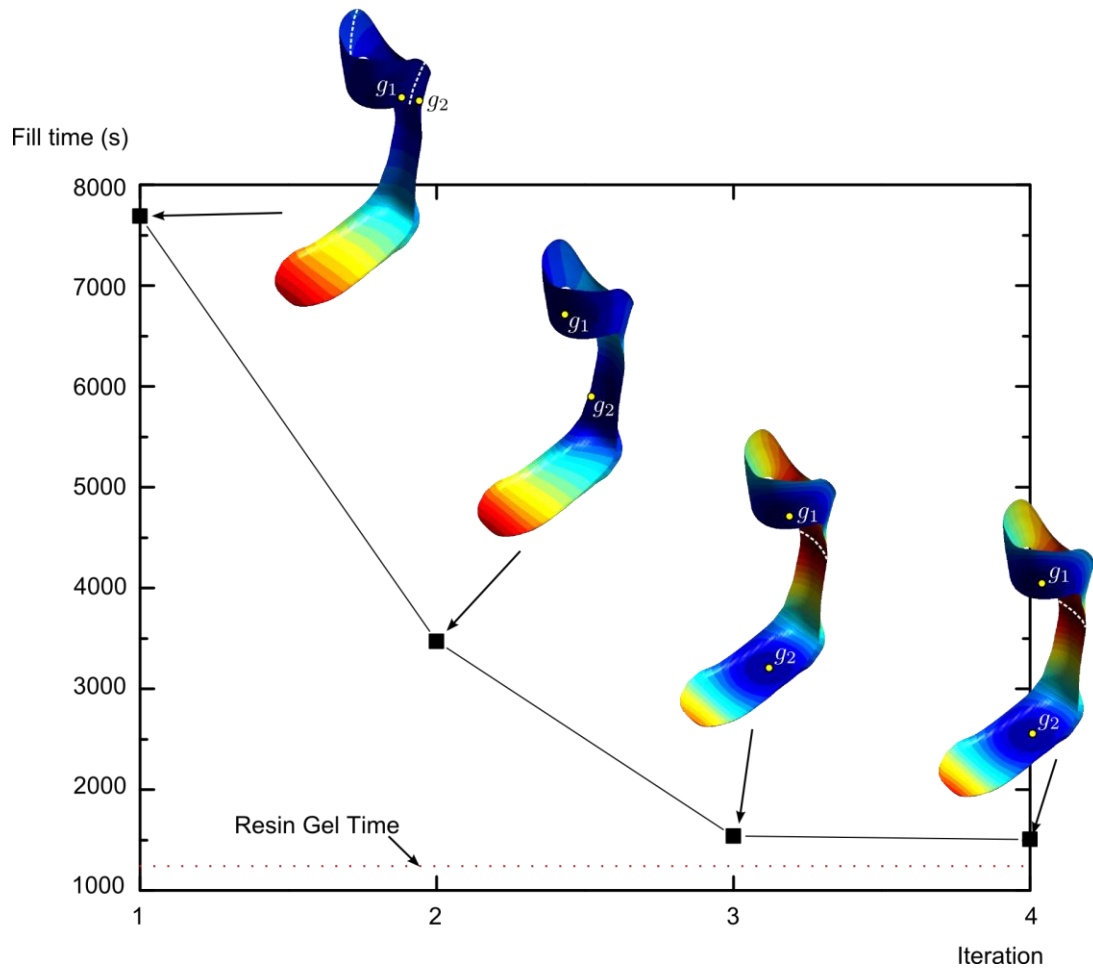


Figure 2-15: Two-gate location optimization for the orthotic leg

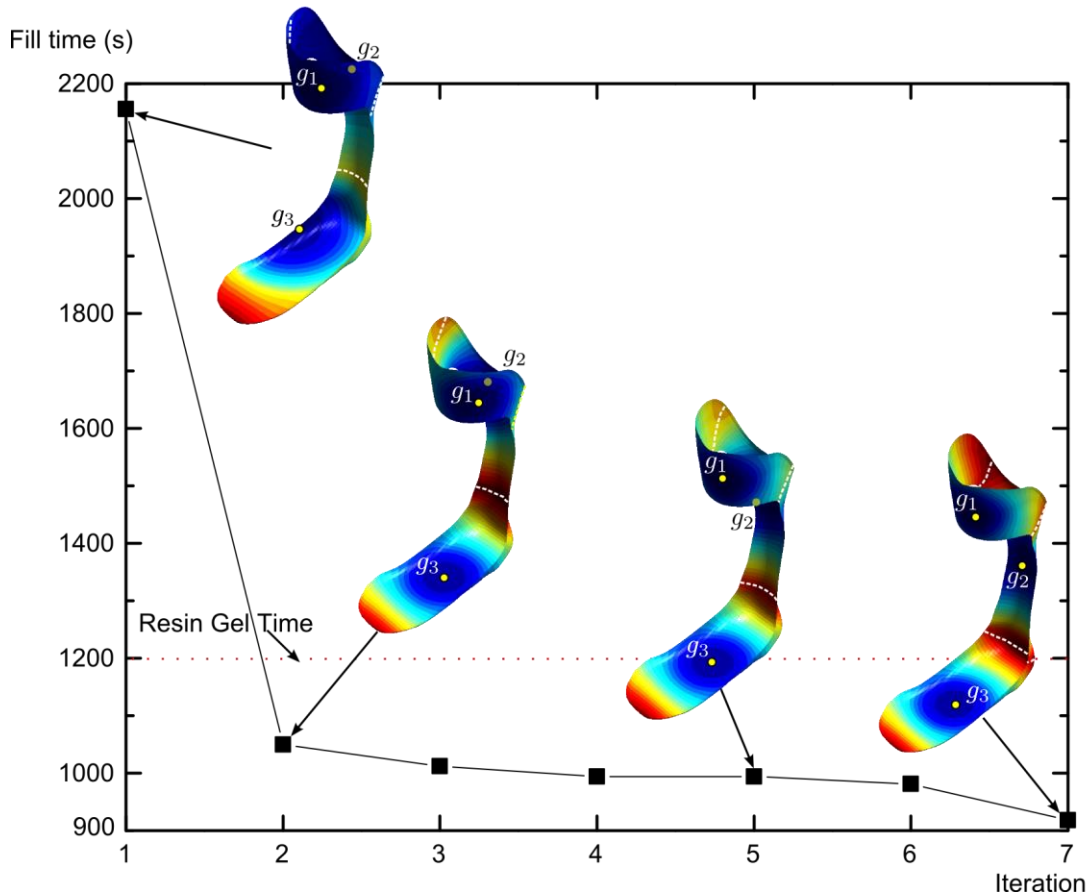


Figure 2-16: Three-gate location optimization for the orthotic leg which satisfies the resin gel time restrictions

### 2.6.2.2 Comparison of two-gate injection optimization using exhaustive search and Genetic Algorithm

First, the two-gate locations for the orthotic part using CVD method is compared with the result returned using exhaustive method by listing all combinations of two-gate injection scenarios. Because the number of scenarios ( $C_{4684}^2 = 11$ million) for this mesh is too large, the part is re-meshed using a larger element size. The coarse mesh (Figure 2-17(a)) has 210 nodes and the number of scenarios to be simulated in LIMS is  $C_{210}^2 = 21945$ . Because the coarse mesh cannot return the accurate fill time,

the location of the gate found using exhaustive search method is then used on the fine mesh, whose nodes that are closest to the locations are set as gates and therefore yield the fill time in Figure 2-17 (a). Next, Genetic Algorithm is used on the fine mesh to find the two-gate injection locations of the optimal two-gate injection locations after 190 simulations with a batch size of 10 (Figure 2-17 (b)). Comparison of number of simulations and minimum fill time returned for the three methods are listed in Table 2-1. Because LIMS simulations requires the most calculation time in each iteration (in the order of  $N^2$ , in which  $N$  is number of nodes in the mesh), the time cost for multiple gate optimization is represented using number of simulations in here.

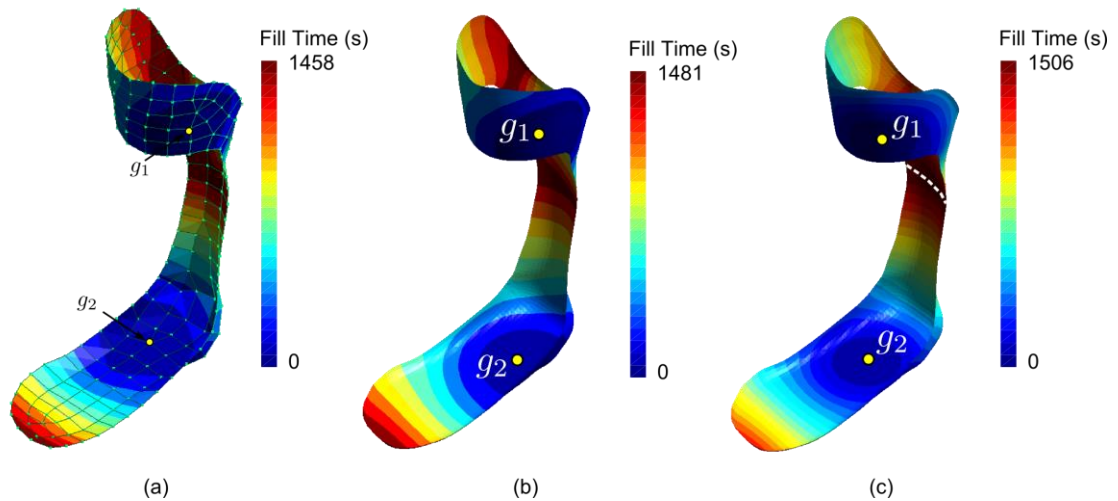


Figure 2-17: Two-gate injection optimization results comparison when using (a): exhaustive search on the coarse mesh with 210 nodes, (b): Genetic Algorithm after 190 simulations, and (c): CVD method after 12 simulations.

Table 2-1: Two-gate injection optimization comparison using different methods

Optimization Method	Exhaustive Search (coarse mesh)	GAs (fine mesh)	CVD (fine mesh)
Minimum Fill Time(s)	1458	1481	1506
Number of Simulations	21,945	190	12 (4 iterations)

### 2.6.2.3 Comparison of three-gate injection optimization using Genetic Algorithm

The CVD results for three-gate injection optimization are compared with that returned from Genetic Algorithm (GA) which is implemented on the fine mesh. GA results were obtained after 23 generations with a batch size of 10. The total number of simulations required is therefore 230. As shown in Figure 2-18,  $g_1$  and  $g_2$  found by both methods are at the same locations, and the gate  $g_3$  on the foot of the orthotic leg are close enough to ensure a shortest fill time found with a 1.8% difference after 28 simulations.

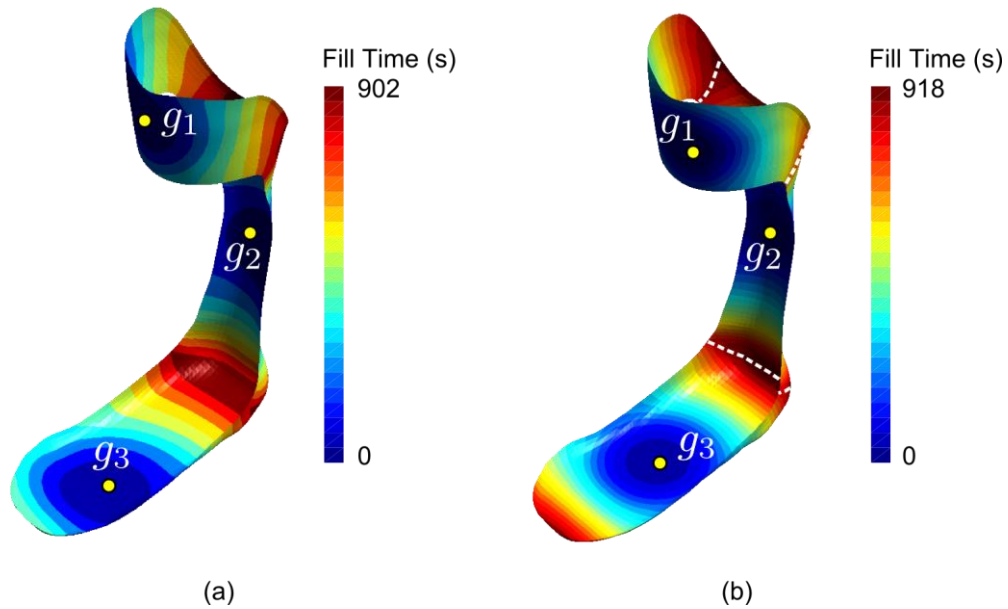


Figure 2-18: Three-gate injection optimization results comparison when using (a): Genetic Algorithm after 230 simulations, and (b) CVD method after 28 simulations.

### 2.6.3 Chassis

The CVD method is then used on a chassis when both a homogeneous material is used as shown in Figure 2-19 (a) and when an insert is added which results in low permeable region as shown in Figure 2-19 (c). The two-gate location for homogeneous part is evenly distributed along the center line as shown in Figure 2-19 (b). Gate  $g_2$  is a little off the center line because of the notch at the left bottom of the part. The two-gate location results when the insert is added in the lower part of the chassis is shown in Figure 2-19 (d). The low permeable section over the insert has moved both the gates into the lower part of the chassis.

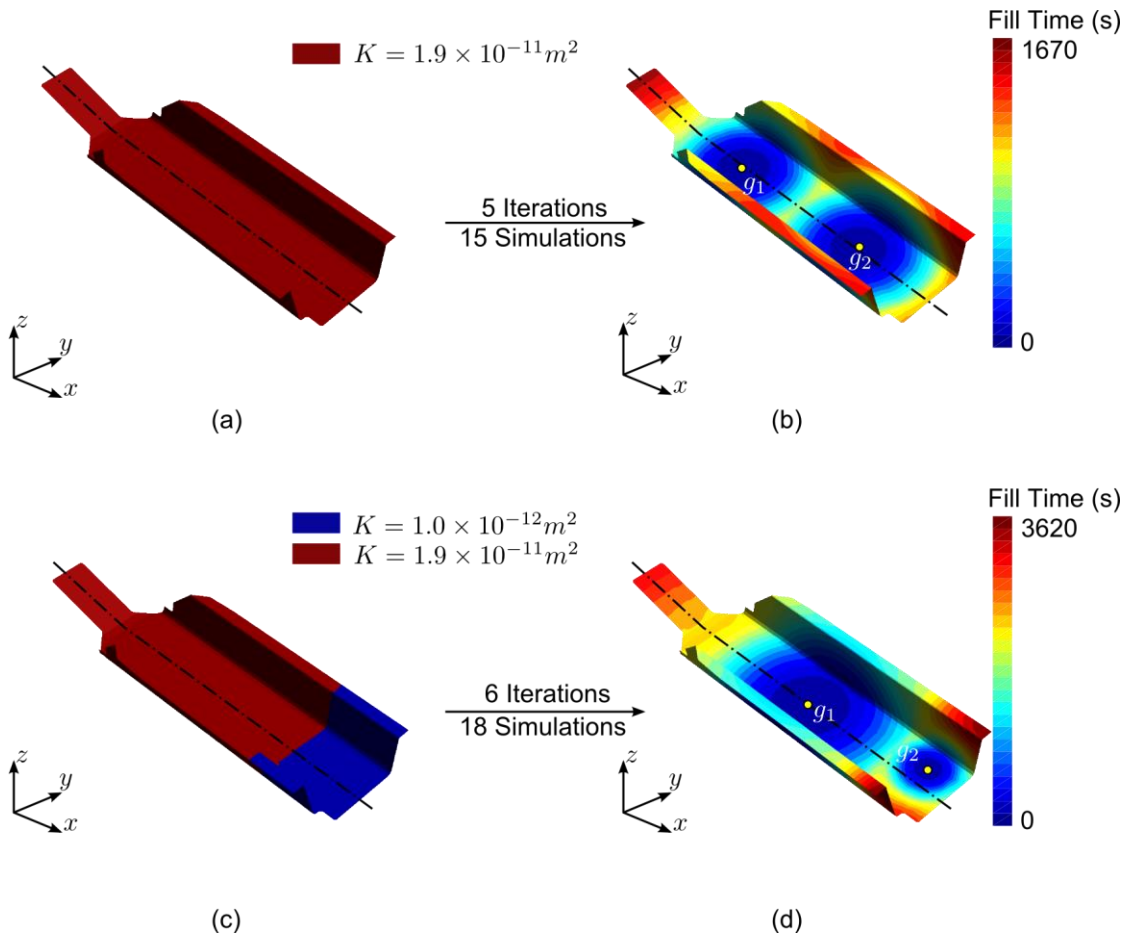


Figure 2-19: Two gate optimization for a chassis: (a) part geometry with homogeneous isotropic permeability, (b) optimal two-gate results after 15 simulations, (c) part geometry with low permeability region, (d) optimal two-gate results after 18 simulations.

However, as mentioned in section 3.4.2, the flow pattern of the part has to be convex to use the CVD method. If the flow pattern in any of the iterations is non-convex, the results returned can deviate from optimal gate locations. For example in Figure 2-20, high permeable region occurs along the corner in lower right of the chassis, because of the gap between preform and the mold surface. When calculating the centroid for the Voronoi Diagram  $V_1$  (Figure 2-20 (b)) associated with  $g_1$  by

selecting the boundary of  $V_1$  as infusion line, the flow pattern has two converging points, one of which is the last fill point, and the other is the point where flow front meets before the region is fully filled. Selecting the last fill point as the centroid which is shown in Figure 2-20 (c) is not accurate, because the extra flow converging point is ignored. The doubly connected flow pattern makes the CVD method inaccurate in placing the gate at the locations which will result in least time to fill.

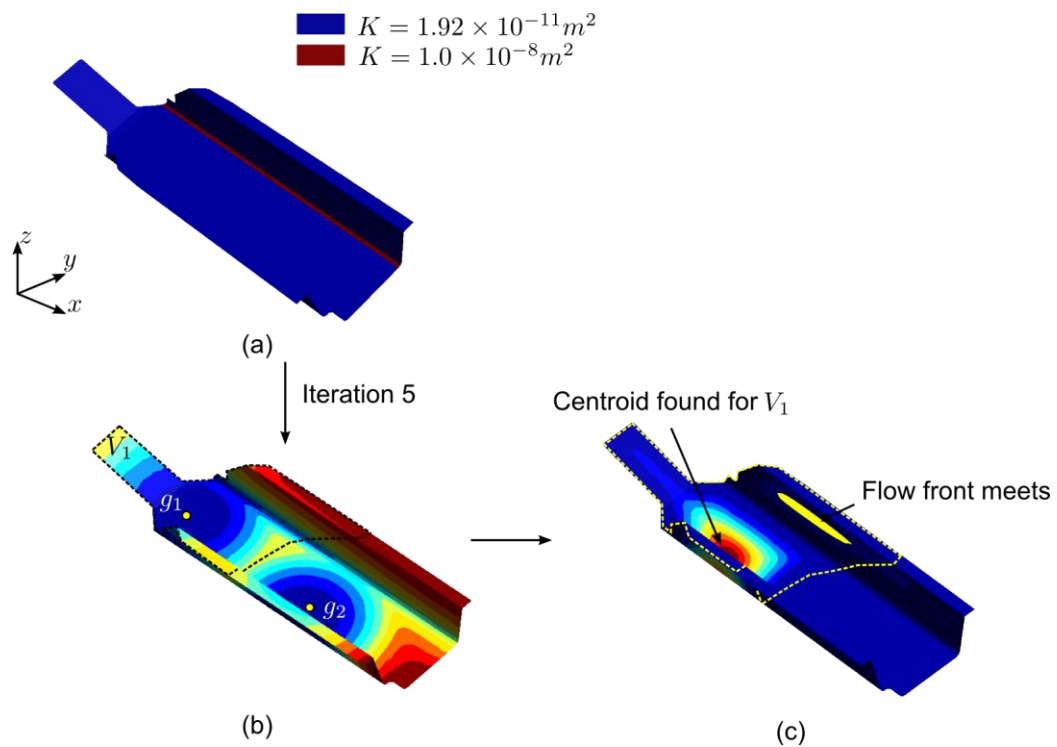


Figure 2-20: Two gate location optimization for the chassis with flow disturbance (high permeability) region shown in (a), and (b) VDs calculation in iteration 5, and (c) inaccurate centroid found for  $V_1$  because of the extra flow front meeting point.

## 2.7 Summary

A one-dimensional model is first developed and discretized using finite elements. Weighted geodesic distance and weighted fill time and their relations to each node is defined based on this one-dimensional model. The weighted geodesic distance and weighted fill time is further generalized for spatial surfaces by considering the surface mesh as a graph. A fill time functional is defined for the surface mesh based on the weighted distance and fill time for each node, and the searching for the minimum of the fill time cost functional is used as the objective function to optimize gate locations. Next, the nodes that are set as gates are used as generators to create the Voronoi Diagram of the part surface, from which the optimal Centroidal Voronoi Diagram of the mold part surface, which will minimize the fill time cost functional, is found using iterative Lloyd's algorithm. It has been shown that the CVD of the part surface will return the gate locations that minimize the fill time cost functional, and requires fewer simulations to be run in LIMS compared to the exhaustive search method and Genetic Algorithms. Although trapping in the local optimum is observed for highly symmetrical geometries using homogeneous and isotropic material when selecting the initial gate location symmetrically, this scenario is highly unlikely for asymmetrical parts with material randomness, and can be avoided by setting random initial gate configurations. Vents are then placed at the places where resin arrives last and the location where the flow fronts meet for the optimal injection scheme from the mold filling pattern returned by LIMS to avoid air pockets being trapped. In this chapter, fill time is considered as the only optimization objective and the number of vents and vent locations do not need to be minimized in our method to achieve minimal fill time.

## Chapter 3

### USE OF MEDIAL AXIS TO FIND OPTIMAL CHANNEL DESIGNS TO REDUCE MOLD FILLING TIME IN RESIN TRANSFER MOLDING

#### 3.1 Introduction

In the Resin Transfer Molding (RTM) process, pre-designed channels branching out like runners from the injection port can be used for faster resin distribution and impregnation as compared to traditional single gate injection to reduce the mold filling time. This chapter introduces another effective and accurate channel design approach for this class of problems in which channels are included in RTM processes whereas high permeable distribution mesh (which is used in VARTM but hard to be implemented in RTM) is not present with the objective of minimizing fill time, when fabricating composite parts that contain complexities in both the geometric features such as compound curvatures and corners and in material properties such as non-homogeneous and highly anisotropic fiber preform permeability.

##### 3.1.1 Resin Transfer Molding (RTM) process using line injection

During the resin injection step, the most important objective is to fully saturate the fibrous reinforcement with resin, displacing all air and volatiles out through the vent to manufacture a void free part. To this end, proper venting schemes are needed so that no voids are trapped within the part. Usually this can be achieved by predicting the resin flow pattern within the mold cavity and placing vents where the resin arrives last [30–32].

Another important objective of this process is to reduce the time it takes to fill the mold with resin. This will increase the production rate and reduce manufacturing costs and also ensure that the empty spaces between the fibers are saturated before the resin gels and is unable to move due to the cross linking of the polymer chains. Two strategies, usually in combination, can be applied to reduce the fill time. First, high injection pressure can be used to increase the resin flow rate through the injection port or gate. This will obviously be limited by the stress or stiffness limits of the mold (or inserts like sandwich cores) and available injection hardware. Thus, this is a brute force method that can be employed up to certain limits after which it will become prohibitively expensive. Second, the injection location or locations may be optimized to evenly distribute the resin within the mold cavity. To improve on this approach, one can use multiple-gate injection systems, and arrange gate locations on the mold wall optimally to reduce fill time [33]. Also, one can create a resin distribution network to speed up the filling process. This can be achieved by either leaving gaps along one or more of the part edges to promote racetracking [34] or fabricating channels within the mold and connecting these channels with the injection port. The former is simpler but the distribution network is hardly optimal in terms of reducing fill time and would be difficult to reproduce from one part to the next. The latter allows one to achieve a controlled and a larger flow rate through the gate under constant pressure, and therefore reduce the filling time significantly, albeit at a cost of more involved flow patterns to be handled by the venting scheme[35]. For example in Figure 3-1(a), channels are machined within the insert on the surface of the core material when processing sandwich structures for faster flow. In Figure 3-1(b), the 3d printed mold is pre-designed with open channels for a faster filling time so the part is fully saturated

with resin before it gels. To effectively benefit from these channels in reducing fill time and prevent void formation, the optimal topology of these channels needs to be determined.

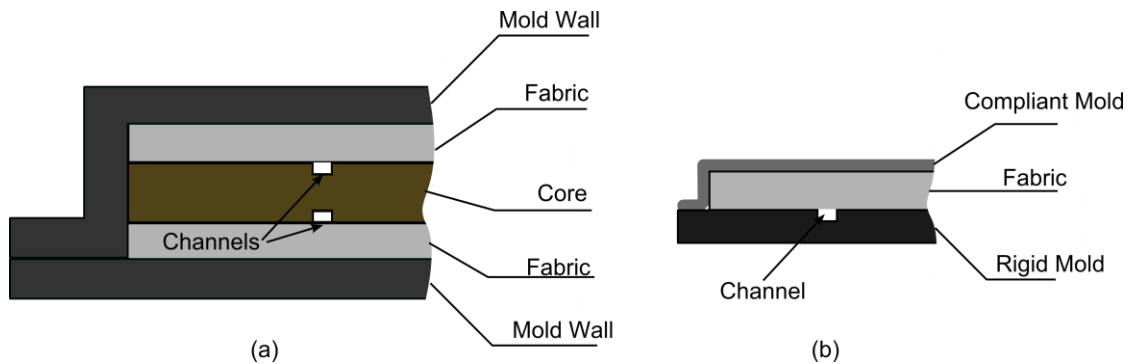


Figure 3-1: Channels used in RTM processes to reduce mold filling times by creating a resin distribution network: (a) sandwich structures where channels are machined on the core material, and (b) channels are pre-printed on the inside surface of the mold wall

For composite shell parts using isotropic or quasi-isotropic, homogenous fabrics of uniform thickness, it is straightforward to place the injection port at the center of the mold surface. If the part is symmetrical, the channel network can be machined along the lines of symmetry. Ideally, this strategy ensures resin arrival at the vent along the boundary in significantly shorter time than single injection gate. However, this task is not easy or intuitive if the geometry of the part is too complicated to find apparent symmetrical lines, or because the complexity in material property such as non-homogenous fabrics or fabrics with highly anisotropic permeability result in more complicated resin flow patterns.

Thus the objective of this chapter is to develop methodologies to find the topology of injection channels connected with injection gate for RTM process to reduce fill time. The method developed herein can deal with parts that include geometry and material complexities such as non-homogeneous material property and fabrics with highly anisotropic permeability. However, as RTM is usually used for shell-like composite parts manufacturing, through-thickness direction of mold flow is ignored and only in-plane mold filling pattern using effective in-plane permeability are addressed. The extension of this method to thick-walled parts with through-the-thickness non-homogeneities would be non-trivial [36], and more criteria have to be designed when through-thickness direction flow needs to be considered.

### **3.1.2 Previous work**

Previously, few researchers have studied the channel topology and location optimization for faster resin infusion in LCM processes. Genetic algorithms have been used to optimize the topology of the injection channel[37,38], but the solution returned from this method does not always guarantee the air and volatiles are displaced towards the boundary, and therefore the resulting venting scheme can be complicated. Distance based Medial Axis concept, which is defined as the loci of points that have at least two distinct closest points to the boundary (Figure 3-2), combined with level set theory and Fast Marching Method has also been used to generate the topology of injection channel [39]. However, certain drawback with this distance-based method limits its use for general injection line design and optimization. First, generating the distance field to the boundary using level set theory and Fast Marching Method is extremely difficult when applied to curved or multifaceted 3D part surfaces without discretizing them. However, the discretization of the part surfaces brings the second drawback of

the distance-based method: extracting medial axis topology by calculating the second derivative of the distance field is difficult and usually inaccurate. Third, the methodology only applies for isotropic material or quasi-isotropic material without thickness variations along the part surface, and the parts that use complicated and varying material properties cannot be addressed. Therefore, new method has to be designed to overcome these limitations.

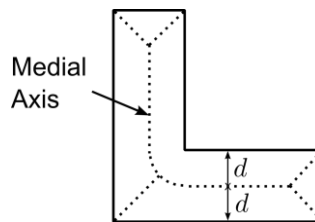


Figure 3-2: Medial Axis definition based on distance for an “L” shape part.

In this work, we modified the definition of the Medial Axis of the part surface based on the mold filling pattern to accommodate the RTM processing practices. Next, a method of separating the part surface into sub regions based on the flow pattern, which is defined as Voronoi Diagram is used to find the fill-time based Medial Axis of the part surface[16,40]. For parts containing preforms that have different permeability and/or thicknesses in different sections (non-homogeneous part), the location of the searched medial axis is further optimized based on the fill time field returned by LIMS. The last section illustrates examples to demonstrate the effectiveness and robustness of our methodology in finding optimal channel topology for parts that contains complexity in both geometry and in material property.

### **3.2 Medial Axis definition based on the fill time**

In computer graphics theory, medial axis is defined based on distance and is the loci of points that have at least two distinct closest points to the boundary. Many models are available to find the points located on the medial axis by calculating the geodesic distance of each point on the surface to the part boundary[41–43]. If the permeability of the fiber preform in the mold is isotropic and uniform, one could apply this to a set of nodes to serve as injection locations within the domain that will ensure that the injected resin reaches two distinct boundaries at the same time. This would create the minimal fill time as moving the injection location toward one of the boundaries will inevitably extend the time required to reach the other boundary and thus extend the total fill time (simple minimum).

There are two embedded assumptions that may not hold when employing this distance-based logic. First, the speed of flow advancement depends on the distance from infusion location(s) and on the flow pattern. Second, and more importantly, it also depends on the permeability and thickness of the material between the injection point and the flow-front and neither property is necessarily constant. In most cases, the composite part design often dictates spatial variation in both these properties for optimal functionality and mechanical performance requirements of the part.

To relax these assumptions in the RTM process, we re-define the part surface medial axis based on the fill time from each point on the medial axis to the boundary rather than just focusing on equal distance from the axis to the boundary. The direction of flow is also important as the time to reach the medial axis from the boundary will not be the same as the time from the medial axis to the boundary if the fiber preform's property is non-homogeneous due to constant pressure at the inlet. An example is shown in Figure 3-3. First, the boundary is discretized into a set of control points

which represent one boundary segment:  $s$ . For each node with coordinates  $(x, y)$  within the discretized part, the fill time from each control point ( $s$ ) on the boundary to node  $(x, y)$  is calculated by assuming constant pressure single gate one dimensional flow along the geodesic line joining the two points, and is recorded as  $t(x, y, s)$ . Next, at the node location  $(x, y)$ , the minimal fill time from all the control points on the boundary is identified. Node location  $(x, y)$  is on the medial axis if two or more control points on the boundary  $s$  provide similar (identical) minimal fill time. As shown in Figure 3-3, point A is on the medial axis and point B is not. All the points within the domain that satisfy this requirement are then joined which will represent the fill time based Medial Axis.

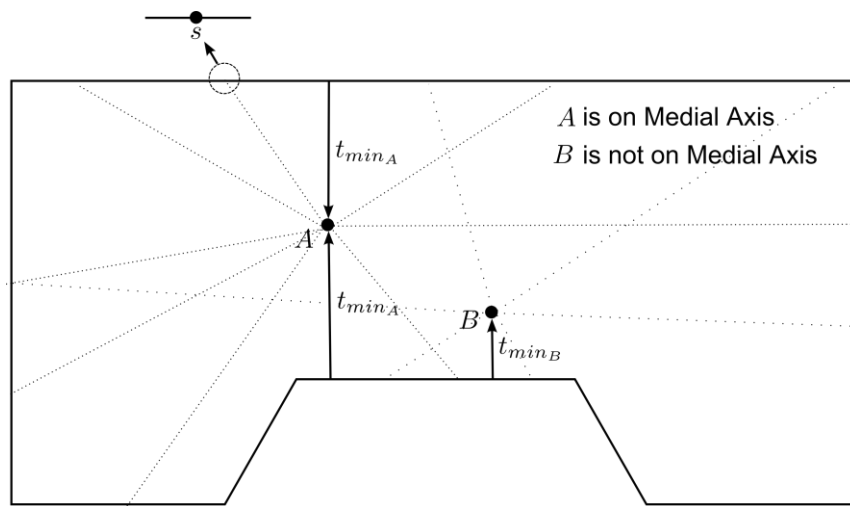


Figure 3-3: Example of the requirement of a node within the domain to be the fill time based Medial Axis: Point A is on the medial axis because two locations on the boundary returns identical minimum fill times; whereas Point B is not on the Medial Axis because only one location on the boundary returns the minimum fill time

It is difficult to find the exact minimal fill times for each node within the part domain from all the control points on the boundary, especially when the part has a complicated geometry and contains preform with anisotropic and non-uniform material properties. Therefore, it is beneficial to define the fill time based medial axis from the Voronoi Diagrams of the part domain surface with respect to a discrete subset of control points on the part boundary. Voronoi Diagram (VD) is the surface partition defined by a finite set of locations on the surface. For a part surface with a total number of  $k$  control points on the boundary, the meshed surface of the part is separated into  $k$  regions, each of which is called a Voronoi Diagram of the part and is associated with one corresponding control point on the boundary. Each region belonging to a control point on the boundary will fill faster from that control point than from any other control points on the part boundary. Therefore, the boundary between two VD regions represents points where the resin reaches at the same time regardless of which of the two control points was used as a gate. The fill time based medial axis is a subset of these boundaries, though most of them (for example those between neighboring points) are a by-product of discretization and must be identified as such. An example of separating a 2D surface into VDs from a set of control points on the boundary is shown in Figure 3-4.

Some boundaries of the VD may be due to the undesirable effect of boundary discretization. Thus, certain selection criteria must be applied to ensure that only the boundaries between two distinct (separated by some distance, not neighbors) control points are being considered, and that some other heuristic rules are observed to prevent unnecessary branching of the medial axis and placing of the inlet too close to

the boundary. Thus, all the internal nodes within the part that satisfy the following criterial are selected:

1. At least two control points on the boundary give the minimum fill time with tolerance  $t_{min} + \epsilon$  ; and
2. The control points on the boundary that give the required fill time within the tolerance are not next to each other.

Joining these identified nodes reveals the topology of the fill time based medial axis. Next, a heuristic parameter  $\delta$  ( $\delta \in (0, 1)$ ) is defined and multiplied by the maximum fill time  $t_{max}$  from the boundary to the injection line. If a node on the medial axis has a fill time  $t$  that satisfies  $t < (\delta \times t_{max})$ , it is considered to be too close to the boundary and deleted (dotted lines marked (a) in Figure 3-4)). Finally, short branches (dotted lines marked (b) in Figure 3-4)) that have length  $l$  smaller than  $\Delta \times h_e$ , in which  $\Delta$  is the heuristic parameter defined by the user and  $h_e$  is the average element size of the mesh, are also deleted. Therefore, the medial axis is the discretized form of a series of connected lines that are defined by the boundaries of the Voronoi Diagram.

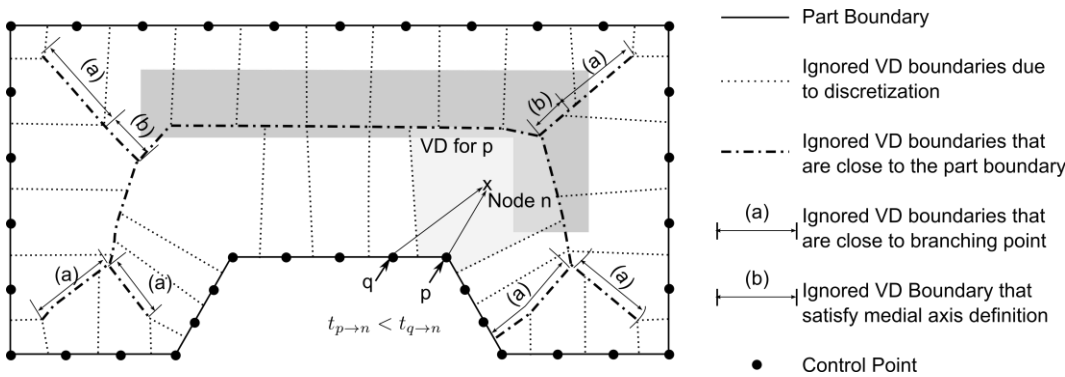


Figure 3-4: Voronoi Diagram of the part geometry from the control points on the part boundary

### 3.3 Optimal injection channel from fill time based medial axis

In this section, a detailed approach is introduced to find the topology of the fill time based medial axis within the part geometry using finite element based mold filling simulation software. This approach addresses the fabric materials that have either isotropic or anisotropic permeability. However, for preforms that are non-homogeneous, a method is proposed to correct the location of medial axis to ensure the resin arrives at the boundary at the same time from the nodes on the medial axis.

#### 3.3.1 Fill time based Medial Axis topology generation

LIMS (details in Appendix A about the mold filling software) is used to generate the flow pattern from a gate under constant injection pressure conditions. As shown in Figure 3-5, first, all the nodes on the boundary of the part surface mesh are selected as control points to represent the boundary curve,  $s$ . The total number of control points on the boundary is  $N$ . For each control point on the boundary, one LIMS flow simulation is executed. Therefore, each node on the part surface will have  $N$  simulation results for fill time:  $\{t_1, t_2, \dots, t_N\}$ , each of which represents the arrival time from a specific boundary control point. Next, the minimum fill time from the set  $\min\{t_1, t_2, \dots, t_N\}$  is selected as the node fill time ( $t_{min}$ ) which represents the lowest fill time at that location when resin is introduced independently from each segment of the boundary to this point. In this chapter, we call the fill time map as the integrated fill time map. Intuitively, one might want to define the injection channel along the “ridge” provided by maximal values in Figure 3-5 as this represents the fill time based medial axis. This is essentially the correct notion but the visual inspection and determination of the ridge must be based on a methodology independent of human observation.

To achieve this, nodal fill time in Figure 3-5 (c) is compared with all simulation results shown in Figure 3-5(b). As shown in Figure 3-5 (c), the nodal fill time  $t_i$  for a specific node  $i$  (which is  $\min\{t_{i,1}, \dots, t_{i,N}\}$ ) is compared with all the scenarios' nodal fill time result for node  $i$  in Figure 3-5 (b). If one scenario  $s$  in Figure 3-5 (b) returns node  $i$ 's fill time  $t_{i,s}$  that falls within range of  $[t_i, t_i + \delta t]$ , then the control point on the boundary for scenario  $s$  is the source gate that fills the node  $i$ . Then the nodes that are filled by more than one control point on the boundary are selected because these satisfy the medial axis definition. For example in Figure 3-5 (c), node  $i$  is on the medial axis, whereas node  $j$  is not.

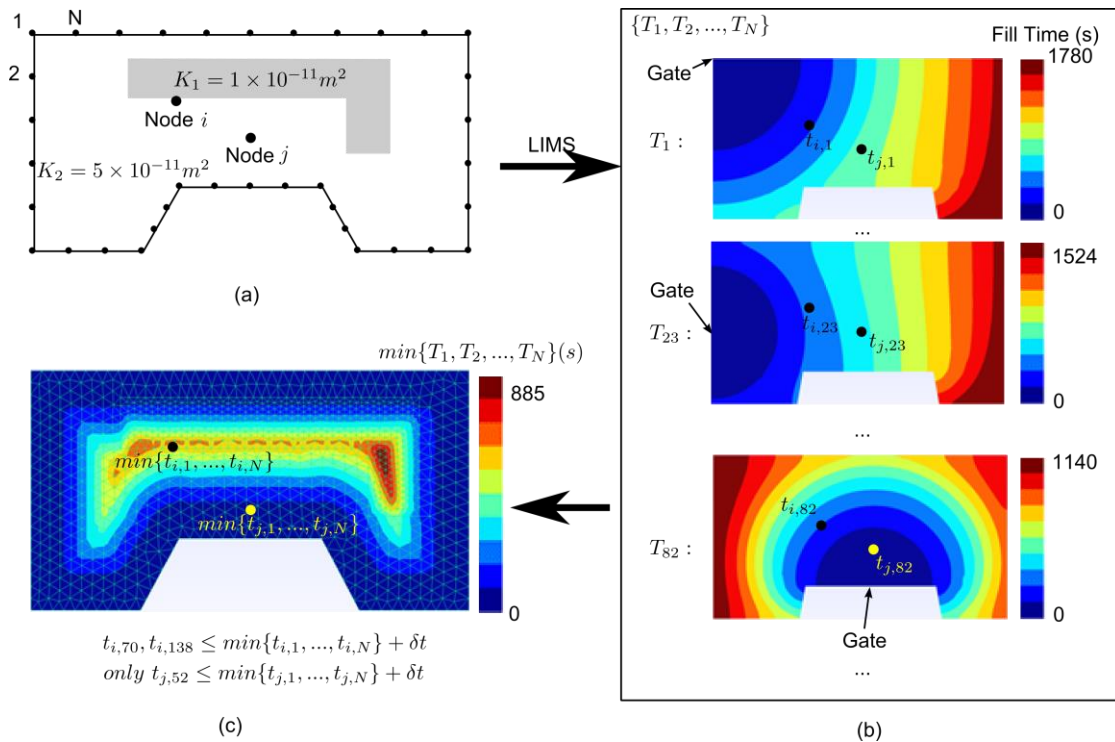


Figure 3-5: Generating the integrated fill time map (a) select N control points on the boundary (b) Record minimum resin arrival time at each interior node from a N flow simulations conducted with each control point on the boundary set as the gate (c) generate minimum fill time map from contours of minimum fill times

Note that in the example shown in Figure 3-5, the number of generators on the boundary can be decreased by e.g. selecting every other node on the boundary as the generator, and therefore decrease the number of scenarios by a factor of two. However, this is an ad-hoc coincidence and cannot be extended to general cases. The reason is that the medial axis generation algorithm developed in here was for spatial surfaces with polygon boundaries. Although in this example the boundaries of the part are connected with straight lines, the general cases usually rely on the meshing strategies to approximate the boundary into polygons. Therefore, using all the nodes on the boundary as the generators are safer when dealing with general cases at the expense of additional computational time.

### 3.4 Medial Axis correction for non-homogeneous preform

#### 3.4.1 Different resin arrival times between two points on the part surface

We have previously stated that the resin arrival time from point A to point B may not necessarily be the same as the resin arrival time from point B to point A. To demonstrate this, consider a 1D example shown in Figure 3-6.

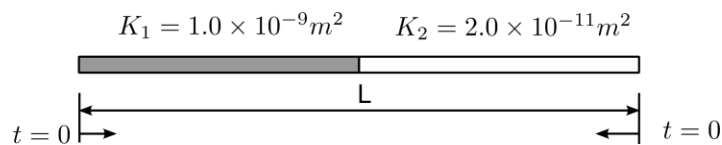


Figure 3-6: A non-homogeneous 1D example that has higher permeability in the left half than in the right half

In this example, the 1D beam is composed of two different preforms: the one that covers the left half has significantly higher permeability than the one that is

placed in the right half of the mold. The goal here is to find the optimal injection location, which will ensure that the resin injected from this point will arrive at both boundaries at the same time. Applying the algorithm from section 3 we identify two control points, one at each end, and two simulations (or closed form calculations[17,18]) can be executed by injecting resin from each boundary control point separately. The time versus location of two flow fronts is plotted in Figure 3-7. The position where the two lines intersect is our medial axis (same fill time from both ends). Thus, the beam is mapped into two domain Voronoi Diagram, each area is assigned to one end accordingly.

Meanwhile, we can find the optimal injection location directly for this 1D beam, because closed form flow solutions are available [17,18]. For each point within the beam, we can set that point as an inlet and plot the time needed to reach left and right end depending on the injection location (Figure 3-8). When these times match, we reach the optimal inlet placement. Note that its location differs from the locations given by the flow-time based medial axis. This is the result of resin arrival time from inlet to ends being different than the resin arrival time from endpoint to the inlet. This is because of the non-homogeneity along the path – permeability or cross-section variations. Note that it differs from the geometric center of the line (conventional medial axis based on distance) as well.

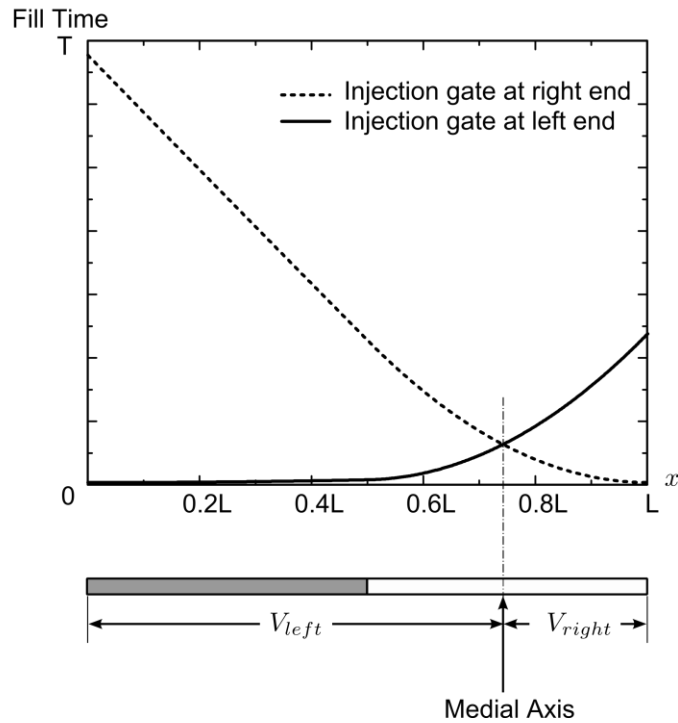


Figure 3-7: Medial axis calculation based on the resin arrival at various locations injected from left and right end respectively.

Figure 3-8 shows that the optimal injection location reduced the fill time by 53% compared with that by injecting at the initial medial axis location. Therefore, it demonstrates that the fill time will depend strongly on the flow direction when the fabric permeability or thickness is non-homogeneous. The important corollary of this results is that the direct use of medial axis as final injection line may still be suboptimal for both 2D (Figure 3-9) and 3D cases, even though in most practical cases the non-homogeneity may be less pronounced than that of our 1D example case. Therefore, it is necessary to accept the medial axis as a first approximation only and to iteratively correct its location.

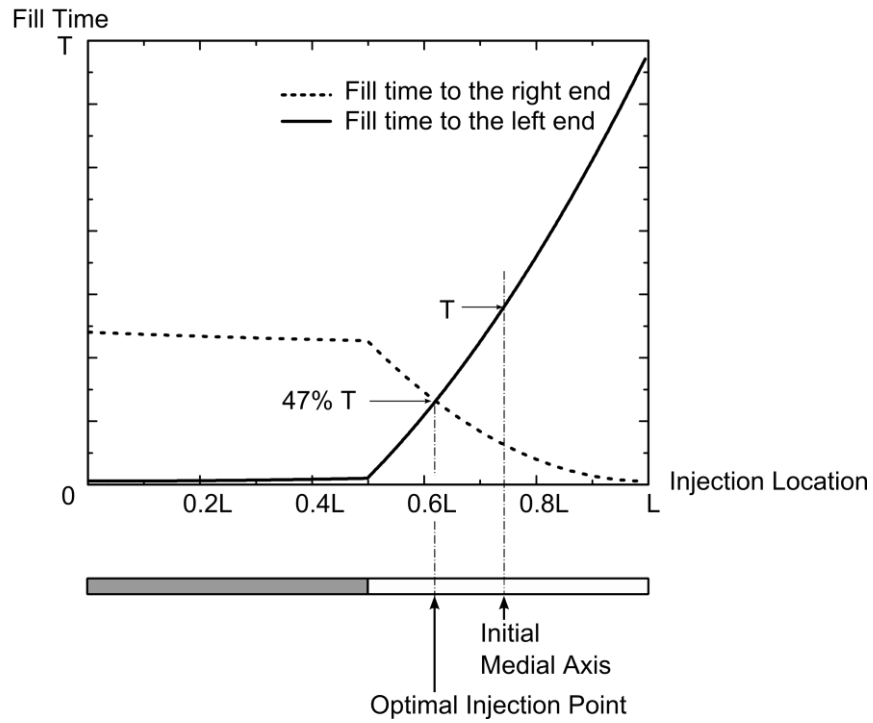


Figure 3-8: Fill time plot from each point in between the two boundary points to the boundary, and the optimal location returns a fill time that is 47% of the initial medial axis fill time shown in Figure 3-7.

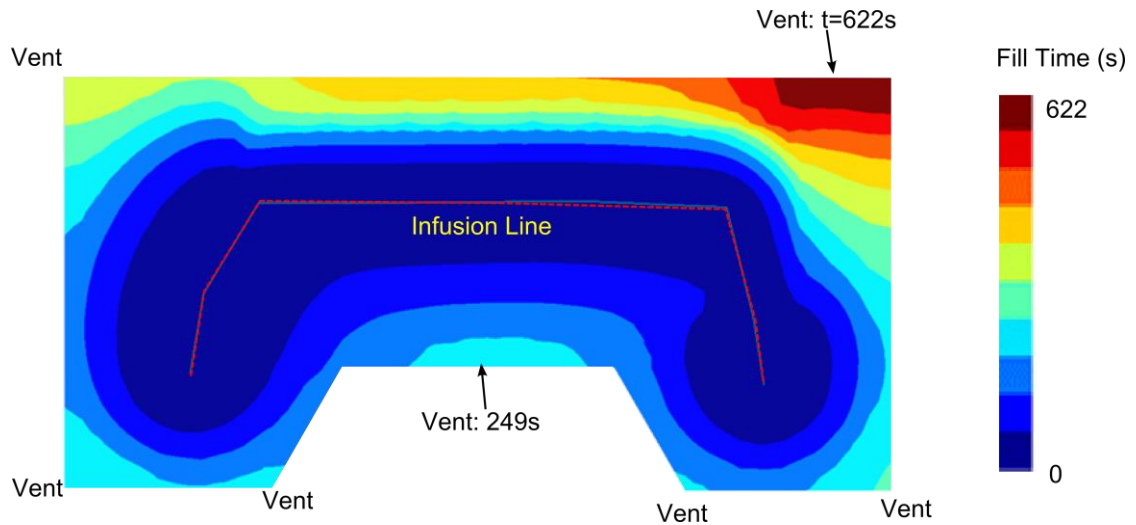


Figure 3-9: Flow pattern when setting the injection channel on the initial medial axis

This raises the question why we want to use the fill time based medial axis in the first place and not just the geometric one. There is no fundamental reason not to do this but two simple practical ones. First, paradoxically, the algorithm to find the time based medial axis is straightforward even on doubly curved surfaces with complex boundary, and it can work with triangulated surfaces easily. On the contrary, the geodesic distance may be surprisingly difficult to determine in these cases [12,15,18,22,33]. Second, as the fill time approach takes into account the permeability and cross-section variations, we would expect it to be a better starting estimate in most cases.

### 3.4.2 Updating the injection line location

The iterative process to correct the injection channel position is again based on flow simulation results. The initial medial axis is used as the injection channel. This line is then iteratively shifted in the direction that reduces the fill time.

As mentioned previously, the medial axis is found by dividing the part domain into a Voronoi Diagram and the common boundaries of the VDs define a series of connected lines that form the medial axis. Therefore, the initial medial axis can be viewed as a connected Graph:  $G\{V, E\}$ , in which V are all the control points connecting the discretized lines and E are all the edges. All the vertices on the injection channel are moved to the new location based on the fill time distribution on the boundary. Based on the fill time results, the flow history can be approximated by identifying each node's most direct upstream nodes. Using this method, the nodes are reconnected into the approximate resin tracing line (Figure 3-10) which intersects each vertex on the initial medial axis channel. Each tracing line will also intersect the boundary in at least two locations. These boundary locations or control points are associated with the specific vertex on the initial medial axis graph. Resin is assumed to originate from the specific vertex on the medial axis and the time for the resin to reach the associated control points on the boundary along the tracing line is calculated. Next, the vertex on the injection channel is moved towards the associated location on the boundary that has the larger of the two fill times. With the path of the control point fixed, the fill time for the boundary node that the control point is moving towards, will decrease monotonically, while the boundary nodes on the other side of the injection line will increase correspondingly. Therefore, there exists a unique location on the path that ensures the resin arrives at the boundary at the same time. Therefore, a simple binary search will converge very fast to the control point location that reduces the final fill time. The process is repeated until the fill time difference from the vertex on the injection line (the medial axis) to the two-control point on the

boundary is smaller than  $\delta t$ , or the step size is smaller than the element size. (Figure 3-10)

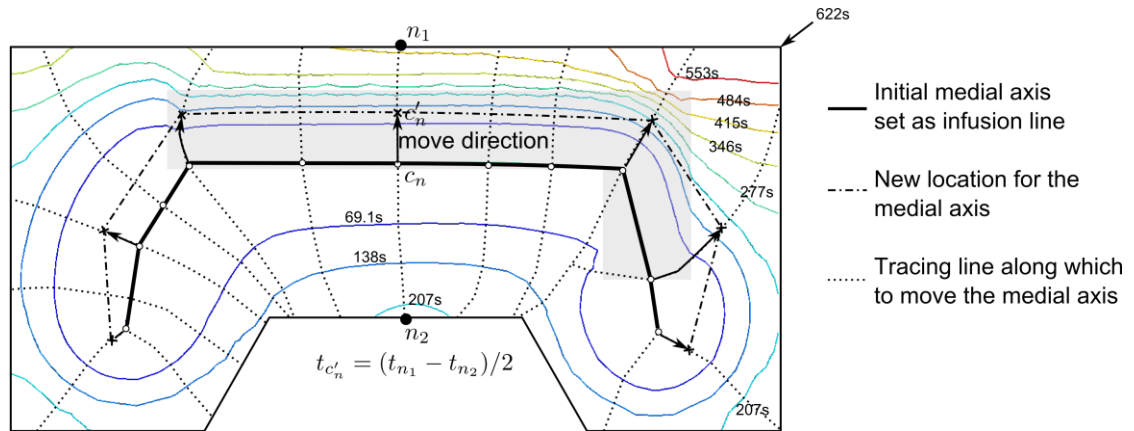


Figure 3-10: Flow contour with the initial medial axis as the injection channel, and the methodology to move the medial axis to the new location.

As shown in Figure 3-11, after four iterations it converges to the injection channel which ensures the resin injected from each control point on the new injection line reaches the associated points on the boundary at about the same time. The processing time is therefore reduced from 622s when using the initial medial axis as the injection channel to 322s for the final injection channel.

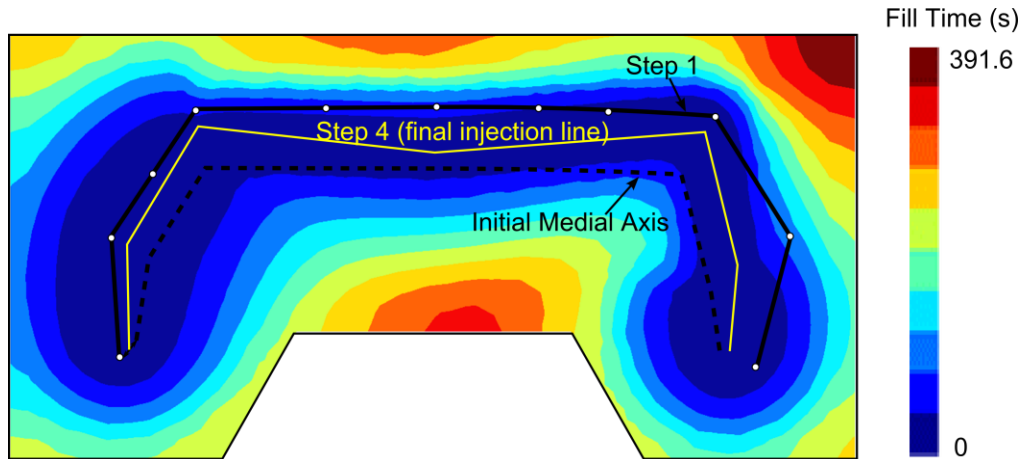


Figure 3-11: Initial medial axis and the arrival at the final injection channel design after four iterations with resin flow patterns when injected from this optimized injection line.

Therefore the entire procedure of using Media Axis to determine the injection location to minimize fill time is separated into two steps: first to calculate the topology of the MA (flow chart has been shown in Figure 3-5), and second to move this initial line to the correct location using the binary search (as shown in Figure 3-11). In terms of computational time requirement to arrive at the optimized injection design, if the surface mesh has  $n$  nodes, there are approximately  $\sqrt{n}$  control points on the boundary, each of which requires a LIMS simulation with the time cost of  $O(n^2)$ . Therefore, finding the MA location step has a time complexity of  $O(n^{2.5})$ . Meanwhile, the MA location correction step requires one LIMS simulation and therefore has a time complexity of  $O(n^2)$ .

### 3.5 Case studies

This section lists some practical examples with complicated part geometries that contain either non-homogeneous or highly anisotropic fabrics to show the

effectiveness and accuracy of the method to find the topology and optimal location of the injection channel. Distance-based method is difficult to implement for such general cases.

**3.5.1 Chassis containing highly anisotropic permeability fabrics**

In the chassis example shown in Figure 3-12, fabric with highly anisotropic material permeability is used for the curved surface. The fabric is aligned 45 degrees along the geometrical symmetry axis.

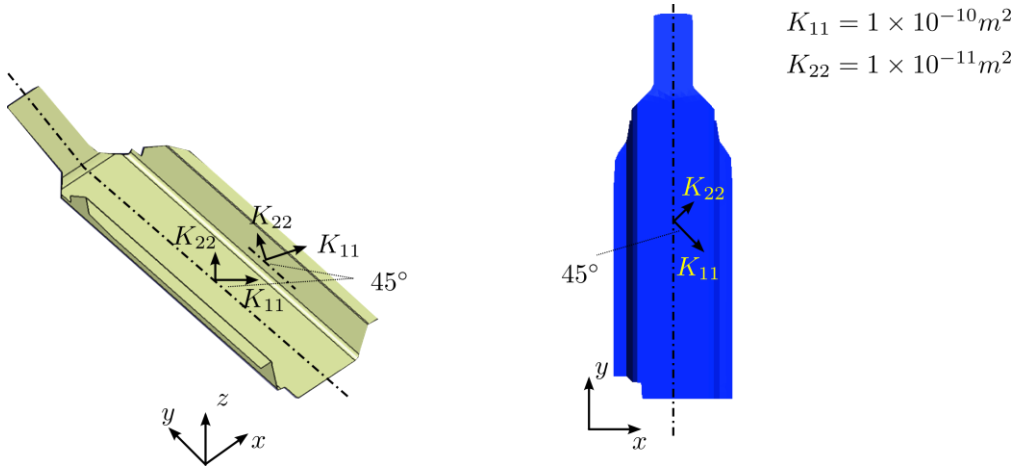


Figure 3-12: Chassis geometry and material permeability specifications.

The integrated fill time is calculated, and the medial axis is found (Figure 3-13) by dividing the part surface into a Voronoi Diagram based on the full set of filling simulation results as described in the previous section. Next, the initial medial axis is chosen as the injection channel, and LIMS is executed to find the flow pattern under constant injection pressure. The flow pattern is shown in Figure 3-14. Because the part material is homogeneous, the initial medial axis will give the optimal injection

line. From the figure one can see that two vents are needed on the boundary, and the resin arrival time at the two vents are 105s and 117s, respectively.

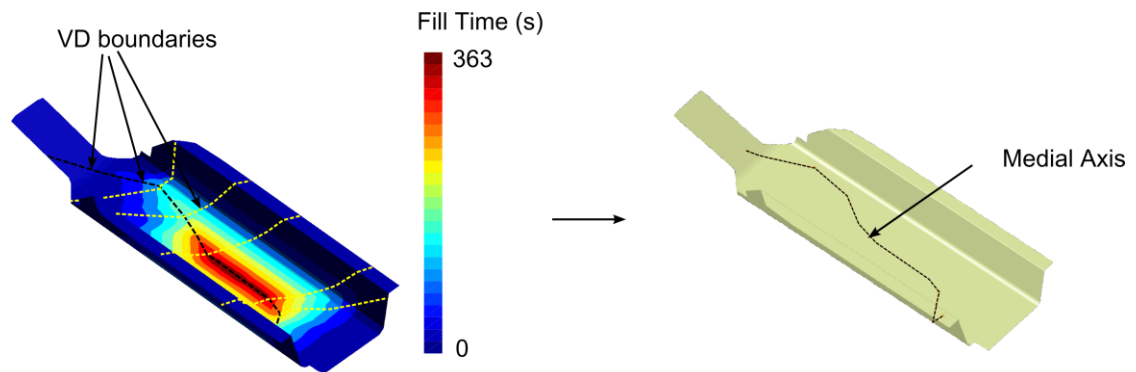


Figure 3-13: Part domain is divided into a Voronoi Diagram based on a set of simulation results from the boundary nodes to select the medial axis which will be the injection channel (right).

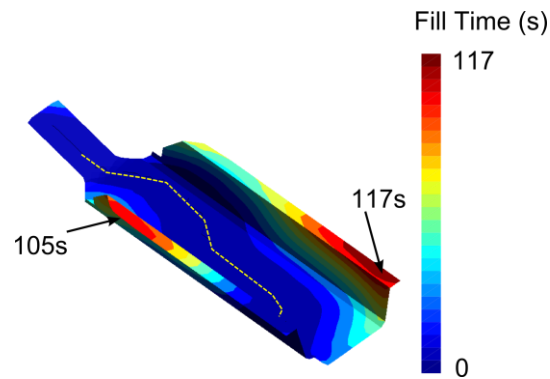


Figure 3-14: Flow pattern when resin is introduced from the injection channel along the medial axis with location of the two vents.

As a comparison, two variations of distance method are simple to implement for this part but the resulting scheme is rather poor. For example, the process engineer

may choose the injection line on the geometric symmetry axis (Figure 3-15(a)), or the geometric symmetry axis rotated according to the material permeability principal directions (Figure 3-15(b)). However, the fill time required is 240% and 450% times larger than injecting from the injection line returned in Figure 3-14, whereas the length of the injection line is approximately the same.

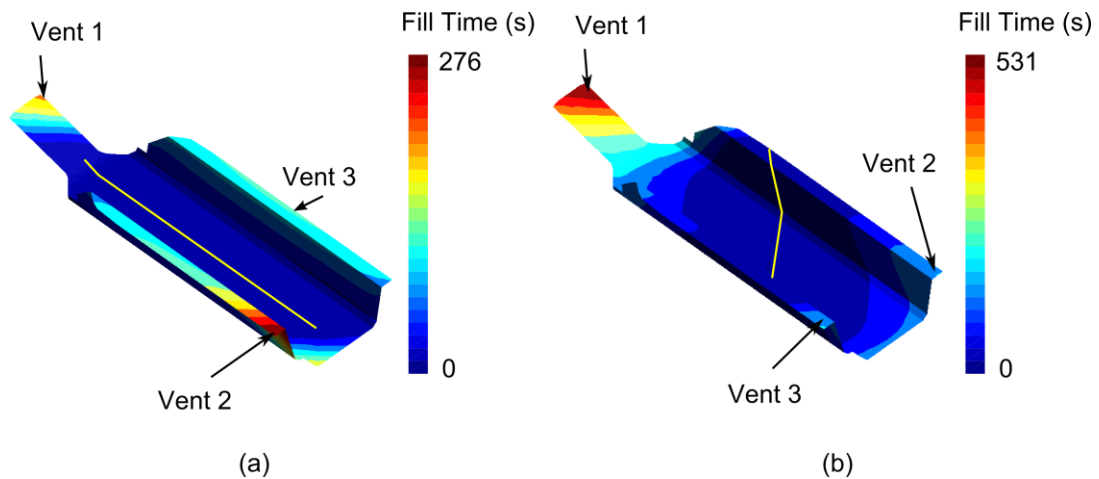


Figure 3-15: Flow pattern if the injection line is selected to be along the (a) geometric symmetry axis, and (b) geometry symmetry axis rotated according to the material permeability principal directions. Fill time in this case is more than twice for case (a) and nearly five time for case (b)

### 3.5.2 Orthotic device with various material configurations

A carbon fiber personalized orthotic device is shown in Figure 3-16. The mold is 3D printed from the scanning data of the patient's foot. Fast cure resin system is used so the resin infusion time to fill the mold needs to be under 20 minutes. In addition, the injection pressure is limited to 1atm because of the mold surface stress requirement for this single-use mold. To infuse the carbon fiber whose permeability is low and to ensure that the mold filling times are below resin gel time (1200s) under

atmosphere pressure, injection lines are pre-printed on the mold surface and connected to the injection gate to increase the flow rate.

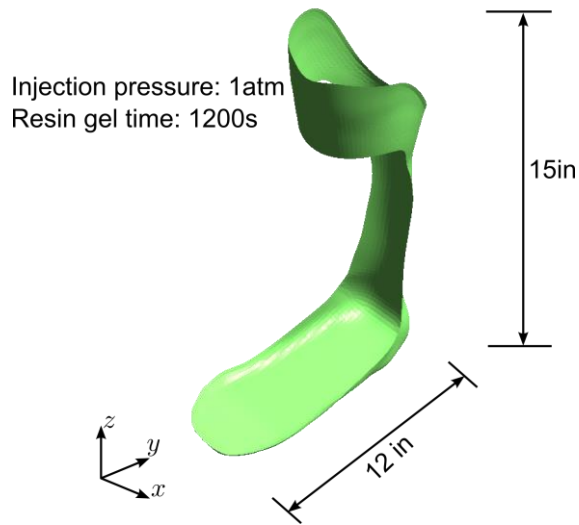


Figure 3-16: A personalized orthotic device with injection pressure and resin gel time constraints

### 3.5.2.1 Fabric with isotropic material permeability

First, the method of finding medial axis is used on homogeneous fabrics with isotropic permeability ( $K = 1.92 \times 10^{-11}m^2$ ). Multiple injection gates have been tried on this geometry[33], but here we design the injection lines connected with a single injection gate to reduce the fill time. The distance based method is difficult to be used on this complicated curved and multi-connected surface. The fill time based medial axis method is therefore used to find the medial axis. First, the integrated fill time is generated, and then the medial axis is calculated by dividing the part surface into a Voronoi Diagram from this integrated fill time map (Figure 3-17). Next, resin is injected into the mold through the medial axis and flow pattern is shown in Figure

3-18. One can see by inspection that for isotropic materials, the medial axis found is the optimal injection channel. The resin arrival time around part edges is distributed evenly towards the boundary, and vents locations are designed on the boundary locations where resin arrives last. This optimal injection channel cannot be easily found through distance-based method.

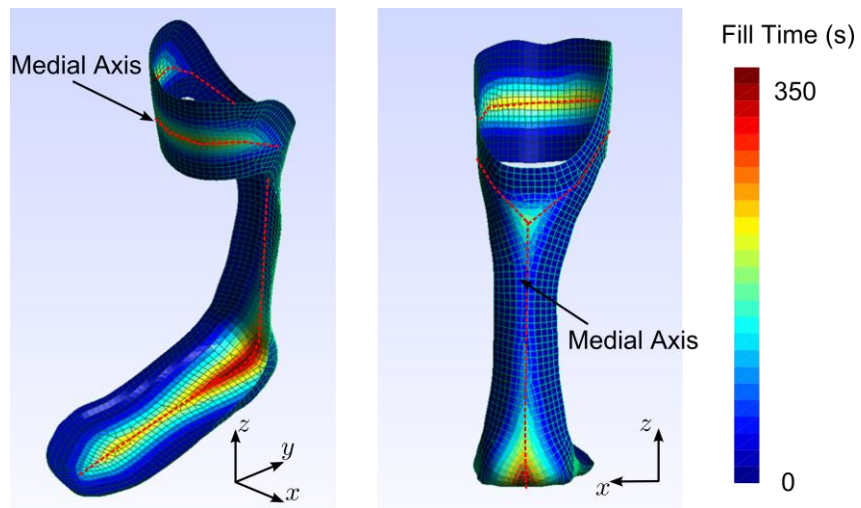


Figure 3-17: Medial axis calculated from the integrated fill time map

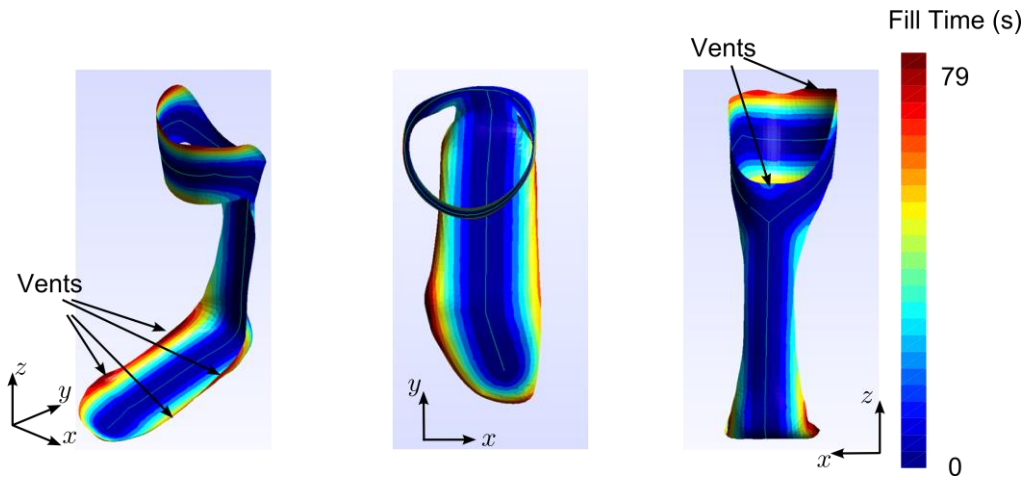


Figure 3-18: Flow pattern with injection line on the medial axis for the orthotic device using isotropic material

### 3.5.2.2 Fabric containing non-homogeneous section

Next, a more complicated case that contains an insert that render the permeability on the foot section non-homogeneous (Figure 3-19) is presented. First, the initial medial axis is found based on the set of filling pattern from each control point on the boundary, as is shown in Figure 3-20.

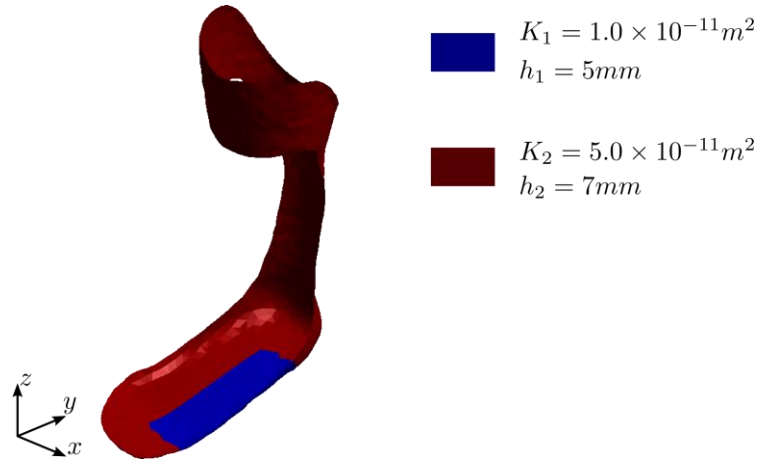


Figure 3-19: Orthotic device with non-homogeneous fabric configuration that contains a low permeable section along the surface edge of the part.

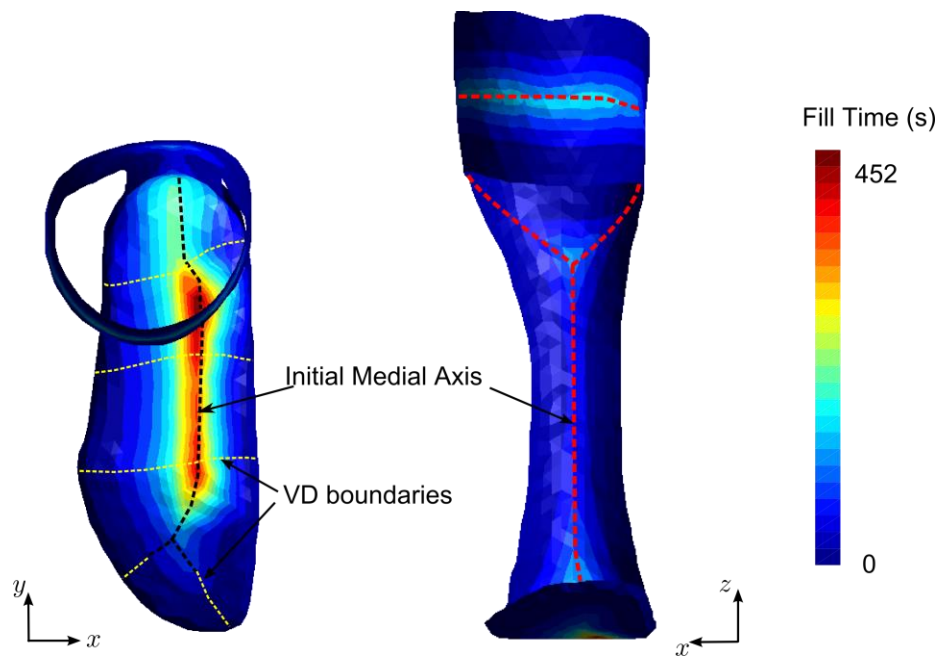


Figure 3-20: Integrated fill time map for the initial medial axis for the orthotic device containing non-homogeneous permeability section as shown in Figure 3-19.

Next, this initial medial axis is set as the injection line, and the resin flow pattern is shown in Figure 3-21. From the LIMS simulation results, we can see that the low-permeability region on the foot section results in the uneven distribution of the resin from the injection line to the boundary. Therefore, this injection line location is not optimal to achieve a minimum fill time using the medial axis topology. Based on the fill time results, the control points on the injection channel are moved towards to boundary segments that have a larger fill time based on the criterial defined in the previous section (Figure 3-21) and connect to a new injection line. Next, final optimal infusion line is searched using the iterative method described in the previous section. In this example, the result for the optimal injection line converges after four iterations when the step length is smaller than the element size. The flow pattern when introducing resin from the final injection line is shown in Figure 3-22, from which one can easily assign all the needed vents on the boundary. Also, fill time contour reveals that the flow is evenly distributed to the boundary of the part surface, and the fill time is reduced from 116s to 105s, compared to injection channel at the initial medial axis shown in Figure 3-21.

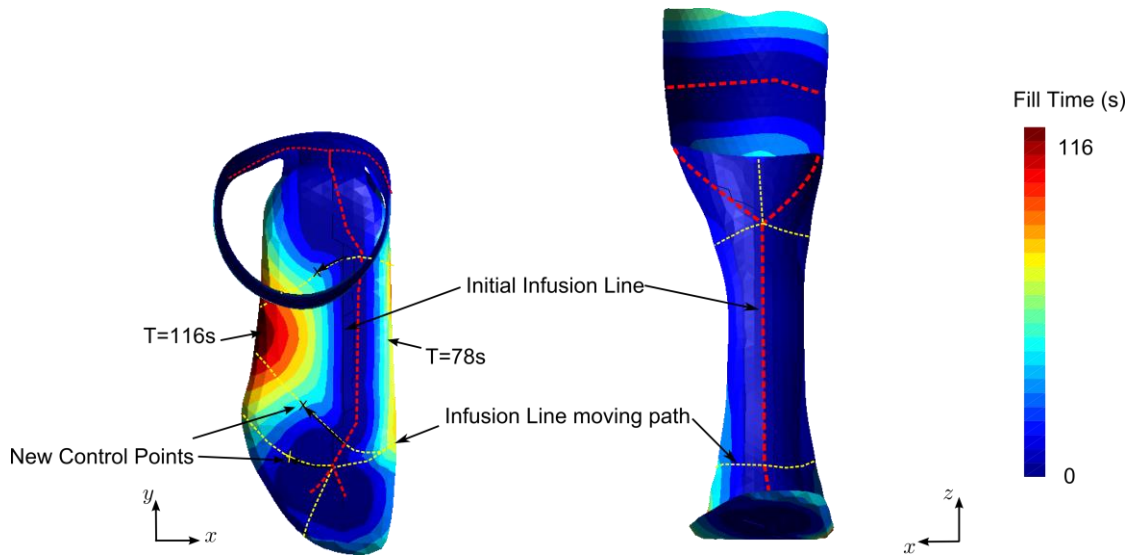


Figure 3-21: Flow pattern if the injection line is placed along the initial medial axis.

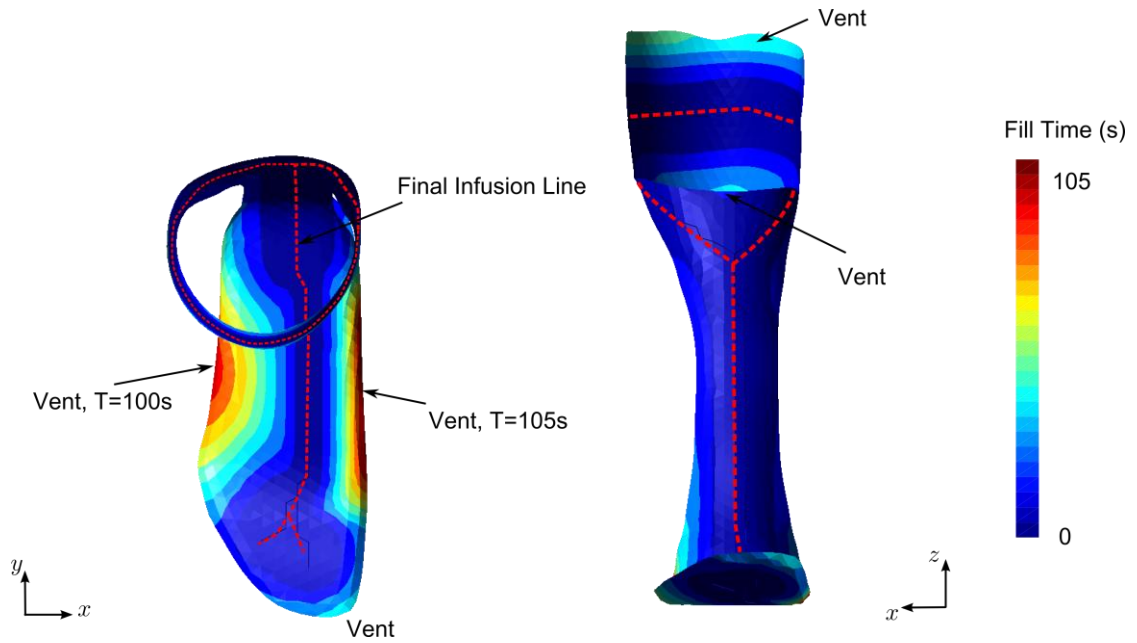


Figure 3-22: Final injection line/vents design and flow pattern after four iterations to move the initial medial axis to final optimal position that reduces the fill time by 10%

### 3.5.3 Humvee hood containing geometrical flow disturbances

Finally, a special type of material non-homogeneity is studied. For the example shown in Figure 3-23, the large curvature causes a small gap between the fabric and the tooling surface, which provide a channel that has higher effective permeability ( $K_{eff} = 8.1 \times 10^{-7} m^2$ ) than other parts of the fabric ( $K = 2.5 \times 10^{-11} m^2$ ). Such unintended channel is coined as “racetracking” channel, and unlike the injection line design in this chapter, the channel may be created randomly during the manufacturing process[32,52,53]. At best, we may know the probability distribution for its magnitude. The non-homogeneity brought by racetracking channel can change the flow pattern significantly. However, the aforementioned method can well reflect the flow disturbances brought by “racetracking” channels, and the initial medial axis and the final injection line design are generated using the methodology presented here as shown in Figure 3-24 and Figure 3-25 respectively. Therefore, this example shows that the fill time based medial axis method can capture the stochastic flow disturbances and generate the injection line accordingly, so it can be applied to the well-developed probability models for these flow disturbances[32,52,53].

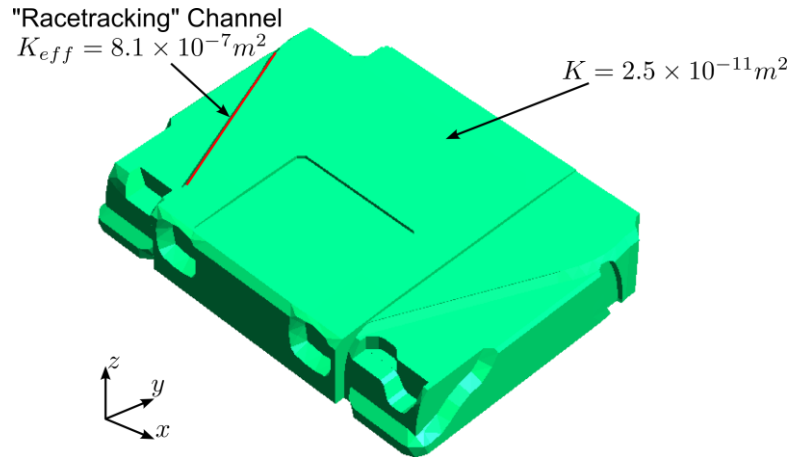


Figure 3-23: Humvee hood geometry and fabric permeability specification with “racetracking” channel located on one internal edge

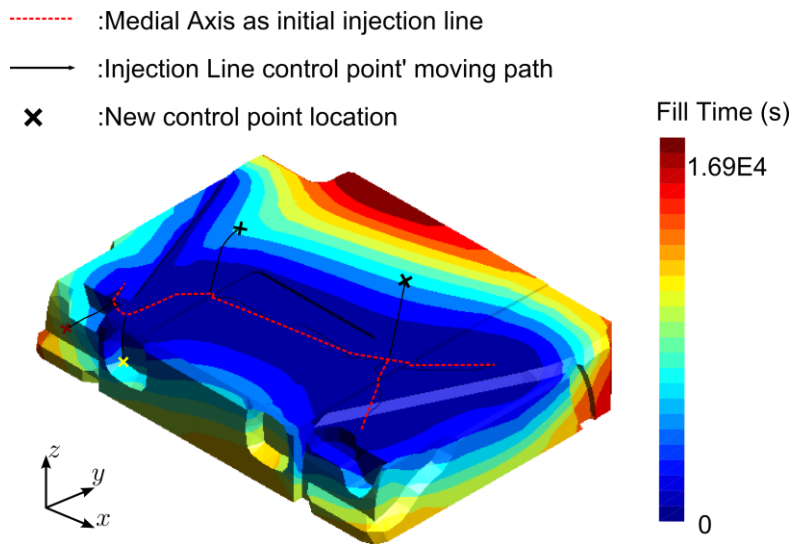


Figure 3-24: Initial medial axis location and flow pattern when selecting it as the injection line, based on which, the injection line moving direction is determined

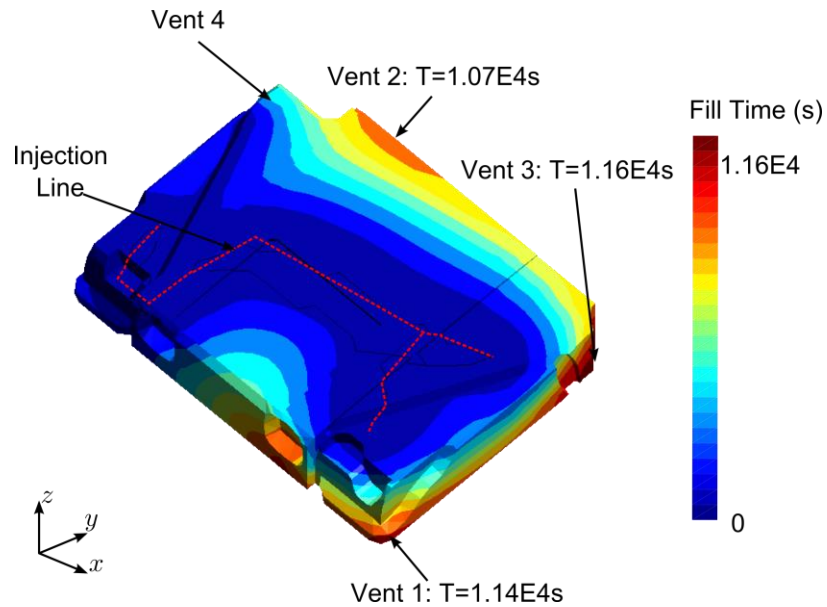


Figure 3-25: Flow pattern for the final injection line design and venting plan. Convergence was achieved in three iterations. The filling time reduced by 46% as compared to the initial medial axis as the injection line

### 3.6 Summary

This chapter introduced an effective methodology for injection line determination in the manufacturing of shell-like composite parts that contain complex geometry and non-uniform and anisotropic material features, using RTM. In this paper, the medial axis of the part surface is redefined to accommodate the mold filling step. An algorithm is developed to find its topology based on the results returned by finite element based mold filling simulation software LIMS combining with the Voronoi Diagram definition that divides the part domain into boundary segments. Next, non-symmetrical fill time between two points on the surface is discussed when non-homogeneous material is used. This finding provided an approach to move the fill time based medial axis to the correct location using binary search algorithm based on the simulation results when injecting the resin through the designed injection line.

Final injection channel topology is obtained when the convergence criteria is satisfied. Three case studies are shown to demonstrate the effectiveness and accuracy in determining an injection line location with the objective of reducing fill time for parts that contain complexities in both geometry and material property variations.

## Chapter 4

### PROCESS AND MATERIAL VARIABILITY IN LCM PROCESSES

#### 4.1 Introduction

Apart from determining the processing parameters that are necessary to run the mold filling simulations, such as the gate/venting schemes, variation in material and process parameters exist in real manufacturing practices that will result in different flow patterns. However, it is often beyond the designers' knowledge or responsibility to recognize these factors by just considering the geometry. This chapter addresses the variability that arises from the designed part by recognizing features that can cause the variability in the permeability of the preform in this region, and then models and develops a methodology to generate a probabilistic flow analysis of the filling process to reconstruct what may occur during the preform layup before the resin is infused during the manufacturing processes. The results are analyzed, consolidated and presented to the designer.

The process of mold filling to manufacture a composite part with LCM initiates when the geometric design along with fiber layup and orientation needed for desired physical and mechanical properties is conceived in a Computer Aided Design (CAD) environment with commonly used design software tools such as CATIA, ProEngineering, Solidworks or SimXpert. The design engineer creates the drawing needed to fabricate the mold in which the fiber preforms can be placed in desired orientations and the resin injected to manufacture the designed part. The resin injection step (also known as the mold filling step) plays a key role as the injected

resin has to saturate all the empty regions in between the fibers to make a successful composite part.

Defects or voids result when the resin does not saturate these regions before it reaches a vent. This occurs because the resin flow pattern avoided these regions, or because entrapped volatiles prevented resin saturation. To prevent voids or dry spots, vents that evacuate volatiles from the mold are placed at all locations where the resin arrives last within the mold cavity. Ideally, such strategy guarantees a part without dry regions or voids. For correct vent placement, many simulation tools [6–23] have been developed to provide a forecast of the filling patterns after an injection gate is specified. However, the inherent material variability and the variability introduced during fabric placement in the mold due to complex curvatures, corners, edges and inserts in the geometric design will dramatically change flow patterns from one part to the next and could result in voids. Thus the flow simulation has to be able to take into account this variability to formulate an injection and venting scheme that is sufficiently robust to manufacture a part without any voids. Thus, one has to accommodate the flow pattern variability into the model. Secondly, the process modeling should be directly connected to the part design, the same way the stress analysis is. Should the modeling results for the designed geometry suggest infusion difficulties, design changes should be considered before the mold cavity is fabricated.

#### **4.1.1 Flow pattern variability and flow disturbances**

In the mold filling simulation, it is assumed that the reinforcement to be saturated constitutes of continuous porous media with known material properties. Under these assumptions, once the inlet gate location and condition is specified for a designed mold geometry, the movement of the flow front can be predicted and last

regions to fill identified as vent locations. This is an idealized case (we will label it as the base case) in which one expects no variation of permeability in the mold from one part to the next. For this situation, only one simulation is necessary to identify the vent locations for complete filling without any dry regions or voids. However the manufacturing practice has demonstrated that the actual flow patterns vary to some degree from this idealized base case. This is due to “flow disturbances” that occur from one part to the next in the same mold cavity. While there are various causes for flow variation, such as reinforcement permeability changes[54–60], the most important factor that changes the resin flow patterns dramatically from the ideal case is race-tracking: Resin racing along gaps between mold walls and preforms, around corners and inserts as these regions offer less resistance to flow than the bulk fabric in the mold.

Race-tracking is likely to occur along the outer edges, fabric folds, bifurcation lines (such as T-shape lines), and tapered regions of the part as shown in Figure 4-1. At these edges, irregular cuts or placement of the reinforcement results in gaps or channels between the fiber preform and the mold wall. Higher permeability will result along these channels or gaps, which will make the resin go faster along the edge, changing the filling pattern and possibly leaving large unsaturated regions as the resin may have found an alternate path to the vent before saturating all the fibers within the mold cavity. Such “race-tracking” channels may not be repeatable from one part to the next during the manufacturing process, though some statistically significant patterns are usually observable.

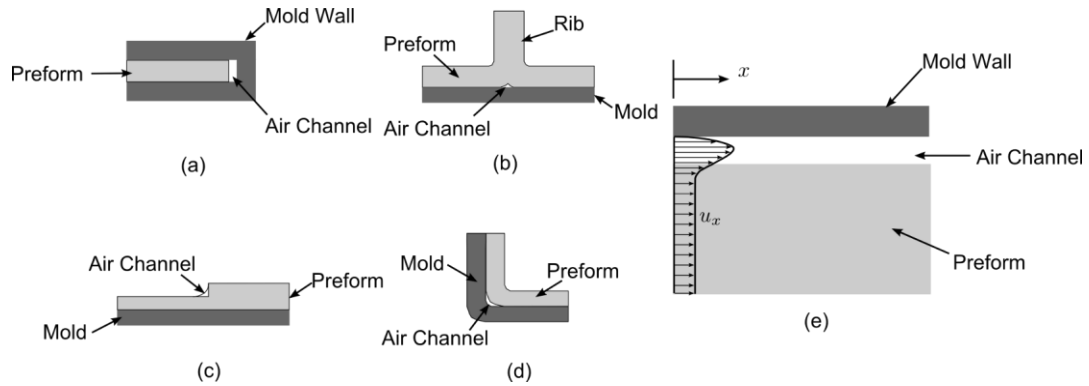


Figure 4-1: Potential race-tracking regions along (a) outer edge; (b) bifurcation lines; (c) tapered regions; (d) sharp corners

Since our goal is to ensure that the mold will fill regardless of any disturbances in the flow, the process modeling must also address the scenarios which account for race-tracking. It is possible to add the race-tracking features to flow models[27], but to actually model all possible infusion scenarios requires significant experience on the part of the analyst. To alleviate this constraint, one needs to develop tools that can:

1. Automatically generate scenarios with various levels and permutations of racetracking along with identified geometric features such as corners and edges and assign a statistical probability to each of them. Even experienced process analyst will not be able to do this manually for a large, complexly shaped part.
2. Create analysis tools to examine individual scenarios and translate the finding in a set of recommendations for robust process design. Again, manual analysis will require tedious examination of many scenarios. The resulting process design will provide the infusion and venting layout and the probability of success of such an injection scheme. If this scheme is too expensive or not possible, the design engineer is notified. Then, the designer can either explore changes in part design to facilitate ease of manufacturing, or explore better production facility that can provide tighter tolerances during manufacturing.

#### **4.1.2 Coupling part design and process analysis**

Accounting for the flow disturbances may not be sufficient to find injection and vent combination for successful mold filling. The outcome of such analysis may be that it is impossible – or requires too many vent locations to reliably manufacture the part by any selected process infusion and vent scheme. If the process analysis feedback is provided to the designer, it can prompt the change of part design for example, the simulation may suggest elimination of certain features (such as sharp corners or tapered inserts) that introduce unacceptable risks of racetracking and make the process less robust.

Currently, the functional design of a composite part is created separately and well in advance of the design of the manufacturing process. In the current part design practice, the designers analyze the part to ensure that the conceived design satisfies the physical and mechanical property requirement but pay no heed to the issue of manufacturability. The designed part that meets the strength and stiffness requirements is sent to the machine shop to manufacture the mold cavity or sent to the process engineer to perform mold filling simulations to determine the gate and vent locations before fabricating the mold. Two aspects are not addressed in this approach. First, the process engineer does not take into account any process variability and manufacturing issues. Second, if the manufacturing engineer cannot produce the part within limits, there is no sensible feedback that the part designer can use to introduce the required changes in the geometry to influence manufacturability.

To address manufacturability, two-way coupling between functional and manufacturing design is necessary. One must integrate process modeling directly into the design loop. By introducing manufacturing simulation tools in the design process, the designer will be able to create a composite part that can be successfully

manufactured. The designer in general does not have the knowledge of the manufacturing process and can seldom use the mold filling simulation tools effectively. However, the designers are not experts in failure analysis either, yet, with the help of software tools, they check for the failure. Thus, goal of the current work is to develop a sufficiently transparent and integrated tool that will provide her or him with (a) the ability to check if the design is workable from the manufacturing standpoint and (b) provide suggestion for changes in part design if it is not able to be manufactured.

## **4.2 Methodology for Automating Effects of Variability in Mold Filling Process**

### **4.2.1 Approach and Procedure**

A methodology is introduced and implemented that applies the existing process modeling and simulation tools to automate process design and evaluate part manufacturability within given manufacturing capabilities and constraints such as time to fill the mold. The resulting output provides suggested infusion and venting schemes within the reliability requirements for the process. If the process is not possible, the methodology can suggest changes in part design.

The following steps were followed to implement the methodology.

- Step 1: The part geometry and material description including laminate orientation and draping information from the design software was converted into a form suitable to simulate the resin infusion during mold filling.
- Step 2: If the inlet configurations are not specified then they are created automatically before executing the resin infusion or flow simulations.

- Step 3: The geometry features of the part are analyzed to identify and classify race-tracking regions in the geometry. Manufacturing data from the fabrication site can be used to assign probabilities and strengths of race-tracking to various identified race-tracking regions. The data is assumed to be available or a probability distribution for the variability can be assigned.
- Step 4: Process simulations are executed for all permutations of scenarios possible based on the probability distribution of identified race-tracking edges and their strengths.
- Step 5: The results record the locations of the dry spots (vents) for each scenario as well as other processing parameters such as the infusion time.
- Step 6: Results are analyzed and assembled to provide suggested infusion schemes, vent locations and expected success rates.

This work will focus on describing the generation of distribution scenarios and analysis of the resulting sets (Steps 3 and 6). The implementation issues will not be discussed in detail here but will be provided in the next Chapter.

## **4.2.2 Logistics and implementation**

### **4.2.2.1 CAD environment and mold filling simulation tools**

A composite part design is usually created using one of the many commercially available CAD software tools such as CATIA, ProEngineering, SolidWorks or SimXpert. The electronic design output format varies with the selected CAD software and often the information, such as dimensions, materials and their orientation and properties are encoded in a way that can only be read by that specific software. All CAD software is capable of creating a finite element mesh of the part which preserves the geometric dimensions and material data and orientation. Hence a tool is developed that can extract the mesh information written in Bulk Data Format

(BDF) by the CAD package and re-arranged to create the data structure necessary to build various scenarios to perform mold filling simulations.

LIMS is utilized to create the filling pattern for all permutations of race-tracking disturbances identified. To realize a seamless integration and coupling between LIMS and the composite part design process, the commercial CAE application ©MSC SimXpert was used as the CAD workbench. Its build-in python script interface enables one to execute mold filling simulation tool from its design environment. Simulation results and analysis suggestions are then transferred back and explicitly displayed into SimXpert CAD part design workbench, allowing the designer to appraise the effect of the part design on manufacturability and tweak the design based on the suggestions offered to improve the manufacturing process.

#### **4.2.2.2 Creation of the base geometry**

Since LCM is most commonly used to manufacture net shape shell structures, it is reasonable to mesh the part geometry with 2-D shell elements which allows one to calculate and provide the material property input of the two dimensional permeability tensor for that element, and the through thickness direction is simplified into an average thickness associated with the element.

Geometry information of the part is explicitly described in the BDF mesh file, including element and nodal information, as well as the nodal connectivity. The preform information in the BDF file is not as explicit as the geometry information, and is written in terms of PCOMP cards which describe the layup and orientation of the fabric or preform. Since preform permeability input is crucial for composite filling simulation, it is necessary to call the material library where unidirectional fiber sheet permeability data is stored, and by combining the unidirectional fiber permeability

with the preform layup sequence described by the PCOMP card, the permeability for the element is averaged in the principal direction of the 2-D preform plane as is described by equations (4.1 to 4.4), in which  $K_{xx}$   $K_{yy}$   $K_{xy}$  are the average 2-D scalar in plane values of the permeability tensor,  $v_f$  is the average fiber volume fraction, and  $K_{xx_i}$   $K_{yy_i}$   $K_{xy_i}$  are the scalar values of the 2-D permeability tensor of the  $i_{th}$  ply,  $v_{f_i}$  is the fiber volume fraction of the  $i_{th}$  ply,  $h_i$  is the thickness of the  $i_{th}$  ply.[62]

$$K_{xx} = \frac{\sum_{i=1}^n h_i K_{xx_i}}{\sum_{i=1}^n h_i} \quad (4.1)$$

$$K_{yy} = \frac{\sum_{i=1}^n h_i K_{yy_i}}{\sum_{i=1}^n h_i} \quad (4.2)$$

$$K_{xy} = \frac{\sum_{i=1}^n h_i K_{xy_i}}{\sum_{i=1}^n h_i} \quad (4.3)$$

$$V_f = \frac{\sum_{i=1}^n h_i V_{f_i}}{\sum_{i=1}^n h_i} \quad (4.4)$$

Since each element in the BDF mesh file is linked to a specific PCOMP card, whose average permeability has been calculated, each element's permeability tensor is then available and is stored as input for the filling simulation input file (Figure 4-2).

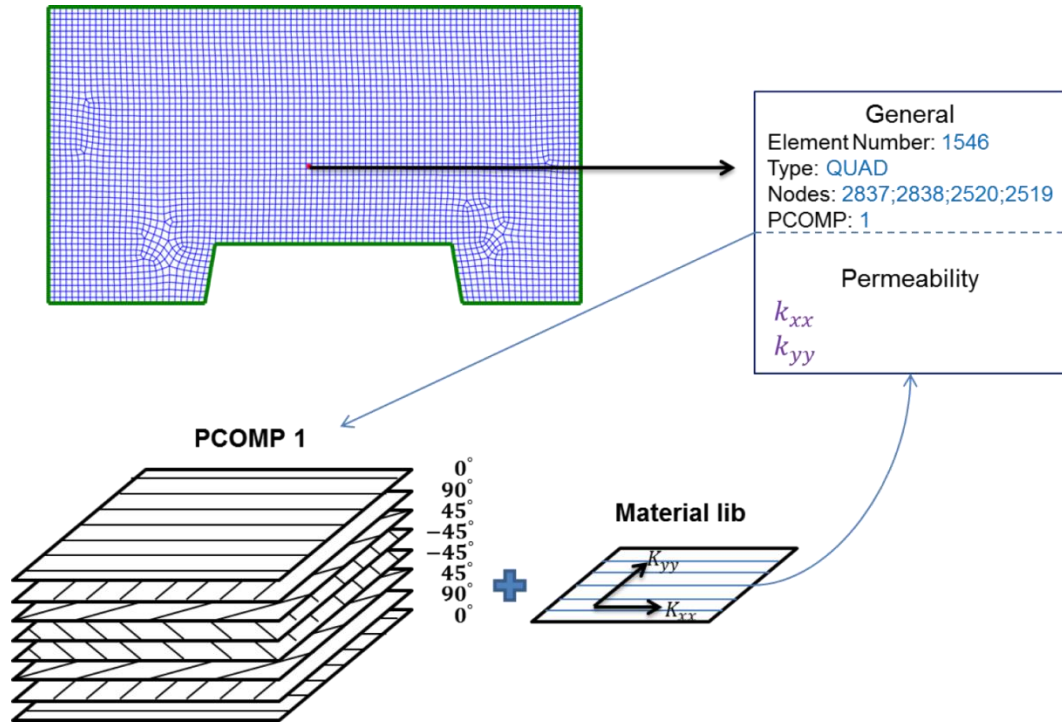


Figure 4-2: Preform permeability is interpreted from PCOMP card and material library information

### 4.2.3 Infusion line or injection gate plan

In addition to permeability tensor input, the mold filling simulation LIMS also requires information regarding the inlet region from which the resin can enter the mold. The resin enters into a mold either through a small diameter hole known as a gate injection or through a channel which is known as a line injection. The selection of this injection location plays a key role in the simulation. The user could specify this location or one could formulate algorithms to pre-select the location and type of gate to execute the filling simulation as discussed in chapters 2 and 3. The gate selection will also depend on the LCM process selected. Figure 4-3 shows the selection of the injection type based on the process. Currently, injection type and locations has been

implemented for RTM, VARTM and RTM-Light but can be expanded to include other gate types and LCM processes.

If the process selected is RTM, the resin enters the mold cavity through a gate as shown in Figure 4-3 (a). If no gate is selected by the designer, the following approach is used to select a gate: the centroid of the part is located by averaging all the nodes' coordinates weighted with the associated element volume, and the nearest node to the centroid is set as the injection gate with positive injection pressure. If VARTM is selected as the process of choice, resin enters the mold through a channel, which is also known as an infusion line as shown in Figure 4-3 (b). This infusion line can either be designated by the designer before the part is meshed, or the program can automatically assign a possible location for the injection line. Currently the algorithm selects an infusion line that connects the elemental edges going through the centroid and along the minor inertia plane. The infusion line is represented as a series of connected 1-D bar elements, whose cross-section area represents the opening area of the pipe or channel through which resin will be injected. Finally for RTM-light process, the resin is injected from the outer boundaries, which can be automatically identified using the algorithm that selects connected element edges which belong to only one element. If more than one boundary is detected, the longest one is selected. As with the VARTM infusion line, a series of 1-D bar elements are automatically built over the boundary, which can be denoted as the infusion line, as shown in Figure 4-3 (c).

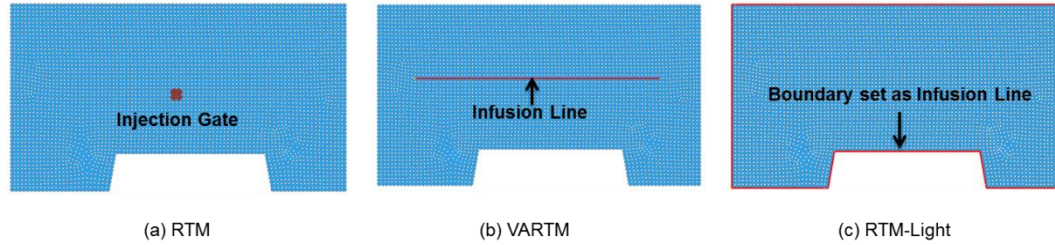


Figure 4-3: Automatic selection of infusion location depends on the type of process and the geometry of the part.

#### 4.2.4 Detection of disturbance regions and generation of possible scenarios

##### 4.2.4.1 Topology analysis and identification of disturbances channels

Nodal and elemental information contained in a typical mesh although sufficient for finite element analysis does not readily provide the topological information such as corners and edges of the meshed part. A new algorithm was developed to automatically build the topology from the meshed part. By interrogating the geometric information, elements are grouped into elemental edges, recorded as a pair of two nodes, which represent the starting and ending point of an elemental edge. Each elemental edge also contains the number of elements sharing this edge. Then all the elemental edges are placed in an array containing the elemental edges which share the same starting node for connectivity analysis. If two elemental edges have the same two nodes, but the sequence of starting and ending nodes is reversed, they are considered as the same edge. Such elemental edges are called twin edges, and each elemental edge includes the information of where its twin edge can be found.

Together with the elemental permeability and the infusion type and location, this detailed rearranged nodes and elements map are stored into the internal data representation which is labeled as SCENARIO. Each elemental edge recorded in the

SCENARIO topology map is examined to identify potential race-tracking regions.

Based on the logic shown in Figure 4-4, one elemental edge is considered to be potential race-tracking edge if one of the following criteria is met:

- Outer edges: those element edges that belong to only one specific element, and this information can be easily read from the data structures which are interpreted from the BDF files, as shown in Figure 4-4 (a).
- Folds: element edges that are shared by two elements that have an angle between their normal directions. These edges are the sharp turns in the geometry that should be avoided, which is shown in Figure 4-4 (b).
- However, even if the turns are smooth, restriction should be added to the curvature as

$$\frac{h}{R} < \lambda$$

in which h is the fiber preform thickness (or element thickness in the mesh file), R is the curvature of the turning surface, and  $\lambda$  is the critical number which can be preset. Such edges are demonstrated in Figure 4-4 (c).

- Bifurcations: which are joints and edges that are shared by more than two elements (Figure 4-4 (d)).

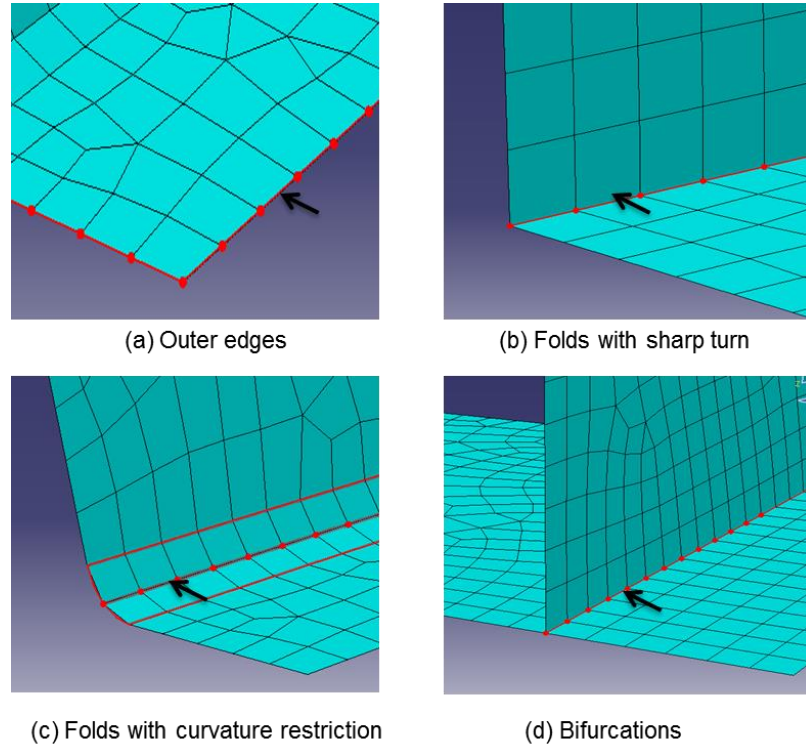


Figure 4-4: Automatic feature recognition of potential race-tracking channels

After all the elemental edges which are potentially susceptible to race-tracking are collected in terms of a discrete set, the geometry and topology information is again interrogated, so the connectivity relations among these discrete edges can be analyzed to form a series of single independent channels. However, some of the channels are too short (length smaller than  $c \times element\ size$  in which  $c$  is a preset constant based on the mesh size) to have significant effects on the flow pattern, so these channels are discarded. On the other hand, when some of the edges are parallel and sufficiently close they can be grouped together to reduce the number of permutations of the simulations to perform. Finally, some of the channels may be broken up due to irregularities in the mesh, but they are still considered.

#### **4.2.4.2 Assigning race-tracking properties to the channels**

Race-tracking channels permeability is assigned in terms of the channel cross-section area. The strength of the race-tracking can be obtained from the manufacturing experience and data. Thus, one can introduce a probability distribution function constructed from actual manufacturing data to define the variation in race-tracking strength from one part to the next.

Gokce et. al. used Weibull density function distribution to represent the race-tracking channel permeability, and created a discrete description of a single race-tracking channel which had two numbers associated with it: strength of race-tracking and its probability distribution[52,63]. To limit the number of permutation of scenarios to be simulated, a coarse discretization is generated, by assigning probabilities for no race-tracking, low race-tracking, and high race-tracking rather than a continuous description (Figure 4-5). It is found that the flow pattern does change significantly as one goes from no to low racetracking but not that significantly as the race-tracking strength is increased. Also, edges, folds, and bifurcation lines are treated separately when specifying the likelihood of race-tracking effects, and different probability maps should be used for different manufacturing facilities.

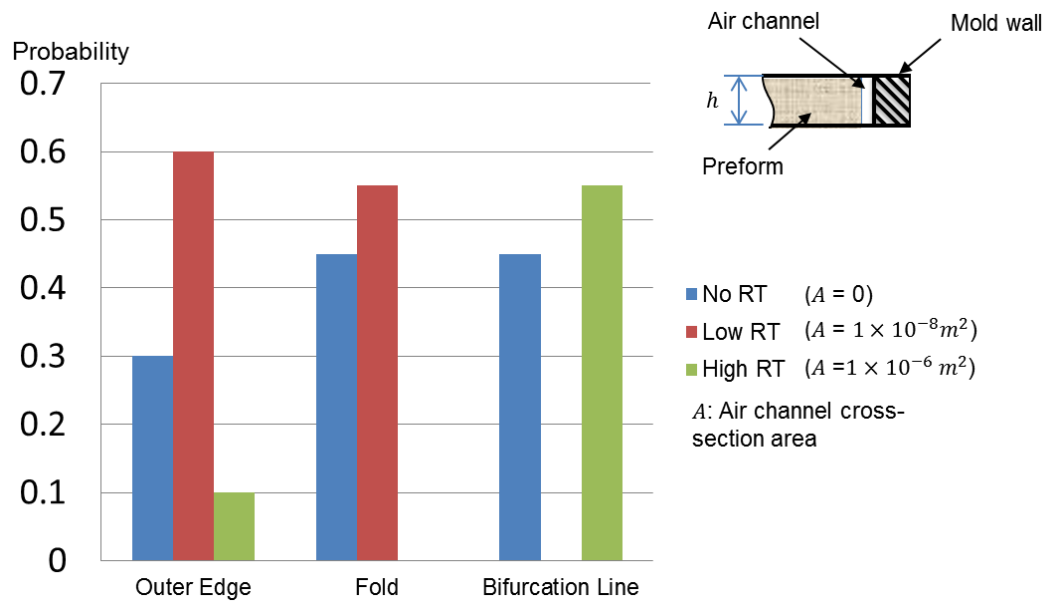


Figure 4-5: An example race-tracking strength with probabilities

#### 4.2.4.3 Automatic generation of possible scenarios

By using the discretized race-tracking strength probability distribution and assuming each of the race-tracking channel is independent, one can build a list of scenarios in terms of permutations and combinations of all the detected race-tracking channels [52] Each scenario in the list has its own race-tracking channels configuration with associated probability.

For the example of a simple sidewall shown in Figure 4-6(a), where 5 possible race-tracking edges have been identified, the race-tracking strengths and their probability provided in the table in Figure 4-6(b) are assigned to the elements in these channels to describe the race-tracking behavior of the channel. Assuming that all five channels are independent and as one channel has three racetracking strengths associated with it while the other four have only two race-tracking strengths associated with them, a total number of  $3 \times 2^4 = 48$  permutations of the flow scenarios are

possible. Each scenario has an associated probability as shown in the scenario space generated in Figure 4-6(c).

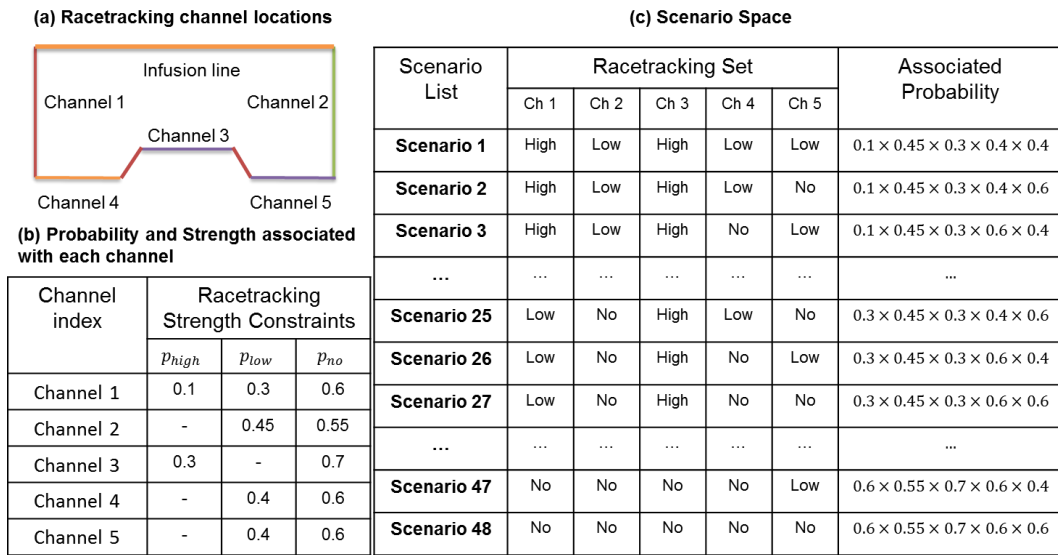


Figure 4-6: Scenario space generation for three potential race-tracking strengths along five edges of a simple sidewall

#### 4.2.5 Mold filling simulations

Having assigned the LCM process and gate locations as explained in section 2.3 and having generated the scenario space as outlined in section 4.2.4, the finite element analysis software LIMS is called upon to execute a mold filling simulation for each scenario in the scenario space (Figure 4-7). Simulation of each scenario is executed twice (Figure 4-8). The first one assumes the mold to be under perfect vacuum (as with a membrane), such that the resin can saturate the entire preform and air is able to escape through the membrane. Filling time is easily acquired from this simulation, but potential defective areas are not obvious from these results. Therefore,

it is necessary to conduct a second simulation on the same scenario, which can predict the regions in the geometry that are least likely to fill. The second simulation sets a non-zero air pressure in the mold and no vents are drilled in the mold. The air in the mold is equal to the resin pressure. All the islands of volume left unfilled are recognized as the last regions to fill requiring a placement of the vent. However, filling time results from the second simulation can be inaccurate. Hence the first simulation gives us the time to fill and the second simulation for the same scenario identifies the regions and the size of the regions that filled last. Each simulation takes only a few seconds to execute for a part with 10,000 nodes on a PC, hence running two simulations is not a taxing overhead to obtain more accurate fill times.

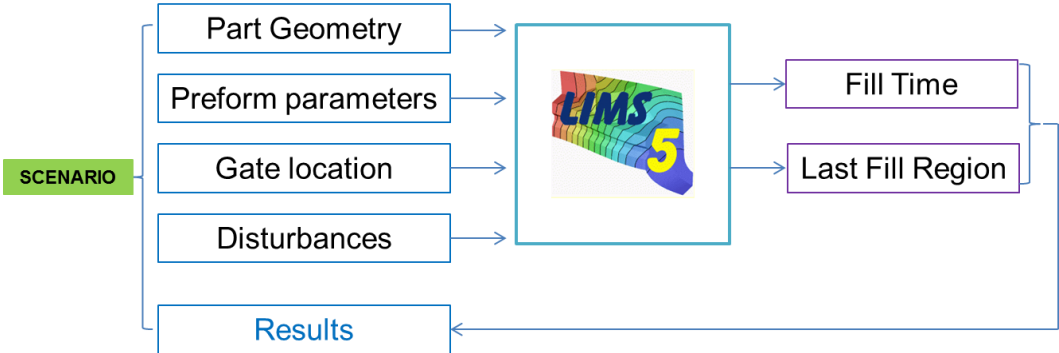


Figure 4-7: Each scenario filling simulation flow chart

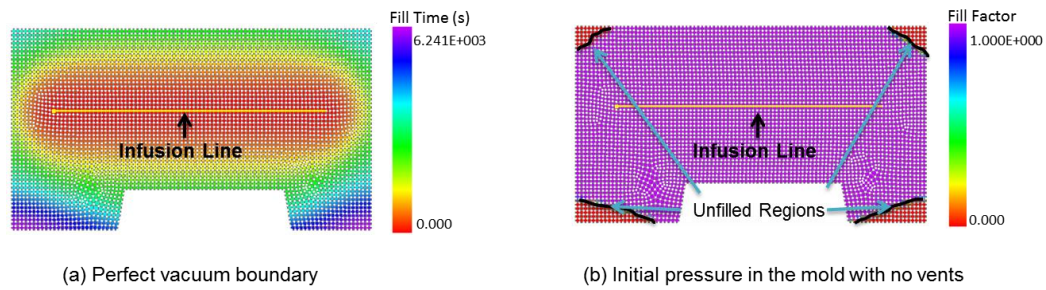


Figure 4-8: Each mold filling scenario is executed twice to find (a) fill time and (b) last region to fill

#### 4.2.6 Analysis of simulation results

Results for each scenario in the list are generated using the mold filling simulation and recorded in the formulated data structure. The results include mold filling time, arrival times of the resin at each node, and node fill factors (all fill factors less than one are classified as unfilled regions). Combining these results with the probability of race-tracking for each scenario, a vent map is created and the success rate is forecasted.

##### 4.2.6.1 Vent map generation

First, the regions that are most likely to be unfilled are identified for each scenario in the entire scenario space. Next, in each scenario all unfilled nodes are weighted with their respective scenario probabilities. These weighted node probabilities are superimposed for the entire scenario space to produce a probability map which denotes the probability for each node to remain unfilled. All nodes with the probability higher than a preset probability value are set as possible vent locations.

Having created this unfilled region map in terms of nodal unfilled probabilities, the topology characteristics of all the nodes set as possible vent locations

is examined to decide if they should be (i) listed as separate vent locations or (ii) they should be grouped together as one vent or (iii) discarded as possible vent location. The approach uses the nodal connectivity information to group all the connected nodes together as one possible vent location. Then it checks repeatedly with the topology of the part in the base data structure, until all the nodes identified as possible vent locations are classified into a group. Each group is a cluster of nodes that are connected. However, it is quite common that some of the groups may contain too few nodes. In practice, these regions are so small that even if there was some trapped air it will not cause any defects. These vents are discarded. Another situation that may occur is that two groups of nodes may be in close proximity and hence can be recognized as one vent. Thus, all the unfilled nodes above a preset probability are screened with the above approach to create the final plausible vent plan for the composite part for the selected injection location which takes into consideration material and placement variability during manufacturing. A schematic of this approach is shown in Figure 4-9.

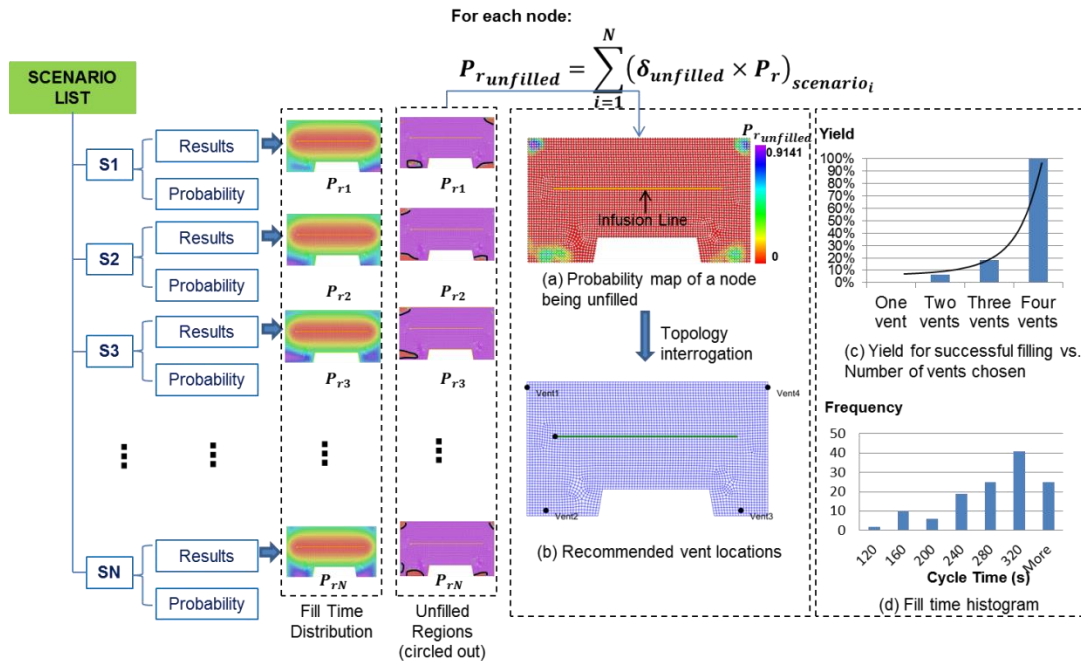


Figure 4-9: The mold filling results from each scenario from the scenario space are weighted with the respective probabilities to generate a vent map denoting the probability of placing a vent at that location for successful filling. In this example, four vents along the four corners ensure that one would be able to fill the mold for any scenarios from the entire scenario space.

#### 4.2.6.2 Success rate for a specific infusion plan

The approach used ensures that for the scenario space identified, if one places vents at all the possible locations as identified by the vent map, one would be able to fill the mold despite the disturbances caused by race-tracking. However, the vent map may suggest vents in locations that may not be possible or may be too many to be practical, in which case, it may be useful to provide the designer with a success percent as a function of number of vents. The success percent or yield is defined as the number of times the mold will fill without any voids when all the possibilities in the scenario space are executed.

To calculate the successful yield for a specific gate/vent scheme, each scenario result is compared with the vent map. Based on the nodal connectivity information, the location of the unfilled nodes in each scenario is used to identify unfilled regions. All the unfilled regions that are geometrically located in close proximity could be grouped together. A vent is placed in each group of unfilled regions in close proximity to avoid formation of voids or dry spots. On the other hand if even one unfilled region is not near any of the vents in the vent map, that scenario is labeled as unable to fill the mold successfully. After all the possible scenarios from the scenario space are executed, each scenario is weighted with its assigned probability to calculate the successful yield for the selected gate/vent scheme.

#### **4.2.6.3 Feedback to designer**

The vent map, filling time and the injection location (if not selected by the designer) are returned within the designer's environment of part design bench for evaluation. All the racetracking regions are identified, injection and vent locations marked and the fill time distribution highlighted. This information reveals to the designer regions which are most likely to have voids. Armed with this knowledge the designer may relax some of the geometric features in part design such as folds with sharp turns and corners which will help reduce the number of flow disturbance regions and hence the scenario space improving the chances of higher yield. Thus this automated evaluation process can flush out troublesome features from the mold filling viewpoint, providing the designer an opportunity to make changes to the geometry accordingly.

## 4.3 Case studies

### 4.3.1 Chassis

#### 4.3.1.1 Disturbances recognition

The CAD model is meshed in MSC SimXpert and is written into Bulk Data Format (BDF) file (Figure 4-10). Based on the race-tracking channel selection criterion, ten channels are automatically detected (Figure 4-11) and assumed to be independent channels, each of which is assigned with a probability of introducing race-tracking effect.

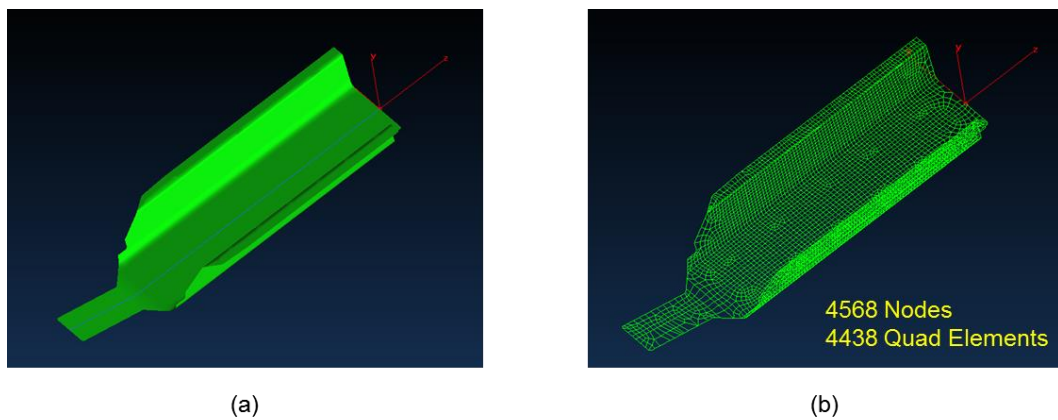


Figure 4-10: (a) Chassis CAD model (b) FE mesh for mold filling simulations

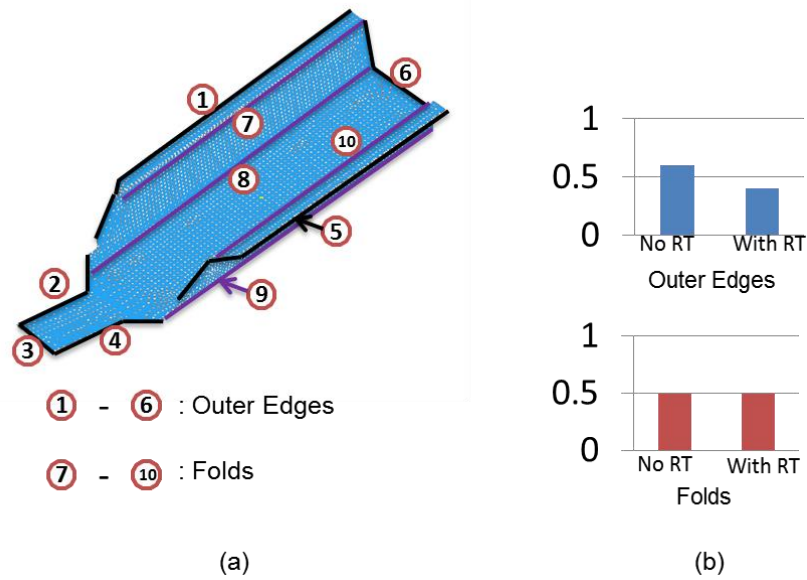


Figure 4-11: (a) Potential race-tracking channels identified (b) Assigned race-tracking distribution along outer edges and along folds

#### 4.3.1.2 RTM-light process

To limit the number of scenarios in the scenario space, a simple discretization of race-tracking strength is used. Each race-tracking channel is described with only two possibilities (no race-tracking or race-tracking) with their respective probabilities specified (Figure 4-12). For race-tracking cases, the diameter of the race-tracking channel is assigned. Race-tracking discretization on outer edges, folds, and bifurcation lines are treated separately. For the chassis example when using RTM-light process, the outer edges serve as the infusion injection lines and hence only four independent potential race-tracking channels along the folds are likely, each of them with an assigned probability. This results in a scenario space of  $2^4 = 16$  scenarios. Each scenario is assigned a probability of occurrence (for the example case, we assume

equal probability for each scenario). The sum of the probability for all the scenarios in the scenario space should add up to unity.

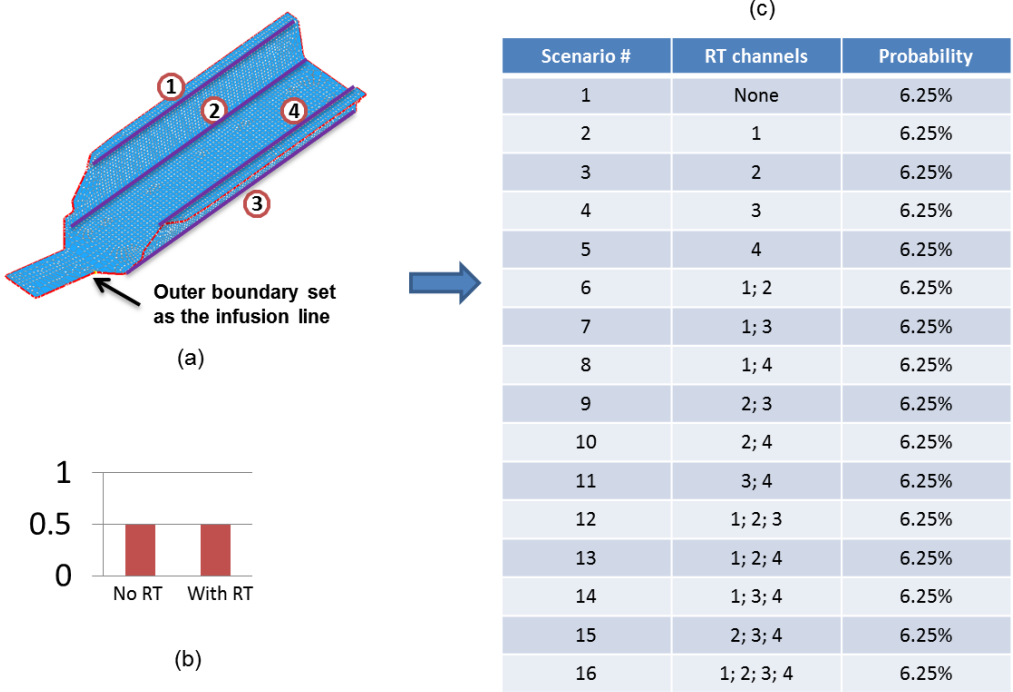


Figure 4-12: Scenario space generation for RTM-light process: (a) potential race-tracking channels identified; (b) race-tracking strength distribution on folds; (c) scenario space generated with equal probability for each scenario.

The entire analysis for these 16 scenarios took about 632s on the computer with Intel® Core™ i7-2600 CPU @3.40GHz, with 16.0 GB RAM. Fill time and the unfilled regions for all of the sixteen scenarios are shown in Figure 4-13 and Figure 4-14. Using the probability analysis approach introduced in section 4.2.6, three vents are recommended as shown in Figure 4-15(a) so that all the scenarios can be successfully filled without voids. Fill time distribution and the relation between

success yield and number of vents are also provided as shown in Figure 4-15(b) and (c).

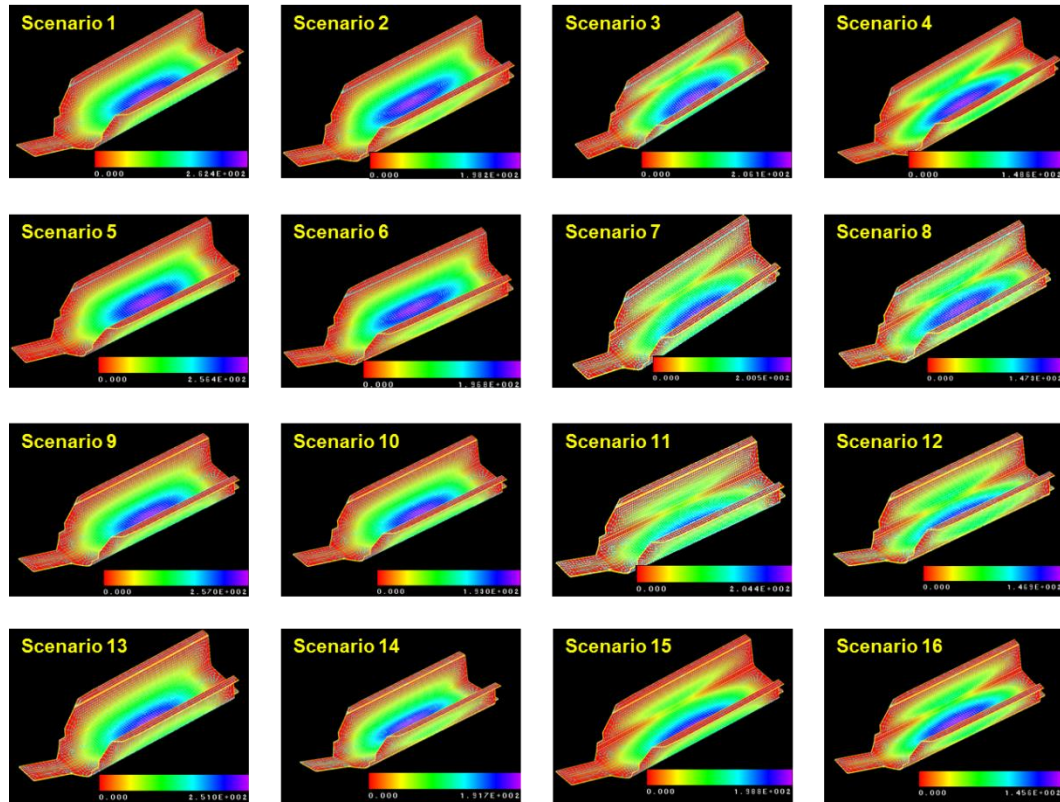


Figure 4-13: Resin flow contours for chassis. Injection is from outer boundaries using RTM Light process

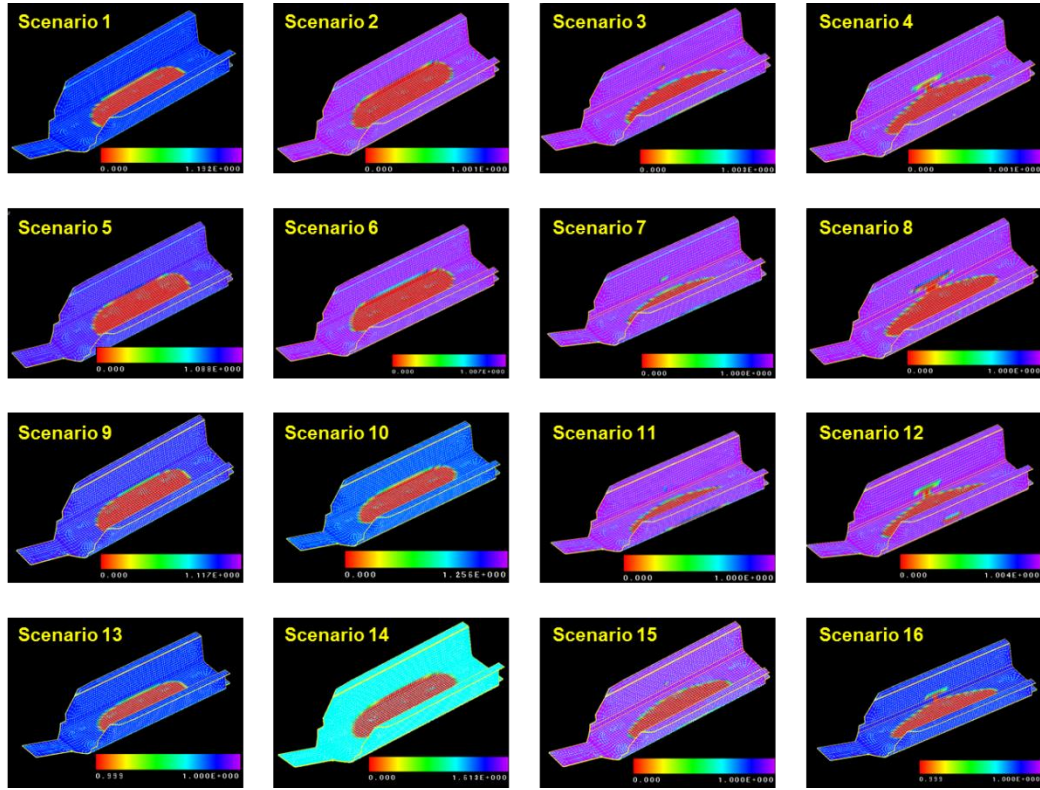
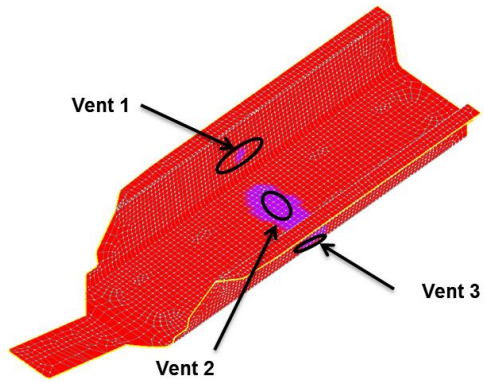


Figure 4-14: Unfilled regions as predicted by LIMS for all 16 scenarios with the RTM Light process



Number of Vents	Vents	Yield
1	Vent 2	87.5
2	Vent 1 & 2	93.75
3	Vent 1, 2 & 3	100%

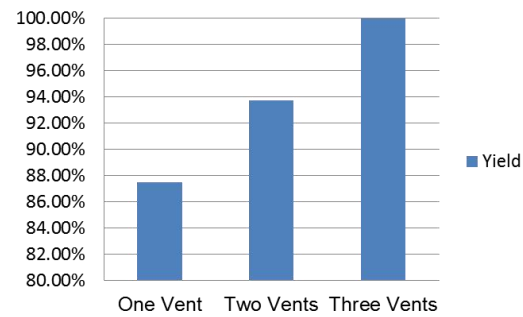
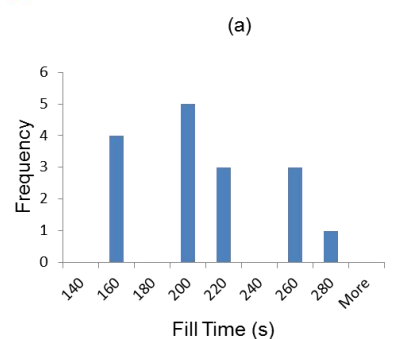


Figure 4-15: Feedbacks and recommendations: (a) vent locations; (b) fill time histogram; (c) successful yield vs. number of vents

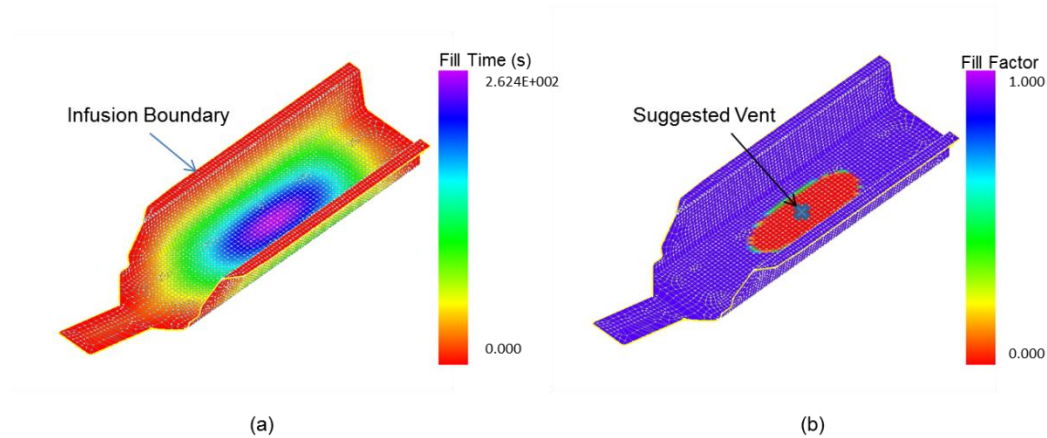


Figure 4-16: Simulation results for (a) Fill Pattern and (b) Fill Factor when race-tracking effect is not taken into account for RTM-light process

The plan for recommended location for the vent is then compared with the mold filling simulation results in which no race-tracking or any other form of flow disturbances are taken into account. This simulation predicts one vent in the center bottom of the chassis, as is shown in Figure 4-16 (b). The two regions on both sides of the chassis where void can be trapped because of the race-tracking effect in the folds will cause voids. As is shown in the Figure 4-15 (c), this one-vent plan will reduce the yield of successfully filling the part by 12.5%.

#### 4.3.1.3 VARTM process

A centerline on the chassis surface is chosen as the resin infusion line for VARTM processing. The six outer edges and the four folds increase the scenario space to 1024 scenarios, as is shown in Figure 4-17 (a) and (b).

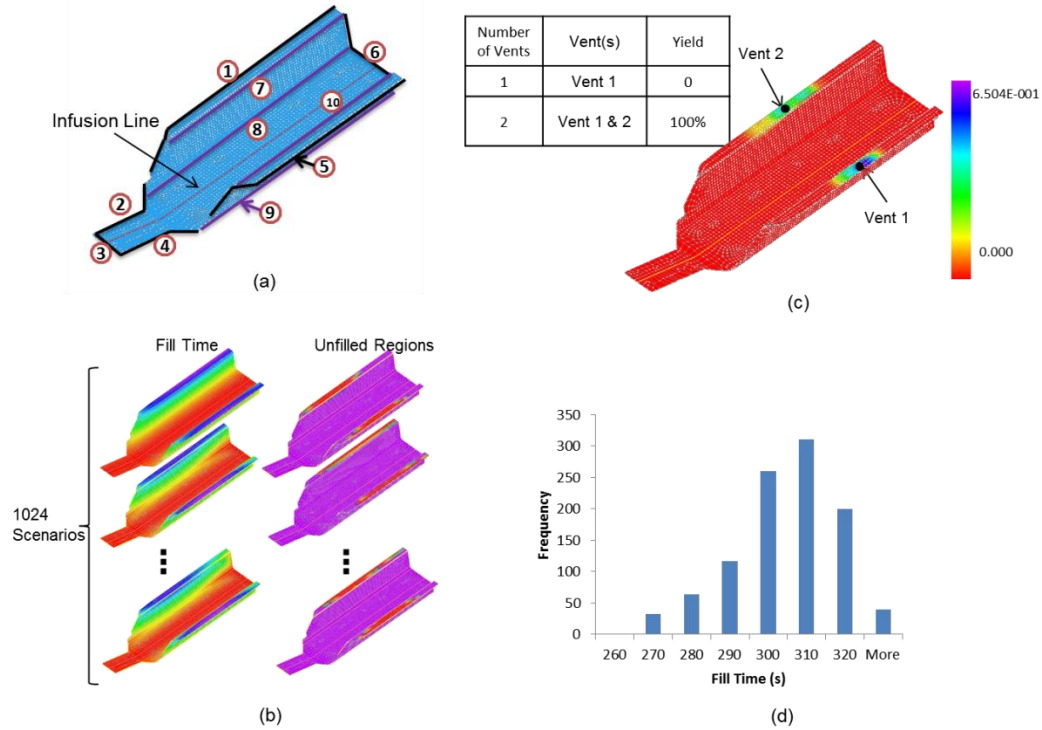


Figure 4-17: Simulation cycle and results for the chassis with VARTM process (a) Infusion line and potential race-tracking channels; (b) Mold filling simulation to find fill times and unfilled regions for all 1024 scenarios; (c) Vent map; (d) Fill time histogram

Two vents are suggested by the simulation results, and the vent locations are shown in Fig. 17 (c). The suggested two vent plan is not different from the scenario in which no flow disturbances are considered as shown in Figure 4-18, because the center infusion line is parallel to most of the race-tracking channels along the outer edges and folds, in which the resistance to resin flow has little effect on the flow pattern. This confirms that two vents as suggested is a robust strategy which will result in 100% yield despite the flow disturbances along 10 regions in the mold. VARTM

process is usually more forgiving due to the ability to introduce line injection schemes for infusion.

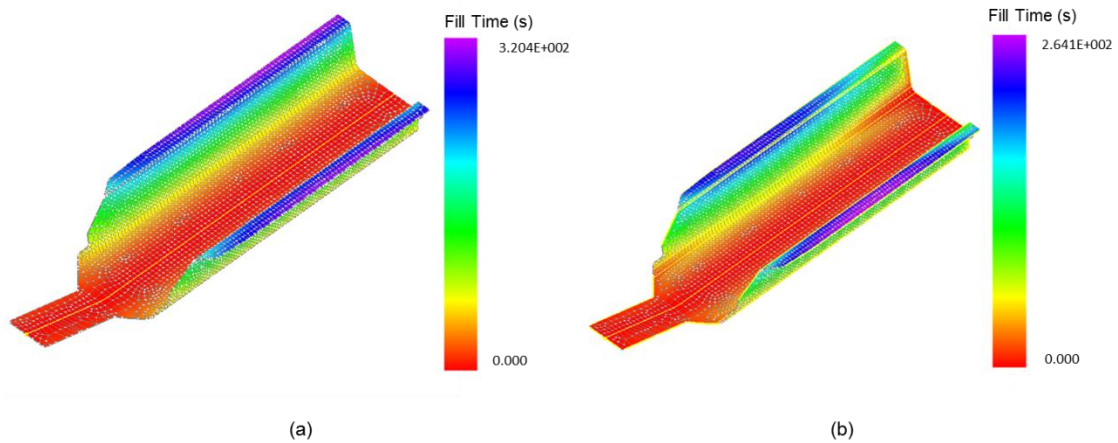


Figure 4-18: Flow front development comparison between the cases when (a) race-tracking effect is not present (b) race-tracking effect is introduced along all of the edges and folds

#### 4.3.1.4 RTM process

The centroid on the bottom surface of the chassis is set as injection gate with a positive injection pressure. Similar to the VARTM process, the ten independent potential race-tracking channels require 1024 scenarios to be analyzed. Six discrete vents are needed along the outer edges for 100% yield (Figure 4-19), whereas if race-tracking effects are not taken into account, only two vents one on each end of the chassis will result in successful filling as shown in Figure 4-20.

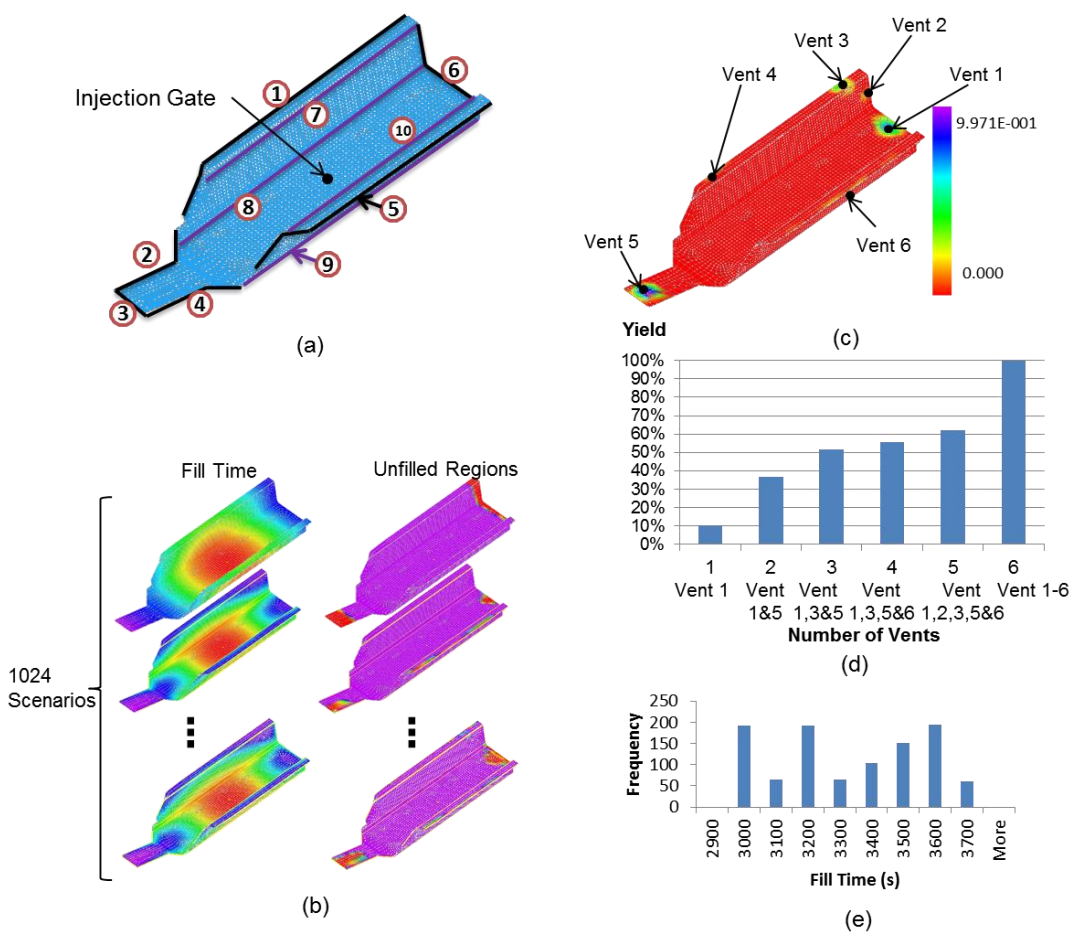


Figure 4-19: Mold filling simulation for the chassis using the RTM process: (a) Injection gate location and potential race-tracking channels identified; (b) Fill time and unfilled regions results for some of the scenarios in the scenario space; (c) Vent map and vent locations; (d) Successful yield vs. number of vents; (e) Fill time histogram.

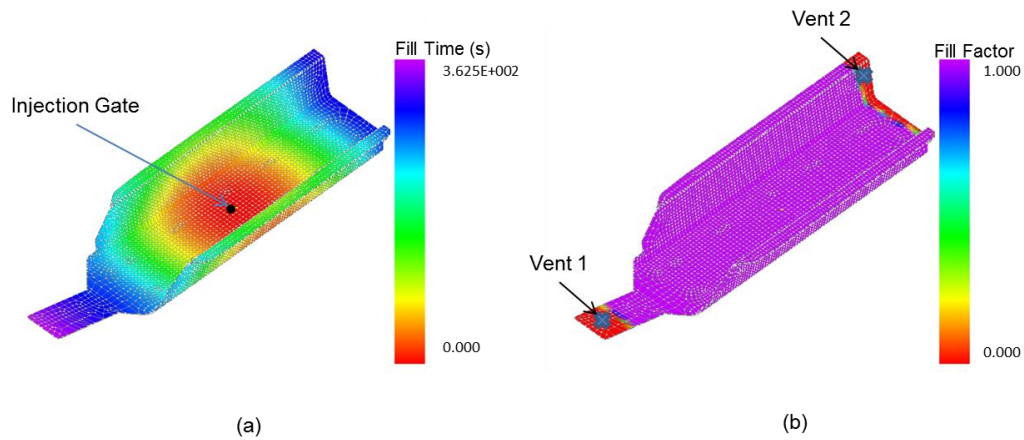


Figure 4-20: (a) Filling pattern and (b) Unfilled regions in the absence of racetracking when the injection gate is located in the center

### 4.3.2 Trailer using the VARTM processes

Next, a trailer that is manufactured using point injection is introduced, as shown in Figure 4-21, and the injection gate is selected at the center of the bottom surface. In this example, only folding lines that can generate potential resin flow disturbances are considered. As shown in Figure 4-21, racetracking channels are automatically detected and grouped into ten independent lines along the folds, each of which is assumed to have equal probability of having no racetracking effect or low racetracking effect (Figure 4-22(a)). Therefore,  $2^{10}=1024$  scenarios are generated in which are executed using LIMS (Figure 4-22(b) (c)). Eight possible vents are identified by aggregating the results for all the 1024 scenarios (Figure 4-22 (c)). Presence of 8 vents will ensure that no voids will be created even when racetracking is present along one or more of the ten identified edges. The simulation took 4.2 hours (with LIMS to run 1024 scenarios) on a machine with Intel® Core™ i7-2600 CPU @3.40GHz, with 16.0 GB RAM. If the production staff can ensure that there will no race tracking at all along any of the edges, one would need only four vents for

successful filling as shown in Figure 4-23. Therefore, to ensure a robust process, one must take into account possible race tracking scenarios to design the process.

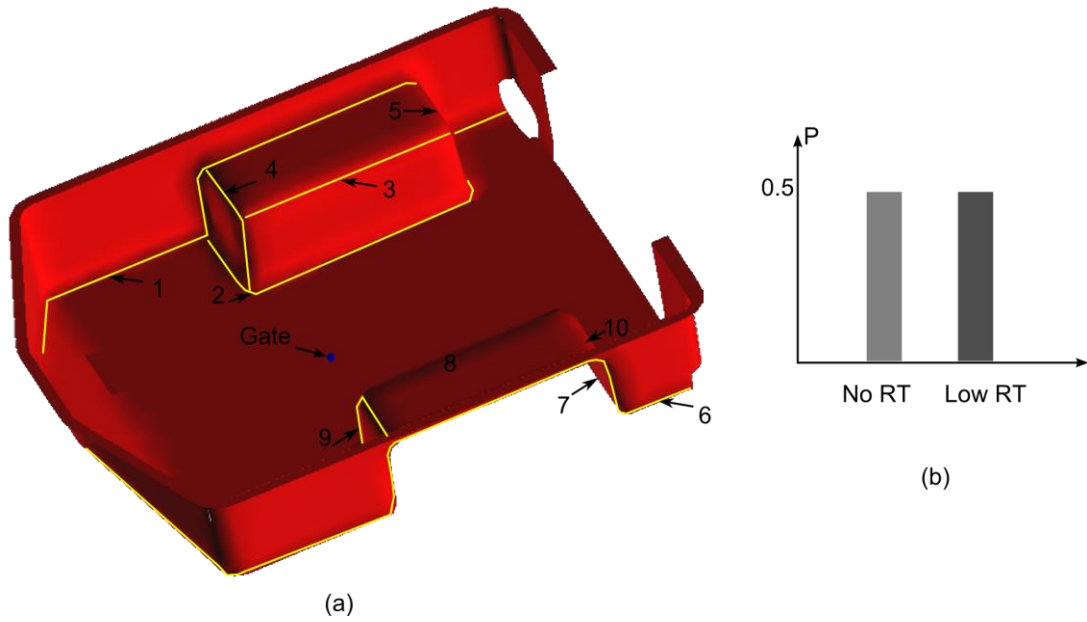


Figure 4-21: Ten race-tracking channels are detected for the trailer along the folds

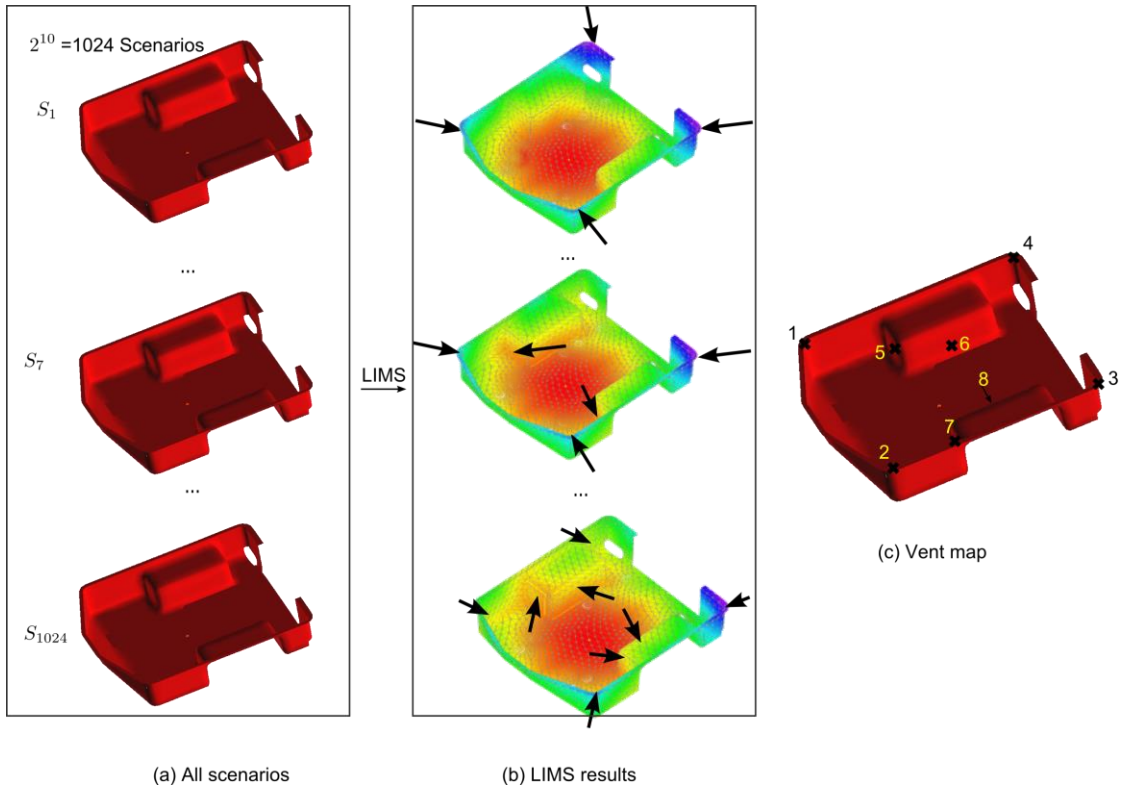


Figure 4-22: Scenario expansion for the trailer and vent map generation using LIMS.

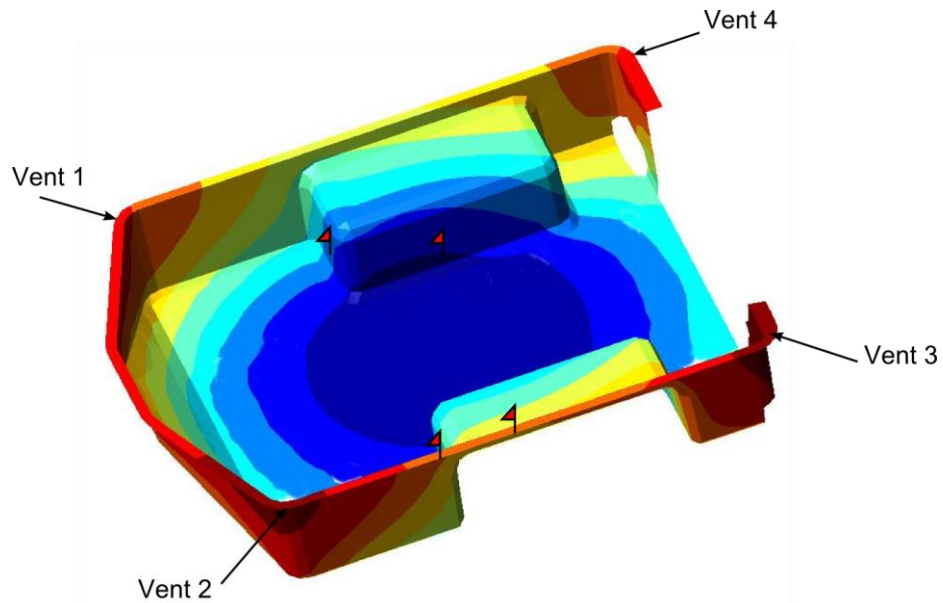


Figure 4-23: Four vents are predicted if only running LIMS for one scenario without considering potential racetracking disturbances along the folding lines, and defect areas are flagged

#### 4.4 Summary

A methodology is proposed by developing an integrated process that can provide information about the manufacturing of a composite part to the designer. It can identify the possible flow disturbance regions, analyze the filling patterns for all permutations possible flow disturbances, and suggest vent locations and the successful yield as a function of number of vents. It can provide this information along with possible injection location and scheme for RTM-Light, VARTM and RTM process choices. The methodology is automated and does not rely on the part designer to provide any input. The automated program takes the meshed CAD file and creates a new data structure with the geometry information, material preform information, and rebuilds the topology based on the mesh file. Potential disturbances channels are automatically detected and race-tracking properties are assigned. The program can

execute all the possible permutations of filling simulation and create a probability map of regions that are most likely to stay unfilled. These regions can be grouped and identified as vents to improve the yield with the infusion scheme selected. The results are returned to the designer in a readable form within the design environment.

An example case study demonstrated this for a chassis validating its usefulness to the designer as a tool to increase the manufacturability of the part by taking steps during the design phase and also providing a comparison between different LCM processes. It can be concluded that race-tracking effect along the outer edges, folds or bifurcation lines can significantly change the resin flow pattern when the mold cavity is being filled, especially when race-tracking regions are not parallel to the flow direction. Without introducing flow disturbances into the mold filling simulation model, the result may not accurately predict all the possible locations in the mold where vents should be drilled, and hence result in lower yield. With the new automated tool which identifies and addresses the race-tracking effects, one can predict the locations and number of vents more accurately. The simulation results and recommendations are provided back to the designer within the part design workbench, so that the designer can make changes to the geometric features to reduce the effect of race tracking and improve manufacturability and yield.

## Chapter 5

### FAST MOLD FILLING SIMULATION BASED ON THE GEODESIC DISTANCE CALCULATION ALGORITHM FOR LCM

#### 5.1 Introduction

Integration of composite part design and manufacturing simulation requires a set of robust processing parameters being established semi-automatically and feedback being provided to the part designer. Accomplishing this may call for simulating all possible scenarios of race-tracking channels, especially when implicit processing parameters are considered. As shown in the previous chapter, if using software package developed based on FE/CV simulations such as LIMS, the time cost to run a set of manufacturing analysis will take too long to be applicable for design-manufacturability integration as it cannot generate real-time feedback to the designer. For example, for a simple mesh containing 5000 nodes, it takes about 15 seconds to run one scenario in the mold filling simulation package LIMS, and running 1000 scenarios will take more than four hours which is too long for real time feedback to the designer, which is a main drawback of the integrating accurate processing simulation with part design.

However, in most cases it is not necessary to provide all simulation outputs but only the estimated impact on flow patterns due to a disturbance created due to design decisions. If there is an approximate method to estimate filling patterns instantly, even with lower accuracy, the feedback to the designer could be in real time to make changes in the design to reduce the impact of disturbances such as race-tracking.

Therefore, this chapter will introduce an approximation of fill time prediction based on distance, so that the integration between design and processing simulation can happen in real time while preserving the accuracy when representing the real manufacturing processes.

## 5.2 Previous work

Predicting fill time based on the largest distance on the surface to the gate was first attempted by Boccard et al.[64] by assuming a radial flow within the mold cavity and channel flow along the edges for flat surfaces. It uses pure distance method on flat surfaces without thickness and permeability changes [15]. This model was also used to predict the fill time and weld lines on a polygon surface [22]. However, their model was concentrated on predicting fill time and is not applicable if the preform permeability varies within the mold or if the mold thickness changes or if higher permeable mat (distribution media) is added to the molding process to accelerate the resin flow as is the case with VARTM, or in the presence of race-tracking channels in RTM.

In this Chapter, a one-dimensional model is developed to relate the fill time with the distance. Combining with Dijkstra's algorithm [65] in search of a path that resin will travel along to simulate the flow front development, fill times for each node on the mesh are predicted. We have modified the method so it can capture the effect of fabric permeability and thickness changes and race-tracking effects for robust vent locations design. The contour plot of the fill time, or the flow pattern which is used for vent location generation, is then compared to the results returned from the mold filling simulation software LIMS. Comparing with LIMS which has (for 2D problems) a time complexity of  $O(N^2)$ , this distance-based model can be reduced to a time complexity

of  $O(|E| + N \log(N))$  ( $N$  is number of nodes in the mesh, and  $|E|$  is number of edges) [24]. The computational savings become significant as  $N$  becomes large.

**5.3 Distance based method for mold filling pattern prediction and its piecewise simplification on FE meshes**

The following section details the equations necessary to evaluate the relations between the time resin flows across one element length on the mesh and its distance to the injection gate. First a continuous model is developed for a one-dimensional flow and then is discretized over the mesh (Figure 5-1). Then this model is used on spatial surfaces to predict each node’s fill time.

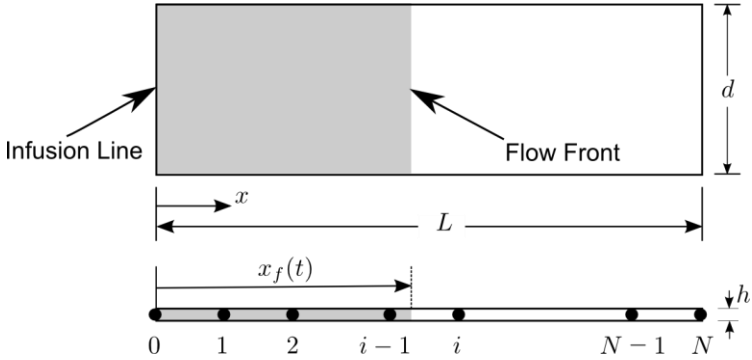


Figure 5-1: One-dimensional flow model (above) and its mesh (below)

**5.3.1 One-dimensional distance time model**

Multiple segments of porous media are injected sequentially, each having a distinct permeability value, thickness and porosity. The relation between flow-front positions versus time is outlined below [17].

For the one-dimensional flow shown in Figure 5-1, under the quasi-steady solution approach, and assuming no dual-scale effects prevalent during the infusion,

the instantaneous governing equations for 1D flow volume averaged velocity  $u_x$  through a thin plate with permeability  $K_{xx}$  according Darcy's Law is:

$$u_x = -\frac{K_{xx}(x)}{\eta} \cdot \frac{dp}{dx} \quad (5.1)$$

where  $p$ , and  $\eta$  are the resin pressure and viscosity respectively. The conservation equation requires that at any  $x$  location:

$$u_x \cdot h(x) = Q = \text{const.} \quad (5.2)$$

in which  $h(x)$  is the local thickness. Combining equation (5.1) and equation (5.2), we obtain the differential equation describing resin pressure field:

$$\frac{dp}{dx} = -Q \cdot \frac{\eta}{K_{xx}(x)h(x)} \quad (5.3)$$

Integrating both sides of equation (5.3), the resin pressure from the inlet to pressure at the flow-front,  $x$  from 0 to flow-front position  $x_f(t)$ :

$$p_{in} = Q \cdot \eta \cdot \int_0^{x_f(t)} \frac{dx}{K_{xx}(x)h(x)} \quad (5.4)$$

This provides the relation between the flow rate  $Q$  and the flow-front position  $L$  as follows:

$$Q = \frac{p_{in}}{\eta} \left( \int_0^{x_f(t)} \frac{dx}{K_{xx}(x)h(x)} \right)^{-1} \quad (5.5)$$

Based on one-dimensional linear flow assumption, the progress of the flow-front can be written as:

$$\frac{dx_f(t)}{dt} = \frac{Q}{\phi(x_f(t)) \cdot h(x_f(t))} \quad (5.6)$$

in which  $\phi$  is the porosity of the fiber preform, and is equal to  $1 - v_f$ , where  $v_f$  is the fiber volume fraction. Substituting equation (5.5) into equation (5.6), the differential equation for the progress of the flow-front can be expressed as:

$$\frac{dx_f(t)}{dt} = \frac{p_{in}}{\eta \cdot h(x_f(t)) \cdot \phi(x_f(t))} \cdot \left( \int_0^{x_f(t)} \frac{dx}{K_{xx}(x)h(x)} \right)^{-1} \quad (5.7)$$

Equation (5.7) can be integrated from node  $i - 1$  to its neighboring node  $i$ , and thus one obtains the flow-front moving time between these two locations (nodes):

$$\int_{t_{i-1}}^{t_i} \frac{p_{in}}{\eta} dt = \int_{x_{i-1}}^{x_i} h(\psi) \cdot \phi(\psi) \cdot \left( \int_0^{\psi} \frac{dx}{K_{xx}(x)h(x)} \right) d\psi \quad (5.8)$$

in which  $t_{i-1}$ ,  $t_i$  are the fill time for node  $i - 1$  and node  $i$  respectively, and  $x_{i-1}$ ,  $x_i$  are their coordinates.  $\psi$  is the flow front position between node  $i - 1$  and node  $i$ . Within each element, permeability  $K_{xx}$  and preform thickness  $h$  are assumed to be constant, which corresponds to element in a usual FE discretization. The discretized

equation for flow-front development between node  $i - 1$  and node  $i$  can then be written as:

$$\Delta t_i = \frac{\eta}{P_{in}} \Delta x_i h_i \phi_i \left[ \sum_{j=1}^{i-1} \left( \frac{\Delta x_j}{K_j h_j} \right) + \frac{\Delta x_i}{2K_i h_i} \right], i = 1, 2 \dots N \quad (5.9)$$

in which  $\Delta x_i = x_i - x_{i-1}$ ,  $\Delta t_i = t_i - t_{i-1}$ . The fill time of the part can therefore be obtained by summing flow development time  $\Delta t$  for each element. Figure 5-2 shows one example of using equation (5.9) to calculate the fill time for each node on a homogeneous plate (Figure 5-2 (a)), and the same plate with distribution media (Figure 5-2 (b), in which through thickness resin impregnation is neglected).

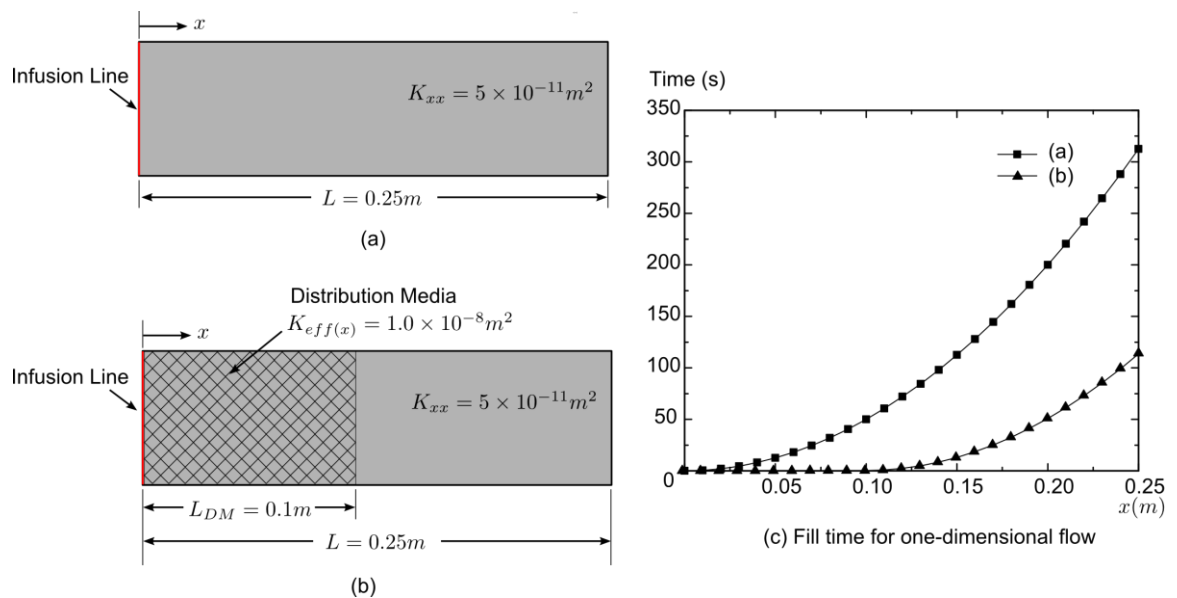
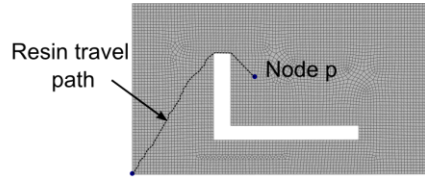


Figure 5-2: Fill time calculation for one-dimensional flow: (a) no distribution media; and (b) with distribution media.

### 5.3.2 Implementation of the one-dimensional flow model on spatial surfaces

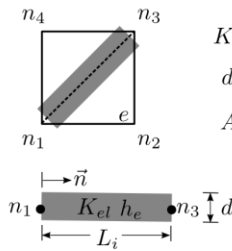
The developed model is then used on the spatial surfaces. To implement the distance prediction of the mold filling time on any curved surface, the FE mesh of the part is treated as a graph. The edges connecting two neighboring nodes are weighted by their length that can be calculated directly from the nodal coordinates contained in the mesh. Next, Dijkstra's algorithm is used to calculate the path for the resin to travel along. When using the discretized equation (5.9) for 2D elements, the preform thickness is substituted with the channel cross-section area as shown in Figure 5-3. Resin travel path consists of connected edges across the elements. Flow progression time across each element is represented by:

$$\Delta t_i = \frac{\eta}{P_{in}} \Delta L_i A_i \phi_i \left[ \sum_{j=1}^{i-1} \left( \frac{\Delta x_j}{K_j A_j} \right) + \frac{\Delta x_i}{2K_i A_i} \right] \quad (5.10)$$



(a) One example of resin travel path from injection gate to node p

$A_e$ : element area  
 $[K_e]$ : element permeability tensor  
 $K_{el}$ : projection of  $[K_e]$  on  $L_i$   
 $h_e$ : element thickness  
 $d$ : width of channel  $L_i$

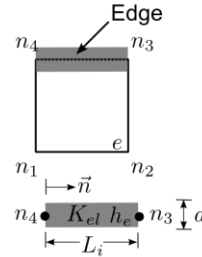


$$K_{el} = \vec{n} \cdot [K_e] \cdot \vec{n}$$

$$d \times L_i = \frac{1}{2} A_e$$

$$A_i = h_e \times d$$

(b) Channel simplification when path goes through the element

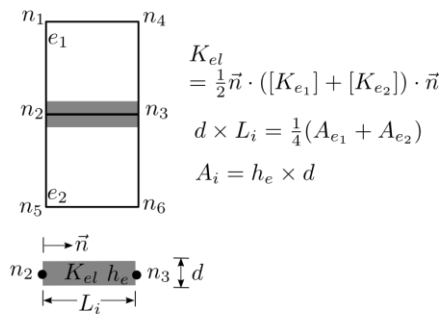


$$K_{el} = \vec{n} \cdot [K_e] \cdot \vec{n}$$

$$d \times L_i = \frac{1}{4} A_e$$

$$A_i = h_e \times d$$

(c) Channel simplification when path goes along the elemental edge on the boundary

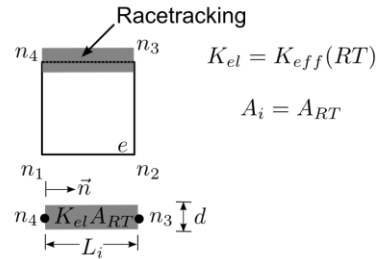


$$K_{el} = \frac{1}{2} \vec{n} \cdot ([K_{e1}] + [K_{e2}]) \cdot \vec{n}$$

$$d \times L_i = \frac{1}{4} (A_{e1} + A_{e2})$$

$$A_i = h_e \times d$$

(d) Channel simplification when path goes along an edge shared by two elements



$$K_{el} = K_{eff}(RT)$$

$$A_i = A_{RT}$$

(e) Channel simplification when path goes through a racetracking channel

Figure 5-3: Channel simplification for 2D quadrilateral elements

The channel simplification enables one to model race-tracking channels by assigning the path through race-tracking channels the cross-section area and permeability accordingly. From equation (5.10), one can see that because race-tracking channels always have higher permeability, resin travels faster when crossing these channels. Pseudocode for Dijkstra's algorithm in moving flow front forward is shown below:

*FUNCTION Dijkstra's algorithm for flow front development*

*SET unsolved nodes to all nodes*

*SET number of unsolved nodes to number of nodes*

*FOR (each node in unsolved nodes)*

*SET fill time of the node to  $\infty$*

*SET fill time of the gate node to 0*

*WHILE (number of unsolved nodes  $\geq 0$ )*

*SET node u to be the node in unsolved nodes with the  
    smallest fill time  $t_u$*

*FOR (every neighboring node v of node u)*

*CALCULATE  $\Delta t_{u \rightarrow v}$  using equation (5.10)*

*IF ( $t_u + \Delta t_{u \rightarrow v} < t_v$ )*

*update  $t_v$  with  $t_u + \Delta t_{u \rightarrow v}$*

*REMOVE node u from unsolved nodes*

*number of unsolved nodes -= 1*

*RETURN nodes with updated fill time*

An example of flow pattern calculation using Dijkstra's algorithm combined with channel simplification is shown in Figure 5-4 for the flat plate with an "L" shape cutout, and the fill pattern is then compared with LIMS result. For both sets of results, each node's fill time is non-dimensionalized by:

$$\bar{t}_i = \frac{t_i}{t_{fill}} \quad (5.11)$$

in which  $t_i$  is fill time calculated for node  $i$ , and  $t_{fill}$  is the fill time of the part returned by distance-based method and LIMS respectively. The CPU time cost comparison between these two methods is shown in Figure 5-5. From the results, one can see that the distance-based model can adequately capture the flow pattern returned by LIMS, however, the savings on CPU time increase significantly as the number of nodes increase. Meanwhile, the distance-based results converged as the mesh becomes finer.

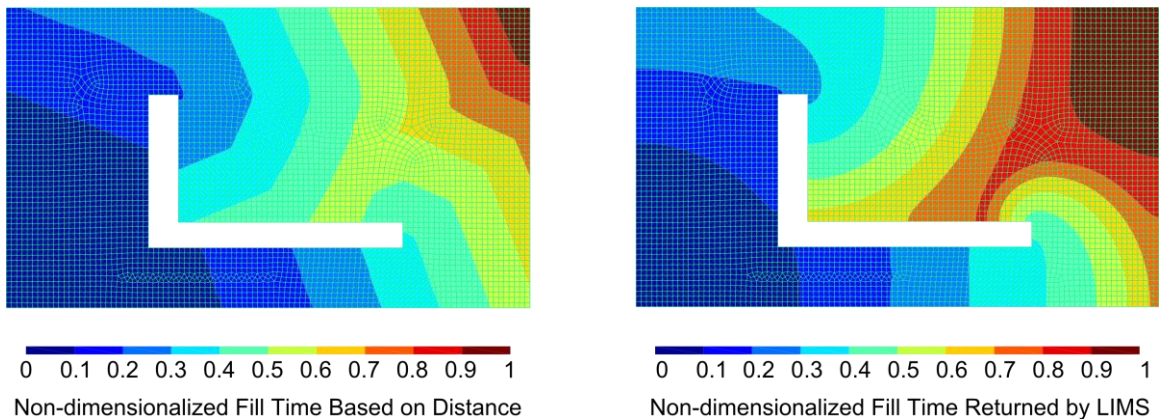


Figure 5-4: Comparison between distance based fill pattern estimation (left) and LIMS result (right)

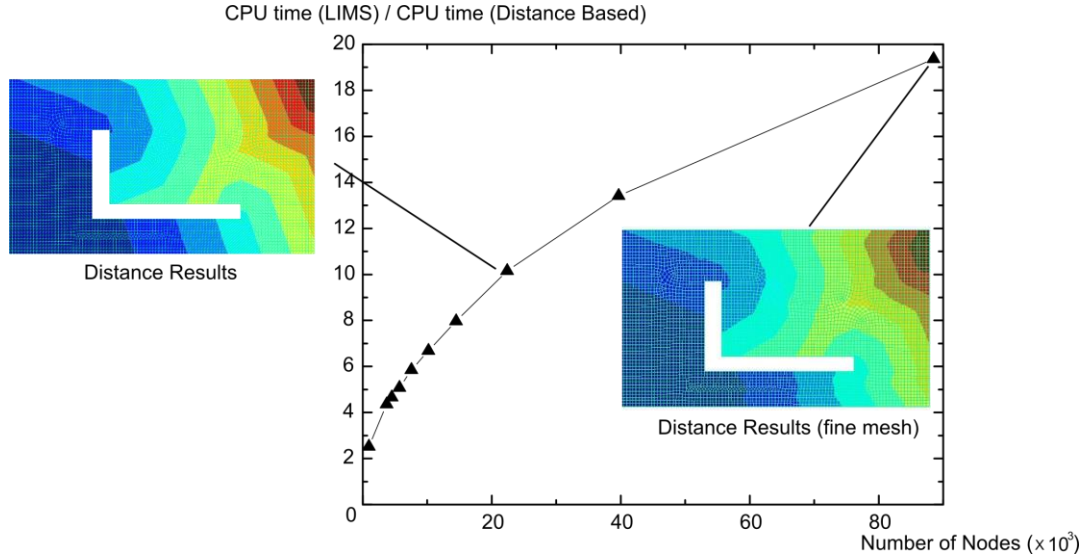


Figure 5-5: Calculation time comparison between distance-based simulation and LIMS simulation with increasing number of nodes. Distance-based flow pattern converges to the LIMS results as shown in Figure 5-4

### 5.3.3 Treatment of permeability variations and the race-tracking channels

Race-tracking channels are simulated as one-dimensional elements, each of which is assigned a permeability in terms of cross-section area. From equation (5.10), because race-tracking channels have a higher permeability, resin travel time is much lower on these edges. Figure 5-6 shows the simulation results for the plate and 4 disturbances occurring at the cutout channels. Flow pattern returned by distance-based model is compared with LIMS result, and it can be seen that the distance-based model can capture very well the flow disturbances introduced by the race-tracking channels.

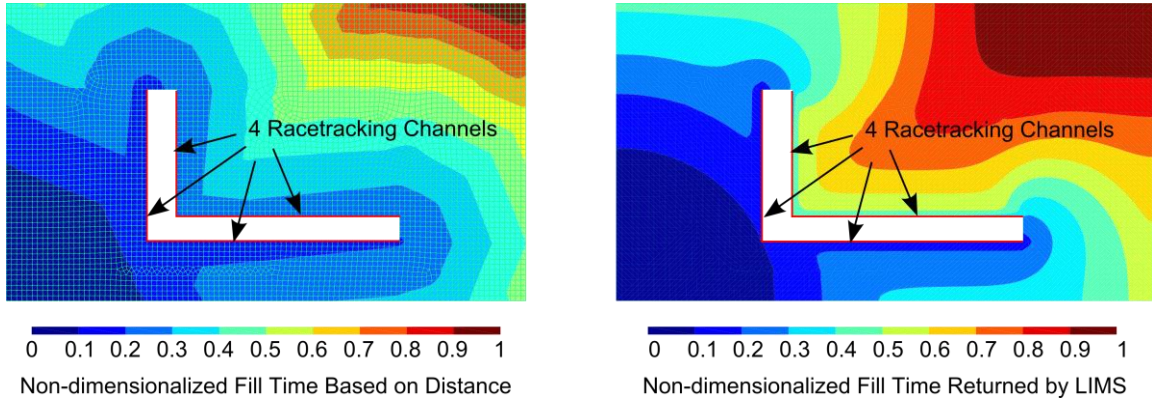


Figure 5-6: Flow pattern comparison between distance-based method and LIMS when 4 race-tracking channels are present at the plate cutout

### 5.3.4 Substitution of distance based flow pattern prediction for robust processing parameters' design

Race-tracking channels can be automatically recognized and a probability model is used to describe the race-tracking strength for each channel. Then the distance-based method is used to generate mold flow pattern for each scenario in the scenario space. For the example of the plate with a “L” shape cutout, seven vent locations are returned by distance-based method and the locations of these vents are the same as the ones obtained from the flow simulation LIMS.

## 5.4 Case studies

Some examples that have complicated geometric features and material variability over the surface are explored in this section to demonstrate the versatility, efficiency and accuracy of the distance-based mold filling simulation by comparing the results with FE based LIMS results.

### 5.4.1 Box

The box shown in Figure 5-7 has four edges on the bottom that use higher permeability material. Both distance-based results (Figure 5-8(a)) and LIMS results (Figure 5-8(b)) show that the venting line should be placed on top of the box if the injection gate is set at the center of the bottom. Moreover, possible flow trapping at four corners of the bottom are captured by both sets of simulation results (Figure 5-8).

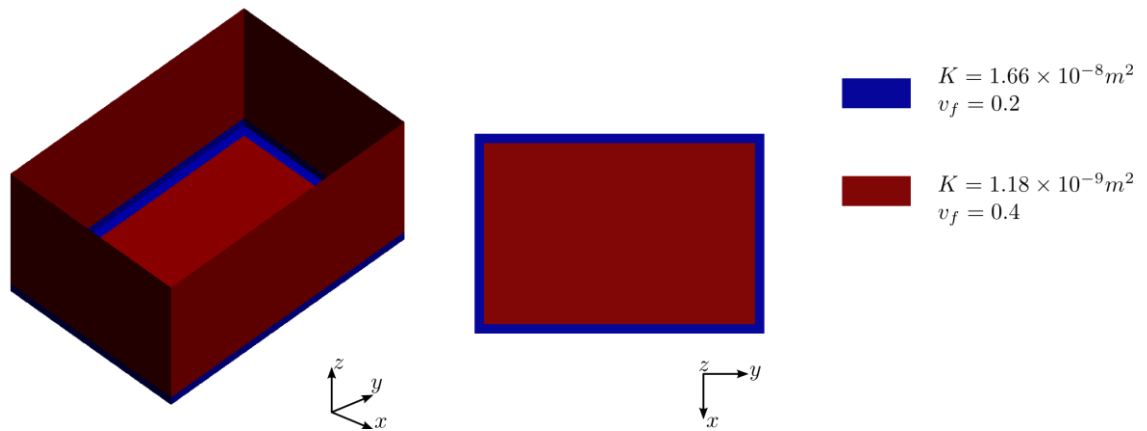
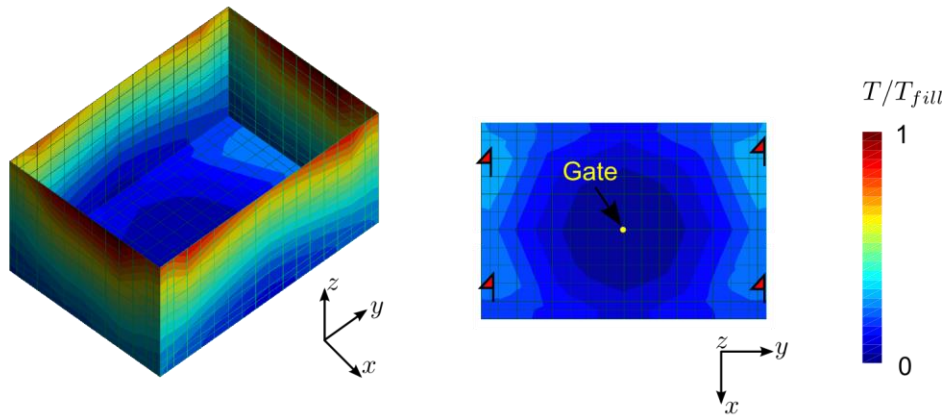
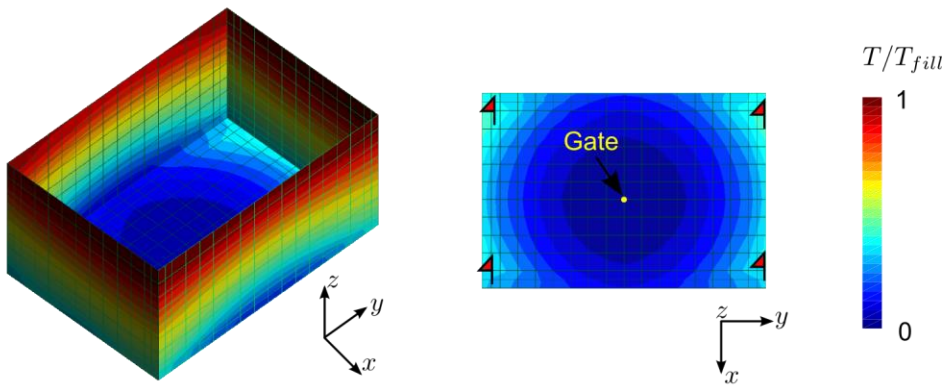


Figure 5-7: Box with preform permeability variations along the edges



(a) Distance-based non-dimensional fill time results for the box

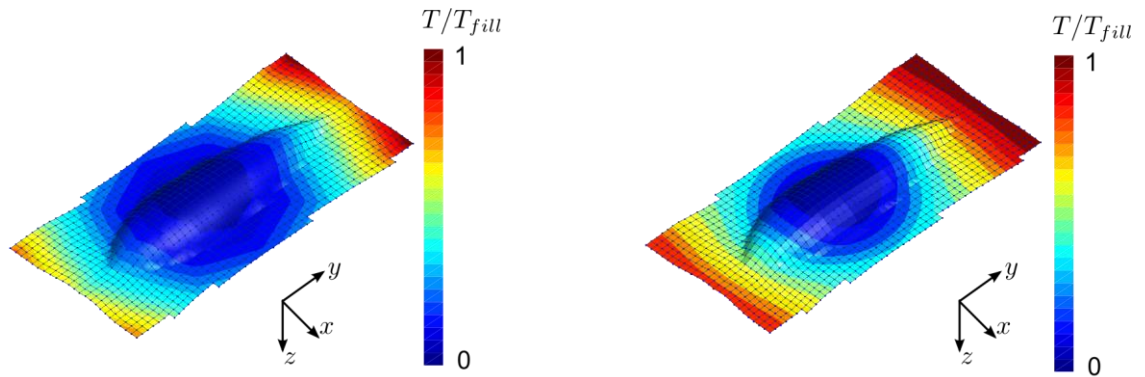


(b) LIMS non-dimensional fill time results for the box

Figure 5-8: Simulation results comparison between distance-based simulation (left) results and LIMS results (right), and possible locations of flow entrapment are flagged where vents should be placed

### 5.4.2 Drop fairing

The drop fairing shown in Figure 5-9 is a doubly curved surface and is injected from the center. Distance-method is able to capture the radial-shape flow development along this curved surface.



(a) Distance based non-dimensional fill time

(b) LIMS non-dimensional fill time

Figure 5-9: Flow pattern simulation results for a double-curved drop fairing using distance-based method (left) and LIMS (right)

### 5.4.3 Humvee hood

A Humvee hood part shown in Figure 5-10 is configured with preform whose permeability varies in several locations on the surface. RTM filling simulation results using both distance based method and LIMS are shown in Figure 5-11 for this case. Humvee hood has one race-tracking channel located on one side of the surface curvature. It can be shown that the flow pattern are the same with these two methods, however, the distance based method reduce the simulation time of 3.46s required by LIMS to 0.104s. These are substantial savings if a scenario space of 256 simulations is analyzed.

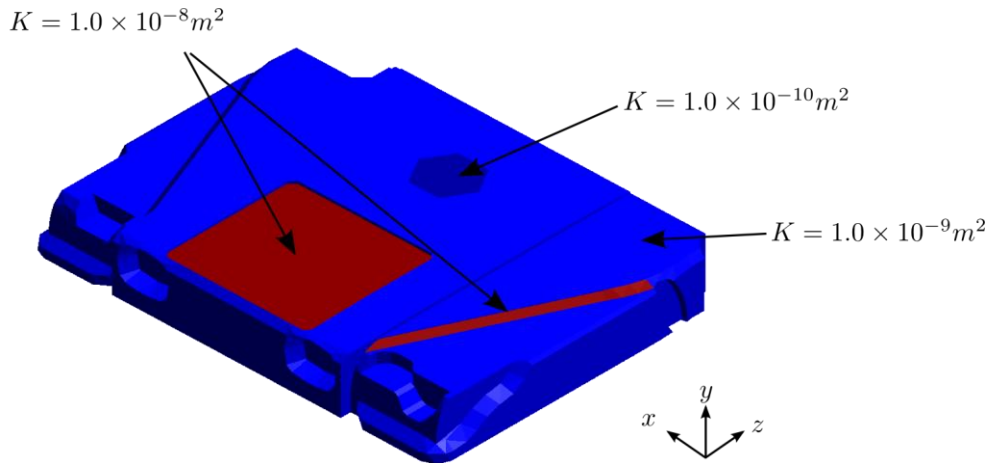


Figure 5-10: Surface geometry and permeability distribution for a humvee hood

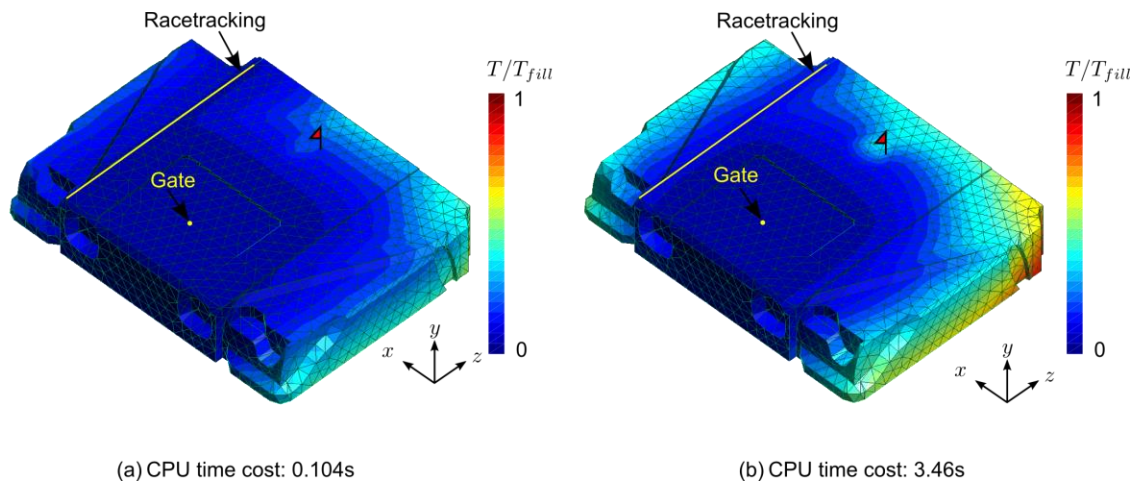


Figure 5-11: RTM simulation results comparison for the humvee hood: (a) non-dimensional fill time results using distance-based method; (b) non-dimensional fill time results returned by LIMS, and possible location of flow entrapment is flagged towards the end of the hood along z axis

#### 5.4.4 Vent location optimization for trailer with many race-tracking possibilities along the edges

Distance-based method is then used in the creation of the vent fitness map for a trailer shown in Figure 5-12(a), in which ten race-tracking channels are detected and 1024 scenarios are generated with the race-tracking strength discretization shown in Figure 5-12(a). Eight possible vents are located by running the distance-based simulation for all the scenarios (Figure 5-12(b)) following the same procedure in Figure 4-22, but the simulation time required is reduced from 4.2 hours (with LIMS to run 1024 scenarios) to 8 minutes.

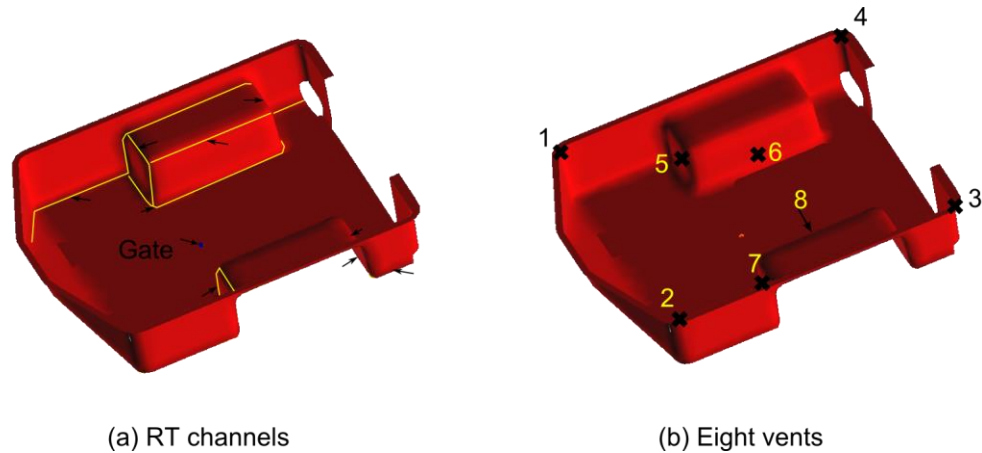


Figure 5-12: Vent map generated using distance based results. The flow front pattern is similar to the one predicted by LIMS (Figure 4-22), and the difference (distance between the vent locations returned by two methods respectively) is smaller than the size of the vents.

#### 5.5 Summary

A one-dimensional resin impregnation model in the fiber preform is developed to calculate fill time approximation based on the distance from the injection gate. Combined with shortest path searching algorithm, Dijkstra's algorithm, this model is

then implemented on spatial surface meshes to calculate fill time for each node and generate flow development pattern. It has been shown that this distance based model can reduce the filling simulation time approximately by the order of  $N\log(N)$  while preserving the flow pattern accuracy necessary to determine vent locations. Our implementation of this method can include variable material properties within the domain, and also accommodate material variability on the surface and can capture very well the flow disturbances from race-tracking channels. Therefore, this distance-based flow prediction algorithm can save significant CPU time when running a large batch of simulations and provide useful vent fitness map information to the designer in real time.

## **Chapter 6**

### **MULTI-TIER STRATEGY TO INTEGRATE COMPUTER AIDED DESIGN AND PROCESSING SIMULATION MODULES**

#### **6.1 Introduction**

In previous chapters, multiple design tools and methodologies have been developed to aid the integration between the designer and processing simulations. However, this task is still not straightforward without applicable framework to use these tools by mimicking the natural design progressions. Therefore, in this chapter, two application strategies to integrate processing simulation and optimization modules are developed to maximize the benefit of the tools.

#### **6.2 Multidisciplinary wind blade design and analysis**

##### **6.2.1 Introduction**

In the theory of engineering design, the design practice converges towards a solution with successive iterations which eliminate uncertainty[66–71]. Multidisciplinary analysis and optimization tools have been developed to aid the designers to select precise parameters that satisfy their pre-determined requirements[72–81]. Conventionally, these analysis tools require the designer to input precise parameter values for analysis. However, at the beginning of the design stage, designers are usually not equipped with sufficient knowledge to uniquely determine all design parameters, which results in many trial and error cycles with a large number of design scenarios, each of which may take a long time to execute using

the analysis module. Thus, the requirement of precise parameter values for the analysis modules is inconsistent with the inherent uncertainty in design space and renders the software ineffective and difficult to use. This disadvantage is even more acute when developing complex composite parts, in which the parameters are co-dependent across multiple disciplinary analysis modules that include structural and laminate analysis modules, composite process simulations, and cost analysis module. Therefore, to better aid the designers make decisions that concurrently receive feedback from all modules with their level of uncertainty at different design stages, this chapter presents a methodology to represent and manipulate the uncertainty inherent in the design parameters, and integrate this approach at each stage of the design process.

Many mathematical models have been explored to represent the design uncertainty, including fuzzy sets theory, frequency probability approach, and interval analysis[67]. Although these methods have shown their capability in the design parameter optimization space, their capability in guiding the development of computer aided software is limited. The mathematical concepts remain unfamiliar to the engineers involved in composite design and development activities. Consequently, these models are limited to academicians only, and a more pragmatic approach has to be developed to bridge the gap. Therefore, this chapter aims at developing pragmatic methodology to manage uncertainty levels throughout the design stage, so that the designer can make informed decisions at each design stage. An example of how one would approach this for wind blade design is presented in this chapter.

### **6.2.2 Design Process as applied to Wind Blade Design**

The design process starts with requirements. In this example of wind blade, this will be limited to turbine location and wind classes, expected performance and some cost limits. The aerodynamics requirements dictate range of sizes, airfoils and so on. The structural integrity then determines the part thicknesses and materials, which contribute to cost. The designer will make decisions based on combined results returned from simulation packages including structural analysis, aerodynamic analysis, laminate design module, manufacturing analysis, and financial calculation package (Figure 6-1). Among these packages, manufacturing is one crucial measure in terms of determining manufacturing steps, predicting cycle time to ensure resin saturation of empty spaces between the fibers before resin gels, and estimating manufacturing cost.

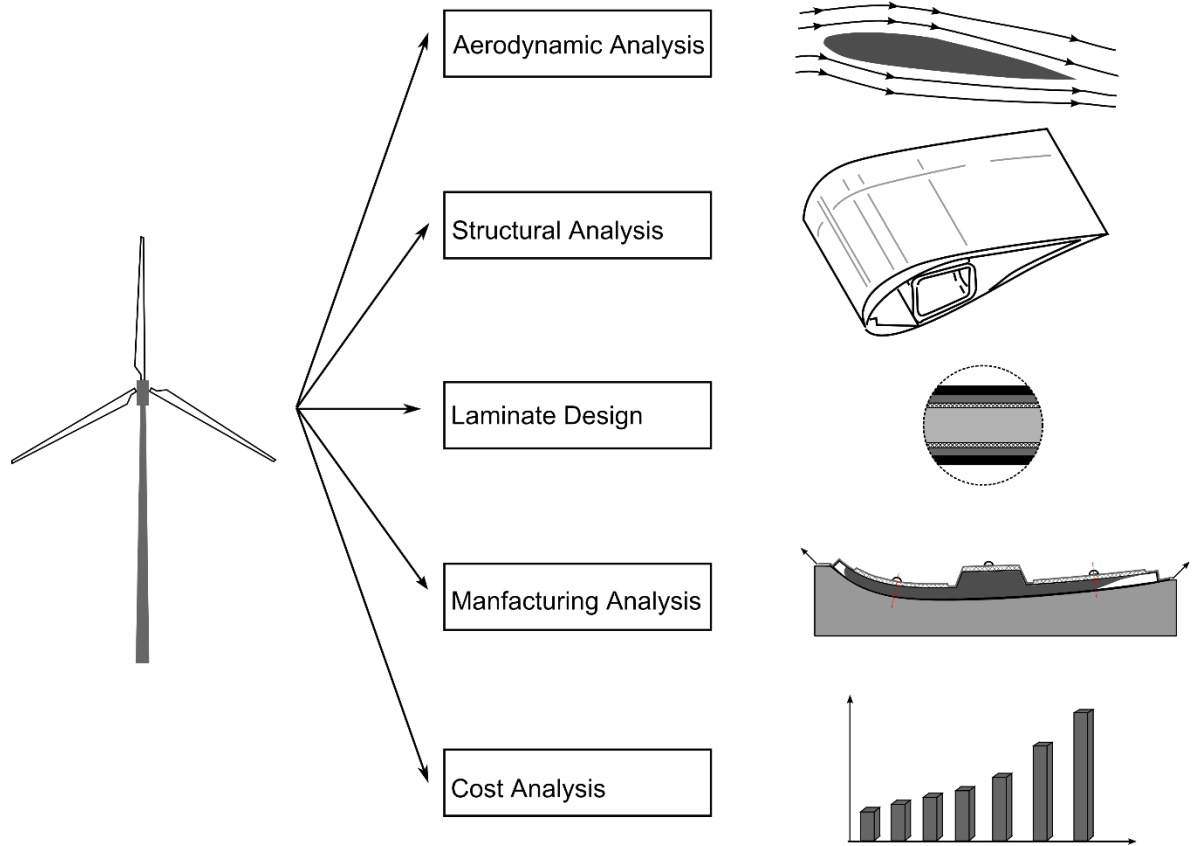


Figure 6-1: Five necessary simulation modules for wind blade design: Aerodynamic analysis, structural analysis, laminate design, manufacturing analysis, and cost analysis

To provide this information, one needs to model the manufacturing process, in this particular wind blade case, the layup of fiber reinforcement for the Vacuum Assisted Resin Transfer Molding (VARTM) manufacturing process, which uses a vacuum to pull the liquid resin from a resin reservoir at atmospheric pressure to saturate all the empty spaces between the fibers in the reinforcement layup. In the VARTM process, layup of fiber reinforcement is placed on top of the one-sided mold, covered with a highly permeable mesh, called the distribution media, and then the assembly is enveloped in a vacuum bag to seal the layups and the mold. Under

vacuum the laminate gets compacted and liquid resin is introduced through the infusion channels connected to the resin reservoir at atmospheric pressure. Resin infusion is discontinued when all the empty spaces between the fibers are saturated with resin. The vacuum is maintained until the resin cures before demolding the part.

During the resin infusion step, processing parameters that need to be specified include infusion pressure, resin viscosity, fabric permeability, and infusion scheme. Due to the large size of the wind blade, resin is sequentially infused into the laminates through a series of open parallel channels aligned along the length of the wind blade. As shown in Figure 6-2, three infusion lines are placed along the bottom surface of the wind blade, the first infusion line that is opened is placed on the middle of the cap, which is the thickest part of the surface. Resin then impregnates the empty spaces mainly in through the thickness direction. Line gates 2 and 3 are opened sequentially when resin arrives there at time  $t_2$  and  $t_3$  respectively.

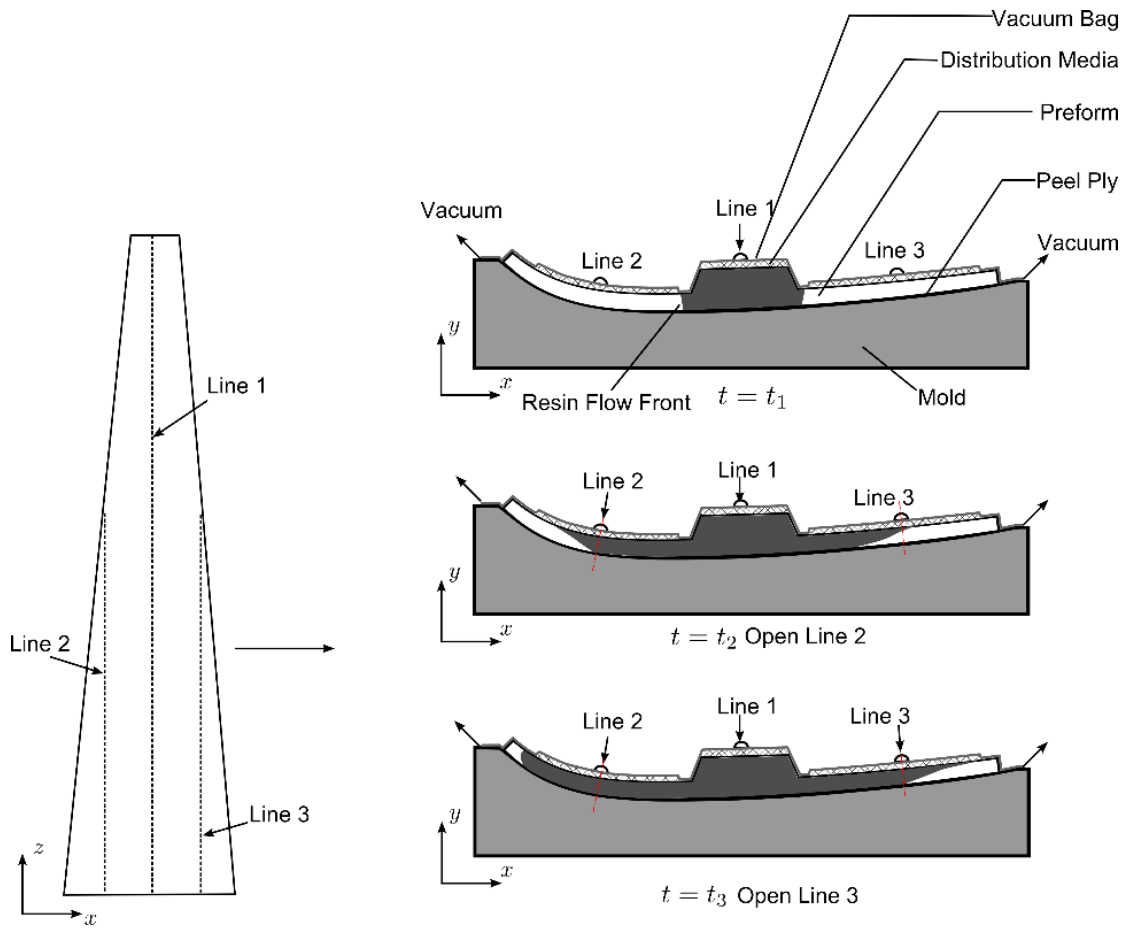


Figure 6-2: Sequential resin infusion to manufacture a composite blade using three infusion lines. Injection lines 2 and 3 are opened when the resin arrives there.

The designer has to specify all the detailed geometry and materials used for the wind blade based on the requirements as dictated by the aerodynamics, structural analysis, and manufacturing. Our goal is to develop a methodology to help the designer use these tools effectively to streamline the design process.

### **6.2.3 Approach**

This section will introduce the uncertainty management approach for the multidisciplinary composite wind blade design and analysis. The methodology is implemented in a software package that integrates various simulation packages for structural, aerodynamics and manufacturing analysis, along with financial cost model, and can handle parameter co-dependencies across these modules. The designer is guided by this methodology to refine the design parameters with the aid of the integrated simulation results. With successive iterations, the software provides the best approximation of the process parameters within the current level of uncertainty.

The software separates input design variables and materials into three tiers of uncertainty levels to match the beginning, intermediate and final design stage evolution (Figure 6-3). To deploy modeling analysis, the model formulation is matched with the uncertainty level of the parameter set that is currently known. To deal with the uncertain or missing information at the preliminary stage and more accurate parameters at the intermediate and final design stage, there are three analysis models of increasing fidelity arranged into three “tiers” of accuracy. The lower tiers replace the unknown parameters by an educated estimate. Although this limits the accuracy of model predictions, this approach allows the lower tier to virtually provide instant feedback so that the designer can tighten the bounds of his design, while retaining accuracy for predictions at the higher tier level where the designed structure becomes fully determined. Number of design alternatives are the largest at the beginning stage, because the designer is incapable of providing all the input parameters with sufficient precision. However, the low fidelity model matched with this tier does not rely on the precise input design parameters and will return the approximate manufacturing simulation results back to the designer in seconds.

Therefore, the designer can explore a large number of design alternatives and exclude unqualified ones. The design space is therefore reduced and passed down to the next tier. After each tier's analysis, the user will have more knowledge and confidence to decide parameters with extra precision, and higher fidelity model is used to return to the designer more accurate results to aid the designer with parameter refinement. The designer can therefore fully use the functionality of the manufacturing simulation tools to gradually reduce the design imprecision and therefore the size of design space (Figure 6-4). Detailed approach for each tier is described in the following sections.

The current implementation of these models may share code and algorithms, and the lower accuracy tier(s) may just fill in the missing information with estimates. On the other hand, simpler (possibly analytic formula based) dedicated models may be used to provide the estimates on the lower level of fidelity. In our case, these approaches are combined.

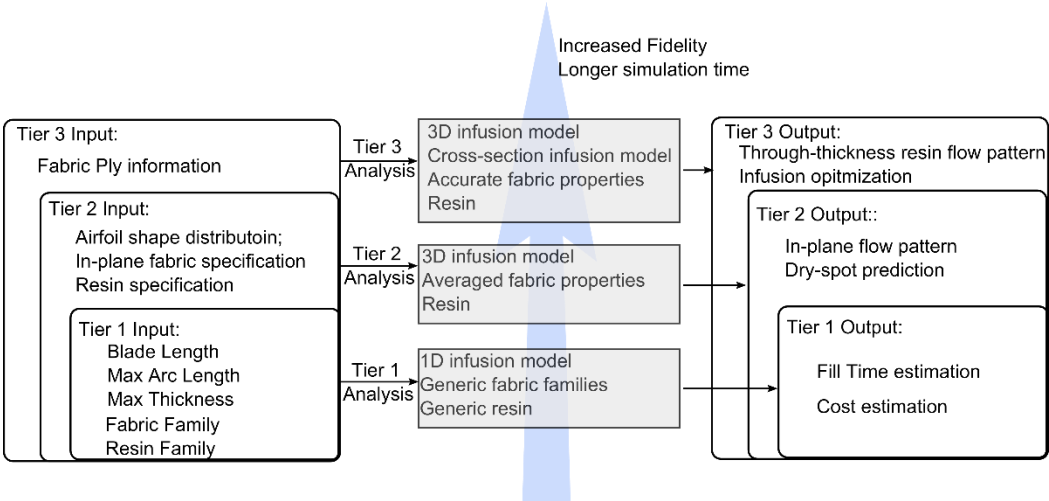


Figure 6-3: Separation of design variables and materials into three tiers with increasing fidelity and decreasing uncertainty for manufacturing analysis

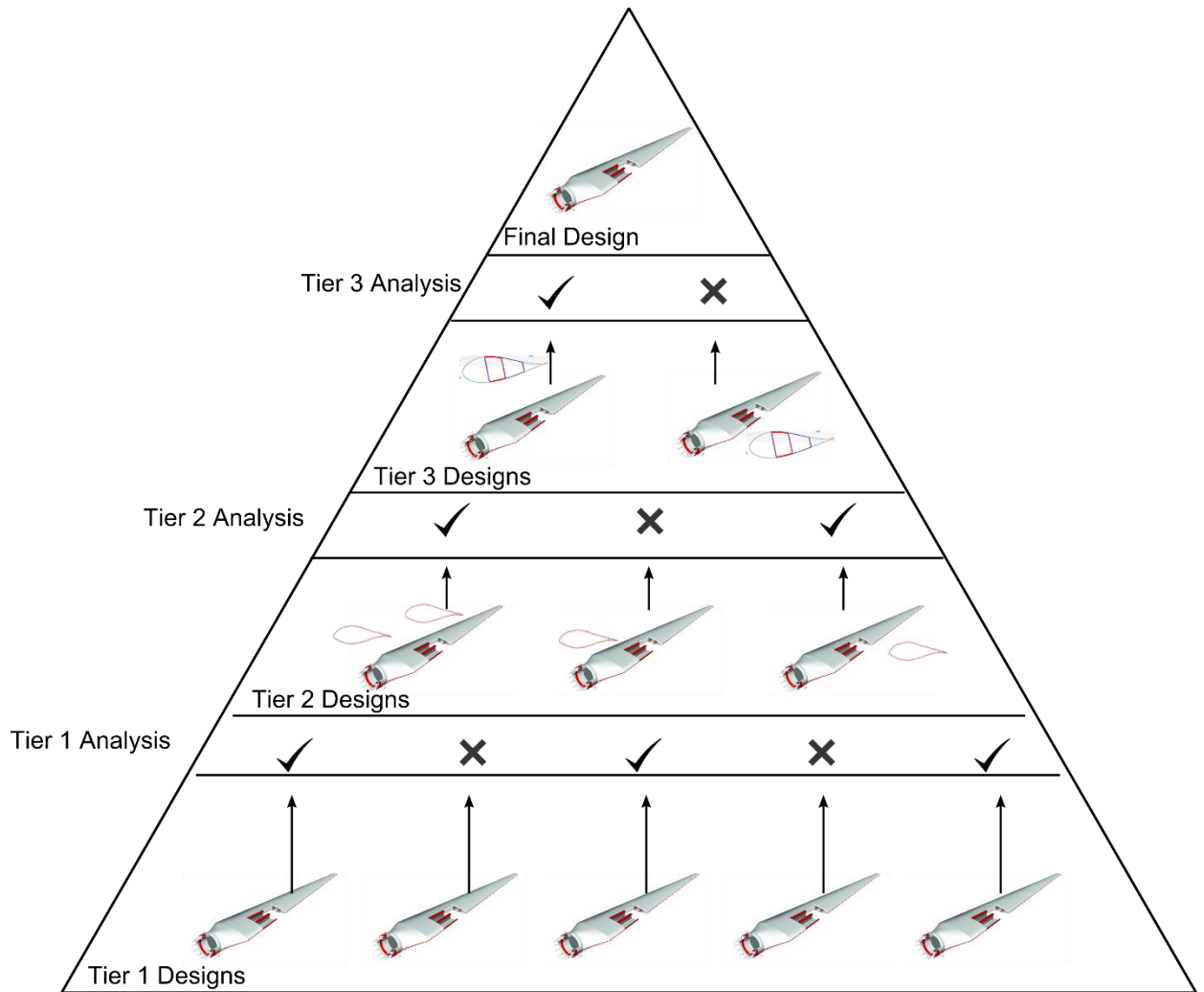


Figure 6-4: Refinement of Design through three-tier strategy manufacturing analysis

### 6.2.3.1 Tier 1: Initial feasibility analysis

The initial tier model matches the preliminary design stage when only a rough idea of the blade dimension is provided based on the wind blade capacity and local wind conditions (Figure 6-5), as provided by the wind blade aerodynamics analysis. The manufacturing module at tier 1 level depends on the one-dimensional Darcy's law to estimate the fill times at the cross section with the longest chord length (Figure

6). The user can choose a typical family of fabrics, such as carbon or glass, and then the controller pulls out the “typical” fabric permeability from the material library. This value is based on the current experience, and, in the long run, may be adjusted to suit the best current practice. Same strategy is used when choosing a family of resins so that a constant isothermal viscosity can be input into the manufacturing analysis model. The processing method used is sequential infusion under vacuum, in which a series of infusion lines are placed parallel along the blade surface with a fixed line spacing. The infusion lines are opened sequentially once the resin reached the trigger point on the tooling side of the blade surface (Figure 6-2). To approximate this process, 1D sequential infusion is specified along the infusion direction of the blade at the location that has the largest chord length. This approximation will return an approximate fill time back to the designer in seconds for a set of input as shown in Figure 6-7. In this example, a tool infusion time module is developed and integrated with other manufacturing, structural and financial analysis modules to return an integrated approximation result which enables the designer to explore a large number of wind blade geometric combinations within the required range, and down select the decision of the blade size based on the real-time simulation results. Along with the beam model stress analysis to calculate the blade’s loading condition, this design step allows one to structurally eliminate unsuitable or overly costly sets of parameters. The acceptable designs, now with properly determined dimensions are then passed on to tier 2 analysis module.

Turbine Capacity: 3MW  
Wind Class: IIa  
Blade length: 45 - 56m

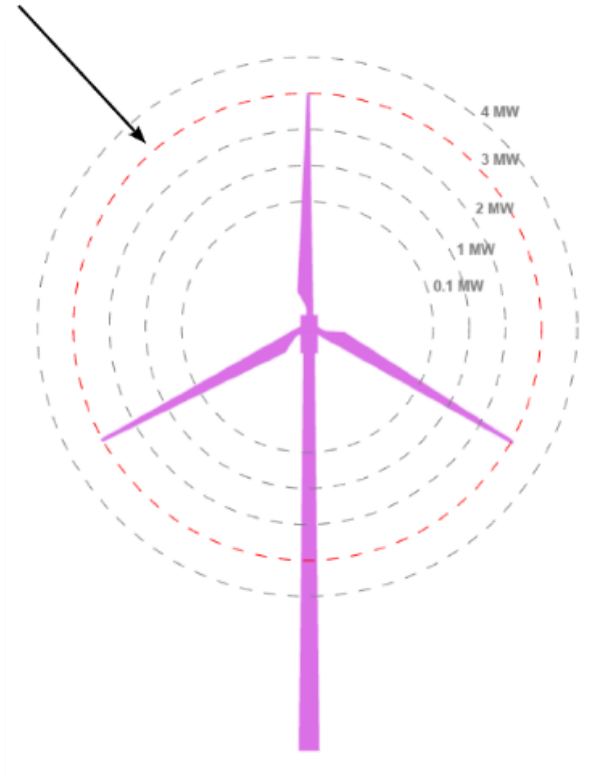


Figure 6-5: Preliminary design parameters based on wind blade capacity with the largest imprecision

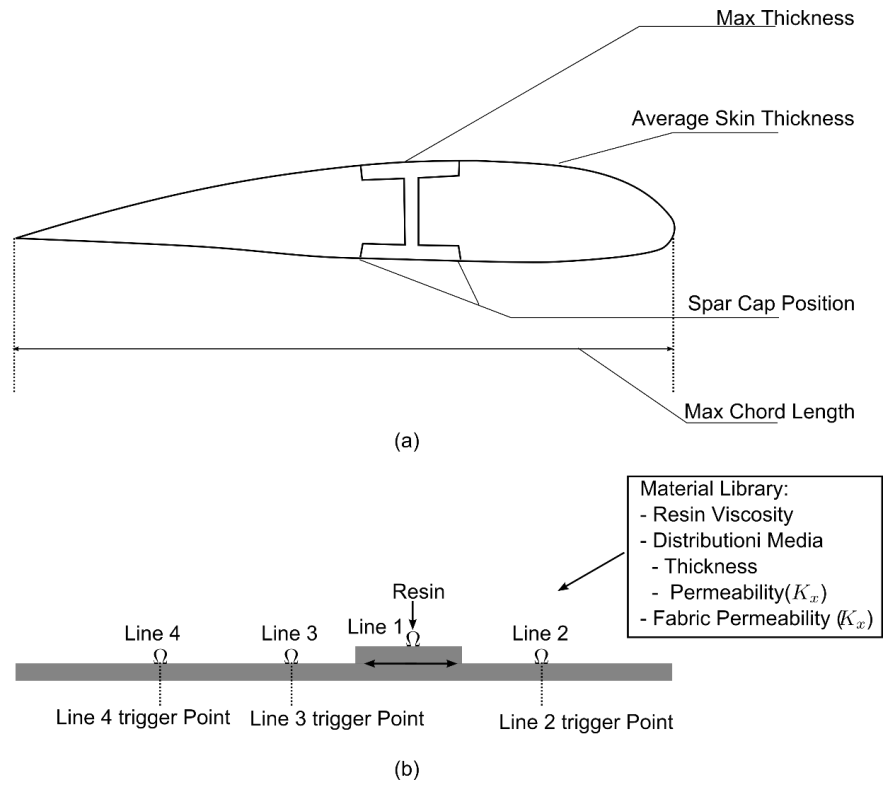


Figure 6-6: (a) Tier 1: Blade geometric approximation at the cross section with largest chord length; (b) 1D flow simplification using sequential injection combining the geometric approximation parameters and material properties.

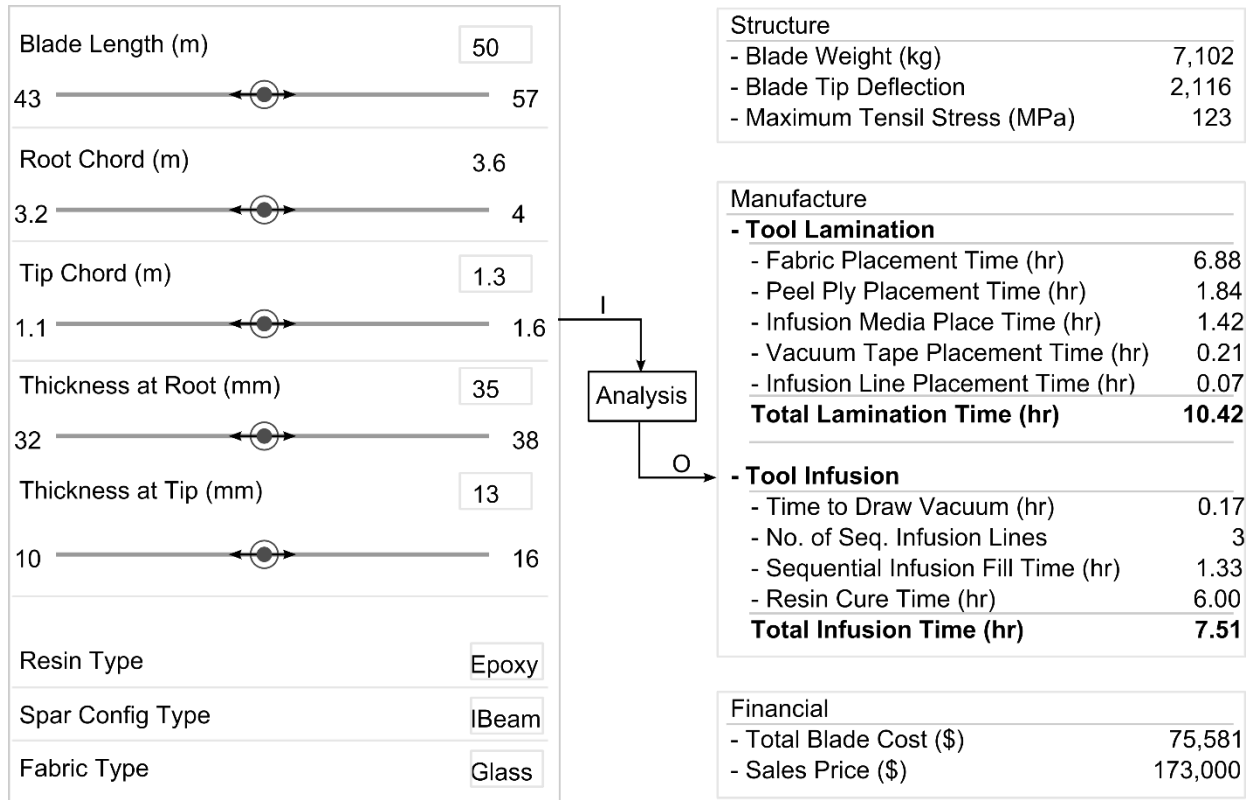


Figure 6-7: Tier 1 input and output (tool infusion analysis package is developed in this work and is combined along with other packaged developed by cooperating teams to generate approximate infusion times and financial cost)

### 6.2.3.2 Tier 2: Analysis for a fixed dimension.

The tier one analysis helps the designer to determine the characteristic part dimensions, such as blade length and chord length at root and tip. At tier 2, aerodynamics simulation is then applied to determine the actual airfoil shape along the entire longitude direction of the blade. Stress analysis can now be carried on with a proper shell structure to further help the designer with the planar form arrangement (Figure 6-8). This provides improved description of geometry and more precise material specification of the laminate pattern by quantifying typical fabric layer orientation ( $0^\circ/45^\circ/90^\circ$ , Carbon/Glass) of the layup on the wind blade surface. Next,

the fabric material selected is passed to the manufacturing analysis simulation model. Then, the user will specify the resin type and transient viscosity and gel-time limitations from the material library. In addition, other detailed processing parameters including infusion line type and spacing, infusion media type are selected by the user (Figure 6-9). Next, a set of 3D meshes are built for each blade part that is going to be undergoing manufacturing analysis independently, based on the precise description of the wind blade surface geometry. Infusion lines are placed on top of the mesh in the format of 1D elements, and material property for each element is automatically calculated based on the selected fabric type, infusion line type, and infusion media. Finally, a well-established FE mold filling simulation software LIMS[27,28] is executed to return the fill time and flow pattern back to the designer (Figure 6-10).

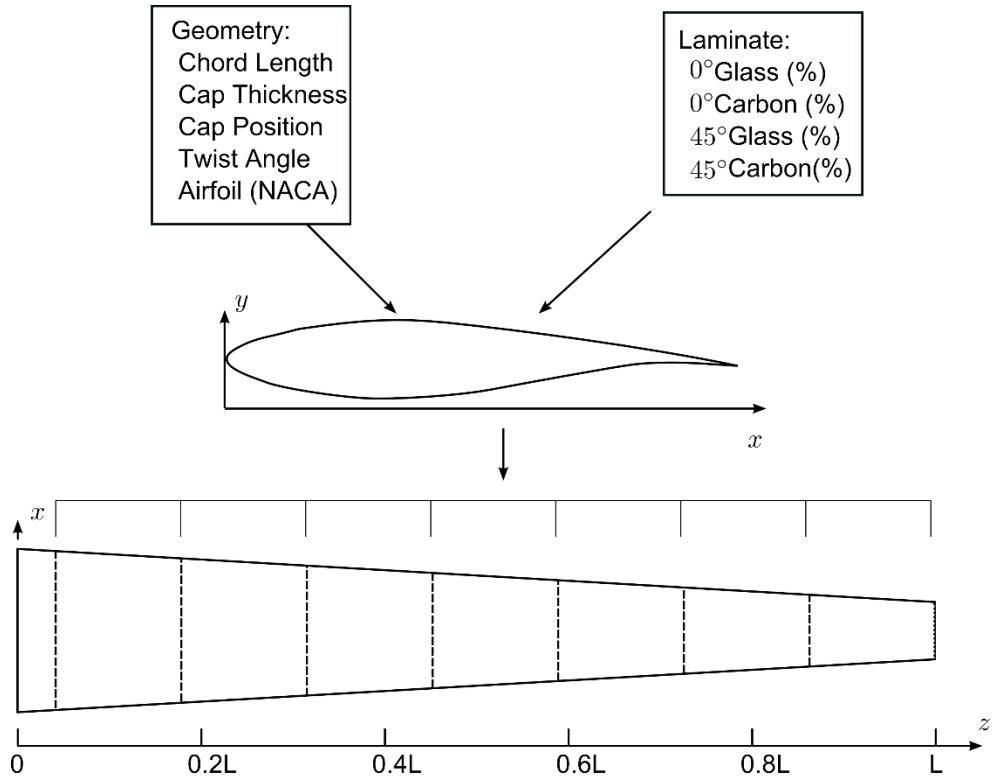


Figure 6-8: Wind blade geometry specification from aerodynamic analysis and laminate material specification for stress analysis

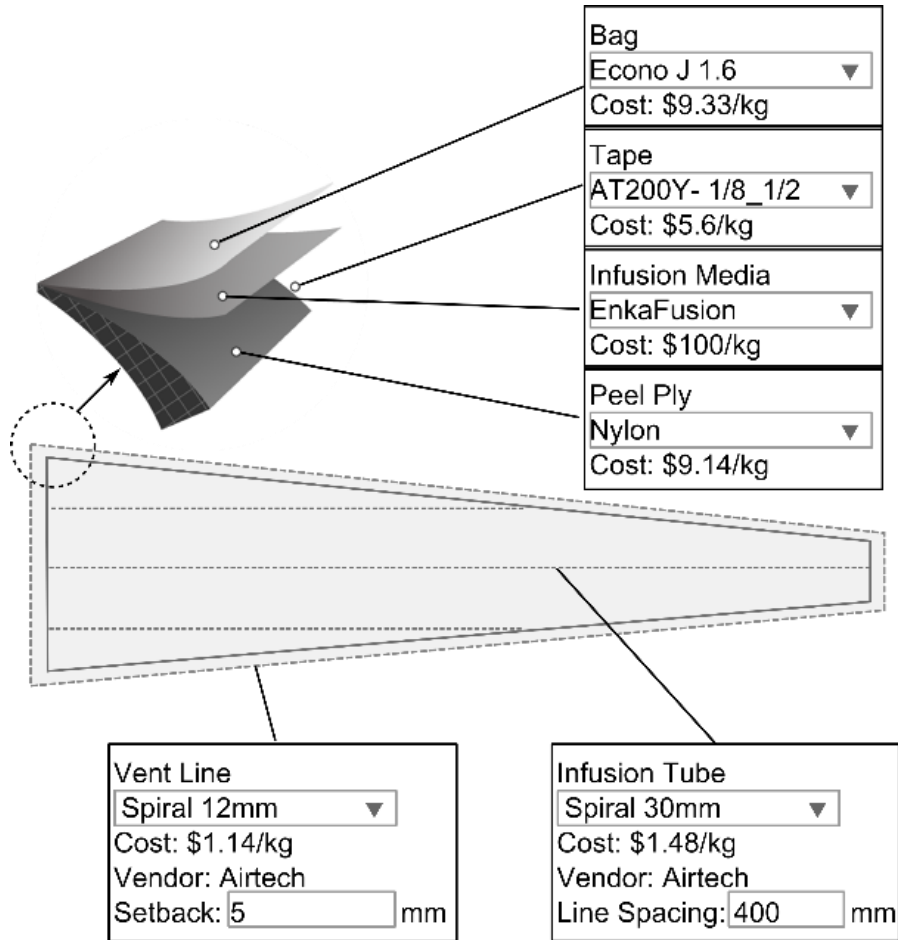


Figure 6-9: Tier 2 material specification for infusion analysis

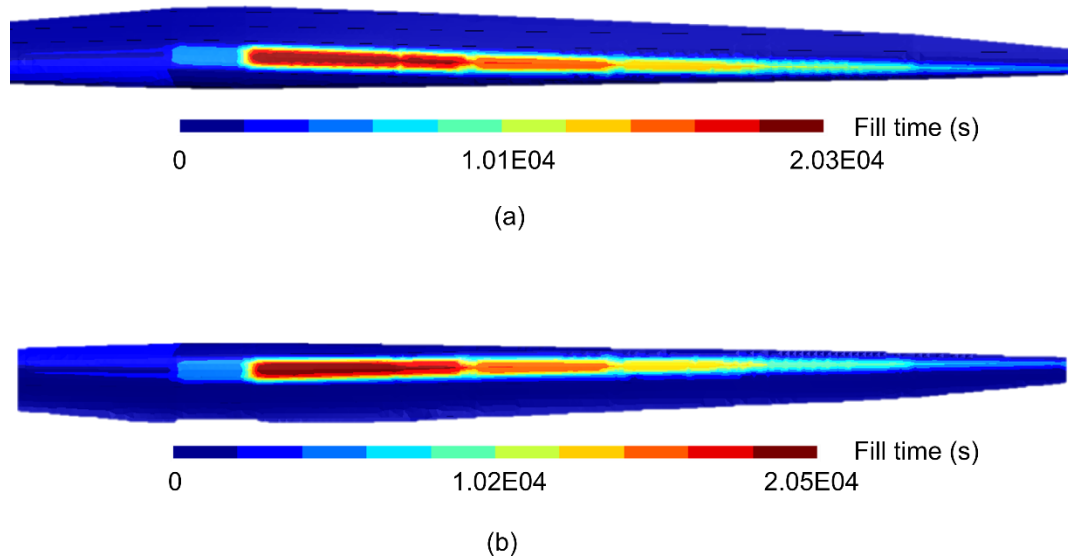


Figure 6-10: LIMS tier 2 output for (a) blade top skin and (b) blade bottom skin, which are infused separately in the manufacturing process simulation.

### 6.2.3.3 Tier 3: Cross-section model introduction

In tier 3, the detailed laminate information is specified (Figure 6-11). This is added into the design parameters for both full structural analysis and processing simulation. The process simulation is again carried on with relatively coarse 3D mesh that is extruded, but on this tier the material properties are no longer “typical” values but rather effective properties based on the laminate information. This provides accurate filling simulation in the blade plane, but is too coarse to determine accurate through-the-thickness flow progression which is crucial for infusion of thick parts, particularly those of varying thickness. To determine that, a series of locations along the longitude direction of the blade are selected and cross-section model is built automatically for the detailed through-thickness flow pattern. The accurate information will help the designer refine the design further and is sufficient for final decision making.

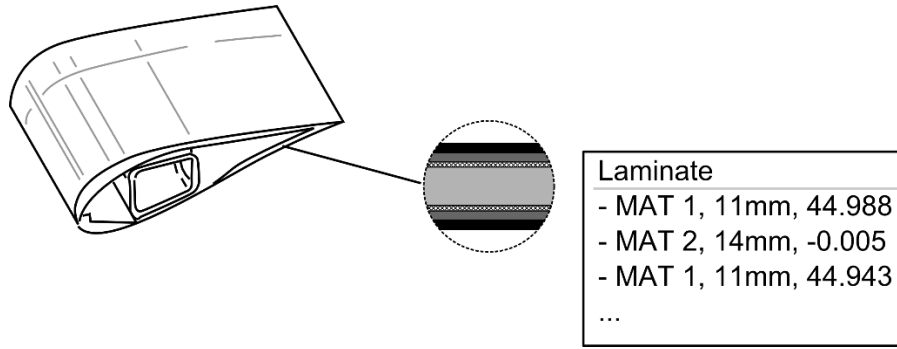


Figure 6-11: Tier 3 laminate specification

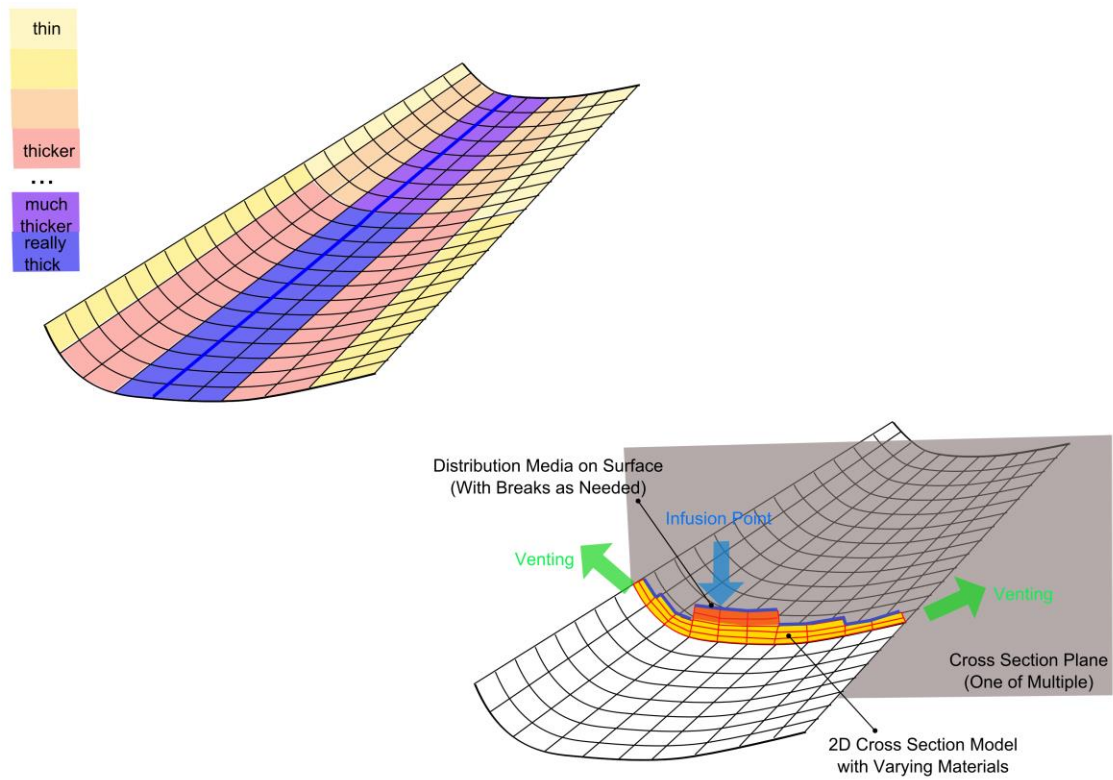


Figure 6-12: Cross section model schematics.

#### **6.2.4 Summary**

This section introduces a methodology of software construction strategy using a management method that supports complicated composite design and analysis tool. Manufacturing packages, structural analysis modules, aerodynamic modules and cost analysis models are integrated together into three tiers. The integration of manufacturing analysis within the software is the focus, but this management approach has also been used on the other two analysis (aerodynamic and structural). In addition, same methodology of separating variables into low to high precision levels can be extended to other analysis tools within the approach. It is shown that this management strategy resembles the practical work flow of design practices for complicated composite part design by taking into account the parameter uncertainties. Therefore, the developed methodology as packaged in a software tool can aid the designer to downsize the design space and select parameters effectively and accurately.

#### **6.3 Multi-tier integration of processing simulation with CAD software SimXpert**

This section will present another software integration framework to fully harness the ability of LCM mold filling simulation packages to simulate the LCM manufacturing processes. To satisfy the requirement in different design stages, it is necessary to perform the manufacturing analysis at three different levels: (Figure 6-13)

- Level 0: Feasibility analysis before flow modeling:  
This level performs the geometry check which will essentially eliminate the elementary conflicts that would make the manufacturing impossible no matter how the resin is introduced.
- Level 1: Selection of processing method and geometric feature recognition:  
Preliminary resin injection scheme is simulated for RTM, VARTM

and RTM-Light; additional infusion schemes can be added as necessary. Different injection and vent schemes are determined and ranked. The scheme that will satisfy manufacturing constraints is returned. Geometric features that have the potential to introduce flow disturbances that will affect the success of mold filling are flagged.

- Level 2: Analysis of sensitivity to disturbances:  
Before exploring this level, the part design already has an injection plan and has identified multiple geometric features that are susceptible to flow disturbances. A full variability analysis is then conducted for the designed part, and a scenario space which represents every possible scenario in manufacturing practice is generated. Injection completion time and the injection location and vent plan is then returned back to the designer.

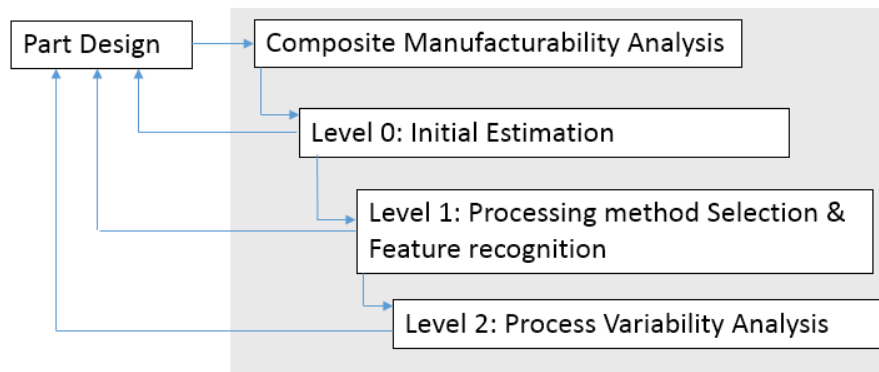


Figure 6-13: Three levels of composite manufacturability analysis

Finally, these three levels of manufacturability analysis are coupled with the commercial CAE software MSC SimXpert. These three levels are arranged in cascade style in the design-manufacturability iteration cycle, and the designer can readily get access to each of the three levels of manufacturability analysis from the design

workbench. Injection and vent plans are returned to the designer with suggestions for modifying the designed part.

**6.3.1 Level 0: Initial feasibility analysis**

At level 0 (Figure 6-14), only a rudimentary analysis is implemented on the geometric limitations of the manufacturing facility and the basic fiber and resin properties. Simple Boolean comparisons between the facility capabilities (weight, size, structure thickness, temperature, humidity, vacuum level, etc.) and the processing needs and geometric description of the part are made. Also the fill time to fill the longest dimension of the part is returned and compared to the selected resin system’s gel time. It is important to note that no further analysis is performed until all of the tests at level 0 are passed.

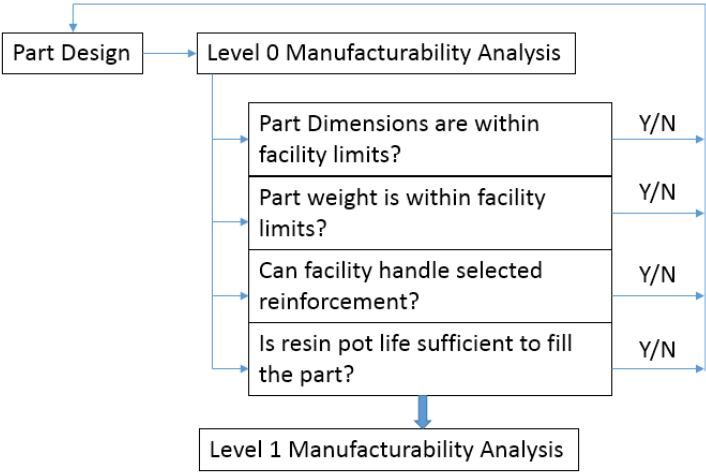


Figure 6-14: Flow chart of Level 0 feasibility estimation based on part geometry dimensions for a preliminary facility requirement check

### **6.3.2 Level 1: Comparison and Selection of Processing Method(S) and feature recognition**

At level 1, the part geometry is analyzed through the mesh file and potential race-tracking channels that will affect the filling time and the success rate of the finished part are identified. The part can be manufactured by either injecting the resin through a small diameter hole known as a gate injection or through a channel which is known as infusion line under vacuum. The selection of this location can be either specified by the user, or the algorithm can automatically calculate the injection gate for RTM, infusion lines for VARTM, and select outer boundaries for RTM-Light.

Race-tracking channels are very likely to occur along the outer edges, around inserts, fabric folds, and the bifurcation lines of the part, and are source of flow disturbances during the mold filling stage. These channels are automatically identified from the CAD geometry and are marked on the meshed part surface, which are categorized into outer edged, folds, and bifurcation lines, accordingly (as described in chapter 4 Figure 6-15) [12]:

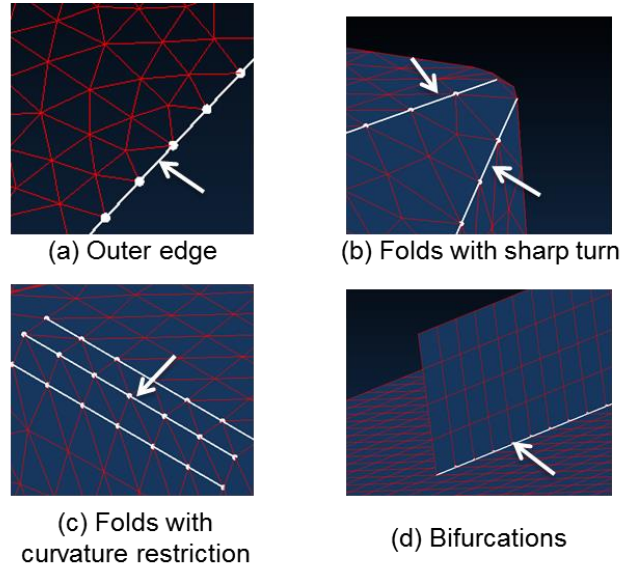


Figure 6-15: Automatic feature recognition of potential race-tracking channels

After all potential race-tracking regions are identified, three LCM processes are initiated for the part: RTM, VARTM and RTM-Light. The injection gate for RTM process is selected by projecting the part centroid along one of the three principle axis of moment of inertia that has the largest value. For VARTM, the intersection line between the part surface and the surface that goes through the centroid and is perpendicular to the smallest principal axis of the moment of inertia. Outer boundary of the part is selected as the infusion line for RTM-Light process. Each infusion scenario is then run through LIMS twice: once with no race-tracking, and again with every race-tracking region active. After the results are calculated and stored, a simple formula is used to determine the infusion scenario that reduces fill time.

$$\begin{aligned}
 Cost = w_1 \times T_{cycle} + w_2 \times L_{racetracking} + w_3 \times N_{vents} + w_4 \\
 \times L_{infusion}
 \end{aligned}
 \tag{6.1}$$

in which  $T_{cycle}$  is the cycle time,  $L_{racetracking}$  is the length of race-tracking channels,  $N_{vents}$  is number of vents, and  $L_{infusion}$  is length of infusion line (0 for RTM). This reduces the number of infusion choices based on both feasibility and ease of manufacturing. The processing method with the lowest cost value is passed to next level's simulation.

### **6.3.3 Level 2 – Analysis of sensitivity to disturbances**

#### **6.3.3.1 Assigning race-tracking properties**

Race-tracking strength is directly associated with the channel cross-section area. Although race-tracking channels may not be repeatable from one part to the next during the manufacturing process, statistical analysis could be used to aid the solution. A probability distribution function from manufacturing floor data (for example the part tolerances) can be introduced to define channel size variations. The same probability distribution function can then be used to describe the statistical variations of race-tracking strength of these channels. Also, it is found that the flow pattern does change significantly as one goes from no race-tracking to low race-tracking, but does not vary much as the race-tracking strength is increased. Therefore, a coarse discretion of the probability distribution by assigning probabilities for no race-tracking, and low race-tracking for each channel is sufficient to capture the race-tracking behavior (Figure 6-16).

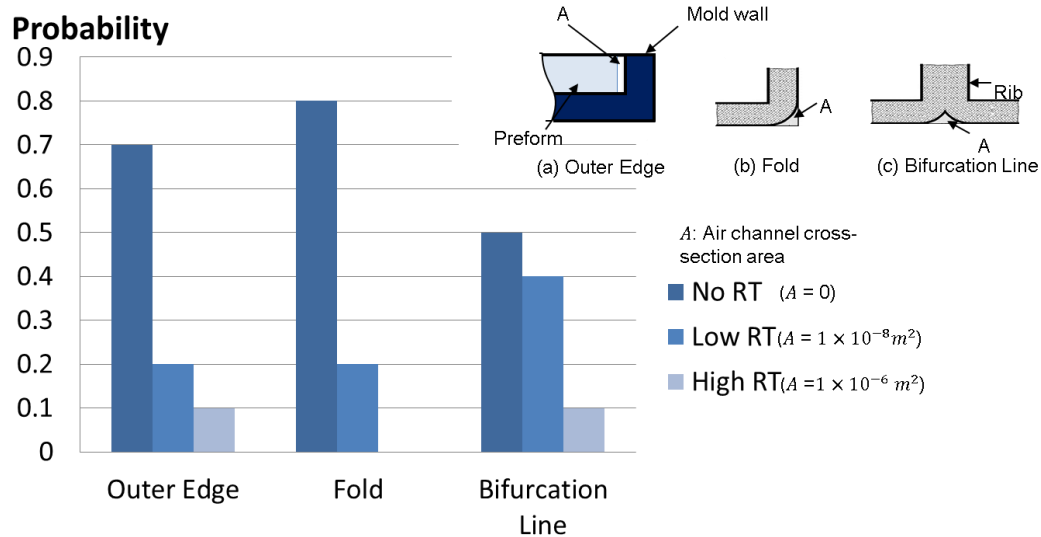


Figure 6-16: Discretized race-tracking strength probability distribution for (a) outer edge, (b) folding lines and (c) bifurcation lines

### 6.3.3.2 Generation of scenario space

Using this discretized race-tracking strength probability distribution, one can build a list of combinatory scenarios, each of which is associated with a certain probability as shown in Figure 6-16. An accurate assessment of the race-tracking probability can thus be ascertained.

For the example of the complex geometry part (trailer) shown in Figure 6-17 (a) where ten possible race-tracking edges have been identified by our edge detection algorithm, the race-tracking strengths and their probability provided in Figure 4 are assigned to the elements in these channels to describe the race-tracking behavior of the channel. Assuming that all ten channels are independent and only two race-tracking strengths are associated with them, a total number of  $2^{10} = 1024$  permutations of the flow scenarios are possible. Each scenario has an associated probability as shown in the scenario space generated in Figure 6-17 (b).

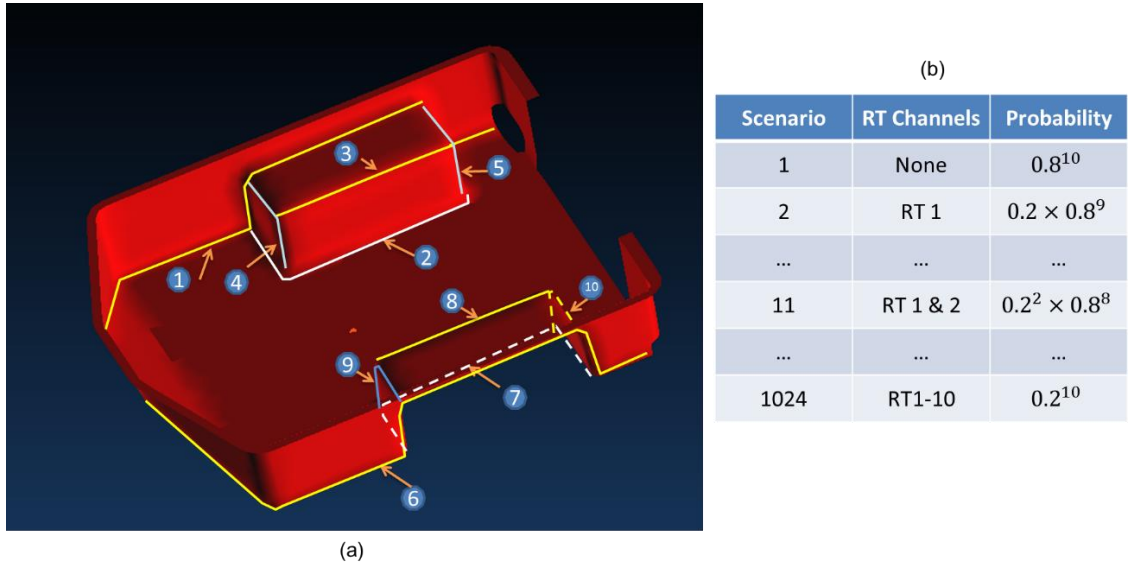


Figure 6-17: (a) Potential race-tracking channels identified around folding lines for a trailer; (b) Scenario space generated with probability distribution in Figure 6-16

### 6.3.3.3 Vent plan analysis

A vent analysis is then executed based on the distance results for each scenario in the list. First, vents should be assigned on the mold wall where the resin arrives last. Second, the regions where the flow fronts meet should also be the location for a vent, because at these locations, air is compressed and trapped within the flow fronts as they merge and cannot dissolve in the resin and needs a vent to escape. These two categories of regions are selected and set as vents based on the distance results for each node on the mesh [12-14].

Vent location is determined for selected gate location for all the scenarios. Each vent location is weighted with the probability of that scenario. After repeating this for each scenario in the list, the weighted node probabilities are superimposed for the entire space to produce a probability map which denotes the probability for a node

to remain unfilled. Thus one can generate a vent fitness map from this information. Nodes that are most likely to be unfilled should be set as vents.

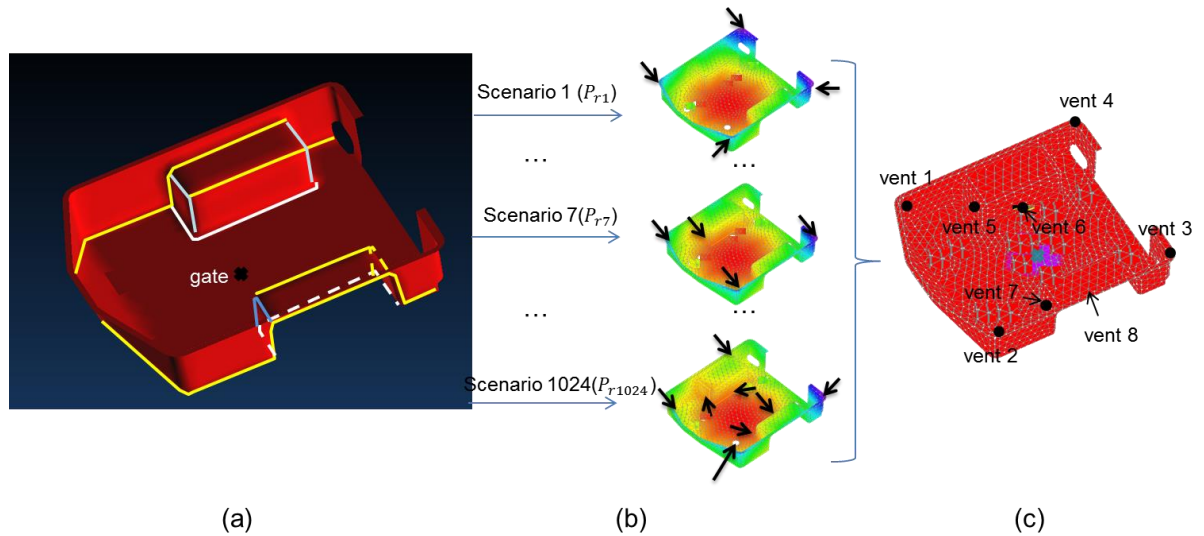


Figure 6-18: Venting plan for the trailer using the RTM process. (a) detect CAD part with 10 race-tracking channels (b) generate vents for each scenario in the list and weight the nodes set as vent with scenario probability (c) superimpose the venting nodes for all scenarios and generate final venting plan.

#### 6.3.3.4 Integrate design-manufacturability iteration

The three levels of manufacturing analysis are integrated with CAE software MSC SimXpert. The interface between MSC SimXpert and manufacturability analysis packages will allow the designer to choose the fiber reinforcement, resin system, and the processing parameters such as which process to use, RTM or VARTM or RTM Light, and where to place the injection gate or the infusion line. If these processing parameters are not set by the designer, the package can generate the optimal injection gate and infusion lines automatically based on the geometry and fiber laminate design pattern. The Level 0 and Level 1 will return the simulation results and feedback in real

time. The Level 3 variability analysis will return the optimal manufacturing design and simulations and modification suggestions for the part design in hours as it does take longer to complete the full simulation analysis with all the possible permutations. The workbench of the manufacturability analysis packages in CAE software MSC SimXpert is shown in Figure 6-19.

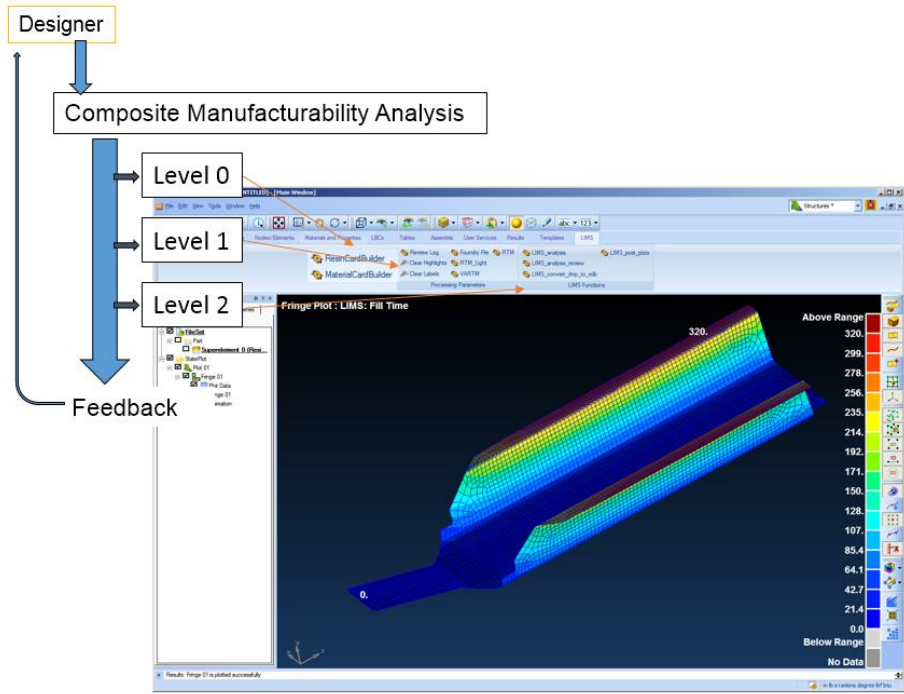


Figure 6-19: Integration of manufacturability analysis packages with CAE software SimXpert

### 6.3.4 Case studies

As an example, complete analysis is performed for the design-manufacturability simulation integration for the part shown in Figure 6-17. After a Level 0 rudimentary test of the part dimensions and weight and comparison with

facility limitations, it is then passed to Level 1 analysis, where ten potential race-tracking channels are recognized and flagged. Then three different processes are automatically generated to evaluate the manufacturing process to be used for the trailer. The injection gate for RTM process is selected by projecting the part centroid along one of the three principle axis of moment of inertia that has the largest value. For VARTM, the intersection line between the part surface and the surface that goes through the centroid and is perpendicular to the smallest principal axis of the moment of inertia. Outer boundary of the part is selected as the infusion line for RTM-Light process. After calculating the cost for the three processes according to Equation 6.1, VARTM with center infusion line is selected as the least expensive process to manufacture the trailer. The trailer along with the infusion plan is then passed to Level 2 analysis, in which the ten potential race-tracking channels generate  $2^{10} = 1024$  scenarios using the race-tracking strength probability discretization in Figure 4. Six vents are returned after Level 2 analysis is complete, and geometry features along the folding lines are flagged for large curvatures and returned back to the designer, as shown in Figure 6-20.

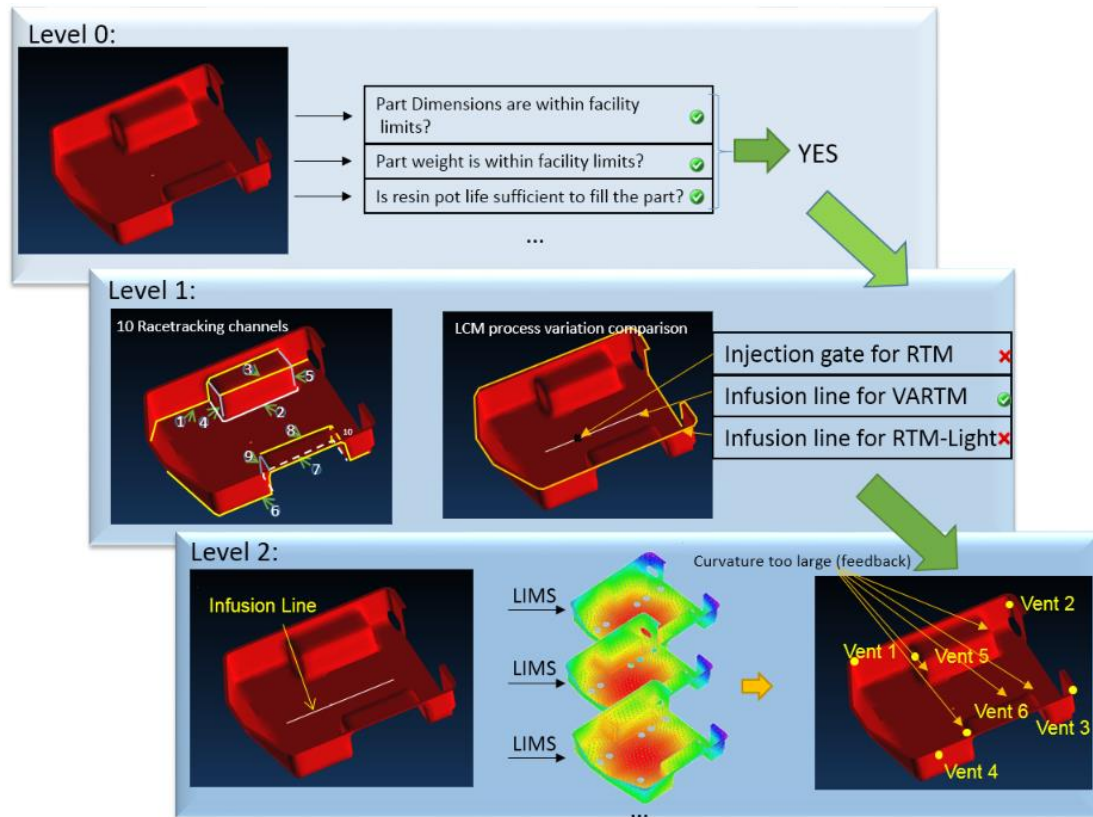


Figure 6-20: Three levels of manufacturability analysis for the trailer

### 6.3.5 Summary

A seamless package is presented that can provide hierarchical manufacturability analysis of a composite part to the designer. This program offers the composite part designer three levels of manufacturability analysis. The initial estimate of the part (level 0) provides the designer an estimated filling time. If the part passes the level 0 test, it then performs level 1 analysis. Potential race-tracking channels that may introduce flow disturbances during manufacturing are flagged and the injection schemes for three different LCM processes are either assigned by the designer or generated by the program automatically to perform the flow analysis for the ideal no

race-tracking case and for the case where race-tracking is present at each identified race tracking channel. The cost analysis (fill time cost in this example, but can be extended to detailed cost analysis using equation 6.1) selects the process and the injection location and is ready for level 2 manufacturability analysis in which a robust venting plan is generated by considering all the possible permutations of possible race-tracking effect that may occur during manufacturing. Cycle time information and infusion/vent plan is then provided to the designer, who then has the option to modify the design to improve manufacturability.

## **Chapter 7**

### **CONCLUSIONS, CONTRIBUTIONS, AND FUTURE WORK**

#### **7.1 Contributions and Conclusions**

The knowledge of LCM processes is growing and mold flow simulation models are becoming more accurate and versatile to describe practical composite manufacturing processes. However, this does not automatically give designers the ease of using these well-defined packages in guiding part design for the purpose of satisfying processing constraints and requirements. The connections between part design and processing simulations and how to seamlessly integrate these two modules are hardly obvious. This work, however, has made several important contributions to fill in this gap and illustrate frameworks to use composite processing simulations effectively so as to guide robust part design.

First, a set of generalized models are developed to automate the determination of process parameters for the designers after the part is drawn. These models free the designers from the intricate task of defining sufficiently robust processing parameters, and therefore reveal a direct and more accurate correlations between part design and its effect during composite manufacturing. Without being an experienced process engineer, the designer can still have confidence to assert that the results returned from the process simulation packages are directly correlated with input drawing after these models are added on top of the interface of process simulation packages. Therefore, the designer can make more informative decisions to implement the design-simulation iterations, and meanwhile with high efficiency and accuracy.

Next, this work improves the LCM simulation packages to reflect the practical composite part manufacturing variability by introducing stochastic models. This stochastic behavior during the mold filling step in LCM processes introduces a series of implicit parameters in process simulation and usually beyond the designer, or the software user's ability to specify. Part geometries are filtered before passing into LCM simulations and a strategic methodology is developed to automatically flag the geometric features that have the potential of generating severe process disturbances. A combinatorial framework is then developed to discretize the scenario space and use the LCM simulation engine as a tool to aggregate the results and generate probability predictions upstream designing for geometry modifications and downstream for designing injection and venting schemes that are sufficiently robust to manufacture a part without voids.

Although full probability analysis brings the designer a more comprehensive and accurate representation of practical manufacturing scenarios, in some cases the calculation time cost is not realistic. Therefore, this work developed another fast yet accurate mold flow simulation substitution tool to reduce the time, yet retain the results' quality when batch runs are submitted. A discretized one-dimensional flow model is developed to predict the fill time based on the distance resin travels. Combined with Dijkstra's algorithm, this model is then implemented on spatial surface meshes to calculate fill time for each node and generate flow development pattern. The computational model developed can predict the mold filling pattern for complex parts even with variable permeability or thickness of the fiber preform, and can capture the disturbed flow behavior along any difficult geometric features at a fraction of the computational cost while retaining the accuracy which is very useful

when one needs to conduct a stochastic analysis that takes into account all permutations of expected flow disturbances.

Finally, this work introduced two unique software packages that integrate composite part design and LCM simulations using cascade style design-simulation patterns. The first example was for composite wind blade design and manufacture. The second example is a unique virtual manufacturing floor called Artificial Vehicle Manufacturing (AVM) simulation software. Two different management strategies are developed and implemented in these two packages when integrating multi-disciplinary analysis modules with CAD software. Both mock up the practical design flow by separating each software in multiple tiers with increasing simulation accuracy and less uncertainty in the definition of design parameters. Therefore, the intuitive strategy will be more natural for the designer to use and make progressive decisions.

In conclusion, major contribution of this work are listed below:

1. Developed optimization algorithms to search for resin infusion/injection schemes for LCM processes effectively and accurately.
2. Formulated and implemented methods to integrate stochastic behavior of mold flow into the design-manufacturing analysis cycle to reflect the LCM scenarios and provide realistic prediction and suggestions to the designer;
3. Developed methods and framework to seamlessly integrate the composite part geometry and material design with LCM simulations with examples that addressed complex geometrical components.
4. Created distance-based model to execute fast mold flow simulations to provide an alternative simulation engine for LCM processes to efficiently run the methods and algorithms developed.
5. Algorithms, methods and models developed in this work can be used to generalize LCM processes combined with composite part designs that include complex geometrical features and material properties.

## 7.2 Future Work

Based on the presented work of this dissertation, three future directions are proposed to address further questions regarding the integration between composite processing simulations and the part design.

First, the optimization methods introduced can be expanded to other generalized LCM processes. Currently, the optimizers developed in this dissertation focuses on RTM processes which use either multiple gate injection or line injection schemes. However, these methods can be modified further to be applied in other LCM variations such as VARTM where line infusion is used and RTM-Light where multiple gates can be fabricated within the system.

Second, probability analysis frameworks introduced in this work combined stochastic models in LCM simulation package LIMS together to generate a comprehensive manufacturing scenario prediction. However, this method requires a large amount of calculation resources allocated to run LIMS by listing all scenarios generated by discretized stochastic models. To reduce the calculation time, apart from searching for faster mold simulation alternatives, it is possible to integrate the material permeability probabilities and stochastic models within LIMS when calculating the flow advancement using previous time step's results. Therefore, number of simulation required to run can be greatly reduced and a lot of repeated calculations are avoided. Thus, the designer can get much faster feedback for a more comprehensive and accurate processing predictions.

Finally, the integrated wind blade design and simulation software demonstrates the potential of repackaging various optimization tools into custom frameworks tailored for different industrial purposes. Meanwhile, alternative approaches such as machine learning frameworks can be modified to integrate optimization modules and

advanced LCM simulation packages to address composite part design iterations for general cases.

## REFERENCES

- [1] Advani SG, Sozer EM. Process modeling in composites manufacturing. CRC Press; 2012.
- [2] Kang MK, Jung JJ, Lee W II. Analysis of resin transfer moulding process with controlled multiple gates resin injection. *Compos Part A Appl Sci Manuf* 2000;31:407–22. doi:10.1016/S1359-835X(99)00086-X.
- [3] Chan AW, Morgan RJ. Sequential multiple port injection for resin transfer molding of polymer composites. *SAMPE Q* 1992;24:45–9.
- [4] Bickerton S, Stadtfeld HC, Steiner K V, Advani SG. Design and application of actively controlled injection schemes for resin-transfer molding. *Compos Sci Technol* 2001;61:1625–37. doi:10.1016/S0266-3538(01)00064-1.
- [5] Berker B, Barooah P, Sun JQ. Sequential logic control of liquid injection molding with automatic vents and vent-to-gate converters. *J Mater Process Manuf Sci* 1997;6:81–104.
- [6] Mathur R, Advani SG, Fink BK. Use of genetic algorithms to optimize gate and vent locations for the resin transfer molding process. *Polym Compos* 1999;20:167–78.
- [7] Gokce A, Hsiao KT, Advani SG. Branch and bound search to optimize injection gate locations in liquid composite molding processes. *Compos Part A-Applied Sci Manuf* 2002;33:1263–72. doi:10.1016/s1359-835x(02)00047-7.
- [8] Young W-B. Gate location optimization in liquid composite molding using genetic algorithms. *J Compos Mater* 1994;28:1098–113.
- [9] Yu H-W, Young W-B. Optimal design of process parameters for resin transfer molding. *J Compos Mater* 1997;31:1113–40.
- [10] Kim BY, Nam GJ, Lee JW. Optimization of filling process in RTM using a genetic algorithm and experimental design method. *Polym Compos* 2002;23:72–86. doi:10.1002/pc.10413.
- [11] Lin MYY, Murphy MJJ, Hahn HTT. Resin transfer molding process optimization. *Compos Part A Appl Sci Manuf* 2000;31:361–71. doi:10.1016/S1359-835X(99)00054-8.
- [12] Jiang S, Zhang C, Wang B. Optimum arrangement of gate and vent locations for RTM process design using a mesh distance-based approach. *Compos Part A*

- Appl Sci Manuf 2002;33:471–81.
- [13] Ye X, Zhang C, Liang Z, Wang B. Heuristic algorithm for determining optimal gate and vent locations for RTM process design. *J Manuf Syst* 2004;23:267–77.
- [14] Luo J, Liang Z, Zhang C, Wang B. Optimum tooling design for resin transfer molding with virtual manufacturing and artificial intelligence. *Compos Part A Appl Sci Manuf* 2001;32:877–88.
- [15] Jiang S, Zhang C, Wang B. A process performance index and its application to optimization of the RTM process. *Polym Compos* 2001;22:690–701.
- [16] Du Q, Faber V, Gunzburger M. Centroidal Voronoi tessellations: applications and algorithms. *SIAM Rev* 1999;41:637–76.
- [17] Lugo J, Simacek P, Advani SG. Analytic method to estimate multiple equivalent permeability components from a single rectilinear experiment in liquid composite molding processes. *Compos Part A Appl Sci Manuf* 2014;67:157–70.
- [18] Wang J, Simacek P, Advani SG. Fast Mold Filling Simulation Based on the Geodesic Distance Calculation Algorithm for Liquid Composite Molding Processes. *Comput Model Eng Sci* 2015;107:59–79.
- [19] Du Q, Emelianenko M, Ju L. Convergence of the Lloyd algorithm for computing centroidal Voronoi tessellations. *SIAM J Numer Anal* 2006;44:102–19.
- [20] Lloyd SP. Least squares quantization in PCM. *Inf Theory, IEEE Trans* 1982;28:129–37.
- [21] Cai Z. Simplified mold filling simulation in resin transfer molding. *J Compos Mater* 1992;26:2606–30.
- [22] Jovanovic V, Manoochehri S, Chassapis C. Parameter estimation for resin transfer molding. *Eng Comput* 2001;18:1091–107.
- [23] Šimáček P, Advani SG. Permeability model for a woven fabric. *Polym Compos* 1996;17:887–99.
- [24] De Parseval Y, Pillai KM, Advani SG. A simple model for the variation of permeability due to partial saturation in dual scale porous media. *Transp Porous Media* 1997;27:243–64.
- [25] Di Fratta C, Klunker F, Trochu F, Ermanni P. Characterization of Textile

Permeability as a Function of Fiber Volume Content with a Single Unidirectional Injection Experiment. *Compos Part A Appl Sci Manuf* 2015.

- [26] Brusckie M V, Advani SG. A finite element/control volume approach to mold filling in anisotropic porous media. *Polym Compos* 1990;11:398–405. doi:10.1002/pc.750110613.
- [27] Šimáček P, Advani SG. Desirable features in mold filling simulations for liquid composite molding processes. *Polym Compos* 2004;25:355–67.
- [28] Simacek P, Advani SG, Binetruy C. Liquid injection molding simulation (LIMS) a comprehensive tool to design, optimize and control the filling process in liquid composite molding. *JEC--Composites* 2004;8:58–61.
- [29] Bickerton S, Šimáček P, Guglielmi SE, Advani SG. Investigation of draping and its effects on the mold filling process during manufacturing of a compound curved composite part. *Compos Part A Appl Sci Manuf* 1997;28:801–16.
- [30] Luo J, Liang Z, Zhang C, Wang B. Optimum tooling design for resin transfer molding with virtual manufacturing and artificial intelligence. *Compos Part A-Applied Sci Manuf* 2001;32:877–88. doi:10.1016/s1359-835x(00)00147-0.
- [31] Lin MY, Murphy MJ, Hahn HT. Resin transfer molding process optimization. *Compos Part A-Applied Sci Manuf* 2000;31:361–71. doi:10.1016/s1359-835x(99)00054-8.
- [32] Wang J, Andres E, Simacek P, Advani SG, Mazzia A, Pini G, et al. Use of Flow Simulation to Develop Robust Injection and Vent Schemes that Account for Process and Material Variability in Liquid Composite Molding Process. *Comput Model Eng Sci* 2012;88:155–82.
- [33] Wang J, Simacek P, Advani SG. Use of Centroidal Voronoi Diagram to find optimal gate locations to minimize mold filling time in resin transfer molding. *Compos Part A Appl Sci Manuf* 2016;87:243–55. doi:10.1016/j.compositesa.2016.04.026.
- [34] Bickerton S, Advani SG. Characterization and modeling of race-tracking in liquid composite molding processes. *Compos Sci Technol* 1999;59:2215–29. doi:10.1016/s0266-3538(99)00077-9.
- [35] Liu B, Bickerton S, Advani SG. Modelling and simulation of resin transfer moulding (RTM)—gate control, venting and dry spot prediction. *Compos Part A Appl Sci Manuf* 1996;27:135–41.

- [36] Ba W, Ren N, Cao L. Geometry of 3D MAT and its application to moulding surfaces. *Graph Models* 2015;82:1–12. doi:10.1016/j.gmod.2015.09.004.
- [37] Hsiao K-T, Devillard M, Advani SG. Simulation based flow distribution network optimization for vacuum assisted resin transfer moulding process. *Model Simul Mater Sci Eng* 2004;12:S175–90. doi:10.1088/0965-0393/12/3/S08.
- [38] Kessels JFA, Jonker AS, Akkerman R. Optimising the flow pipe arrangement for resin infusion under flexible tooling. *Compos Part A Appl Sci Manuf* 2007;38:2076–85. doi:10.1016/j.compositesa.2007.04.008.
- [39] Sánchez F, Domenech L, García V, Montés N, Falcó A, Cueto E, et al. Fast and reliable gate arrangement pre-design of resin infusion processes. *Compos Part A Appl Sci Manuf* 2015;77:285–92. doi:10.1016/j.compositesa.2015.04.018.
- [40] Lu L, Lévy B, Wang W. Centroidal Voronoi tessellation of line segments and graphs. *Comput. Graph. Forum*, vol. 31, 2012, p. 775–84.
- [41] Peyré G, Cohen LD. Geodesic remeshing using front propagation. *Int J Comput Vis* 2006;69:145–56.
- [42] Fletcher PT, Lu C, Pizer SM, Joshi S. Principal geodesic analysis for the study of nonlinear statistics of shape. *IEEE Trans Med Imaging* 2004;23:995–1005.
- [43] Dey TK, Sun J. Defining and computing curve-skeletons with medial geodesic function. *Symp. Geom. Process.*, vol. 6, 2006, p. 143–52.
- [44] Brusckke M V, Advani SG. RTM: Filling simulation of complex three dimensional shell-like structures. *Sampe Q* 1991;23:2–11.
- [45] Brusckke M V., Advani SG. A numerical approach to model non-isothermal viscous flow through fibrous media with free surfaces. *Int J Numer Methods Fluids* 1994;19:575–603. doi:10.1002/flid.1650190704.
- [46] Chan AW, Hwang S-T. Modeling of the impregnation process during resin transfer molding. *Polym Eng Sci* 1991;31:1149–56.
- [47] Coulter JP, Guceri SI. Resin impregnation during the manufacturing of composite materials subject to prescribed injection rate. *J Reinf Plast Compos* 1988;7:200–19.
- [48] García JA, Gascón L, Sánchez F, Chinesta F. Mould filling simulation in RTM processes. *Reveu Des Compos Des Mater Av* 2003:85–98.

- [49] Gascón L, García JA, LeBel F, Ruiz E, Trochu F. A two-phase flow model to simulate mold filling and saturation in Resin Transfer Molding. *Int J Mater Form* 2015. doi:10.1007/s12289-015-1225-z.
- [50] Sánchez F, García JA, Gascón L, Chinesta F. Towards an efficient numerical treatment of the transport problems in the resin transfer molding simulation. *Comput Methods Appl Mech Eng* 2007;196:2300–12. doi:10.1016/j.cma.2006.07.018.
- [51] Soukane S, Trochu F. Application of the level set method to the simulation of resin transfer molding. *Compos Sci Technol* 2006;66:1067–80. doi:10.1016/j.compscitech.2005.03.001.
- [52] Gokce A, Advani S. Combinatorial search to optimize vent locations in the presence of disturbances in liquid composite molding processes. *Mater Manuf Process* 2003;18:261–85. doi:10.1081/amp-120018909.
- [53] Gokce A, Advani SG. Vent location optimization using map-based exhaustive search in liquid composite molding processes. *Mater Manuf Process* 2004;19:523–48. doi:10.1081/amp-120038659.
- [54] Comas-Cardona S, Bickerton S, Deleglise M, Walbran WA, Binetruy C, Krawczak P. Influence of Textile Architectures on the Compaction and Saturated Permeability Spatial Variations. *Recent Adv Text Compos* 2008:3–10.
- [55] Deleglise M, Binetruy C, Krawczak P. Simulation of LCM processes involving induced or forced deformations. vol. 37. 6 SPEC. IS, Elsevier Ltd; 2006, p. 874–80. doi:10.1016/j.compositesa.2005.04.005.
- [56] Comas-Cardona S, Binetruy C, Krawczak P. Unidirectional compression of fibre reinforcements. Part 2: A continuous permeability tensor measurement. *Compos Sci Technol* 2007;67:638–45.
- [57] Lomov SV, Verpoest I. Compression of woven reinforcements: a mathematical model. *J Reinf Plast Compos* 2000;19:1329–50.
- [58] Long AC, Rudd CD, Blagdon M, Kendall KN, Demeri MY. Simulation and measurement of reinforcement deformation during preform manufacture. *Polym Polym Compos* 1996;4:335–41.
- [59] Long AC, Rudd CD. A simulation of reinforcement deformation during the production of preforms for liquid moulding processes. *Proc Inst Mech Eng Part B J Eng Manuf* 1994;208:269–78.

- [60] Robitaille F, Long AC, Rudd CD. Permeability prediction for industrial preforms. *Plast Rubber Compos* 2002;31:238–48. doi:10.1179/146580102225004992.
- [61] Simacek P, Sozer EM, Advani SG. User manual for DRAPE 1.1 and LIMS 4.0 liquid injection molding simulation. *CCM Rep* 1998:1–98.
- [62] Advani SG, Sozer EM. *Process modeling in composites manufacturing*. vol. 59. CRC; 2002.
- [63] Gokce A, Advani SG. Simultaneous gate and vent location optimization in liquid composite molding processes. *Compos Part A-Applied Sci Manuf* 2004;35:1419–32. doi:10.1016/j.compositesa.2004.05.001.
- [64] Boccard A, Lee WI, Springer GS. Model for determining the vent locations and the fill time of resin transfer molds. *J Compos Mater* 1995;29:306–33.
- [65] Dijkstra EW. A note on two problems in connexion with graphs. *Numer Math* 1959;1:269–71.
- [66] Ertas A, Jones JC. *The engineering design process*. Wiley New York; 1996.
- [67] Antonsson EK, Otto KN. Imprecision in Engineering Design. *J Vib Acoust* 1995;117:25. doi:10.1115/1.2838671.
- [68] Fernandes J, Henriques E, Silva A. A Method for Managing Uncertainty Levels in Design Variables during Complex Product Development. *Complex Syst. Des. Manag.*, Springer; 2014, p. 113–24.
- [69] Otto KN, Antonsson EK. Design Parameter Selection in the Presence of Noise 1994;6:234–46.
- [70] Wood KL, Antonsson EK, Beck JL. Representing imprecision in engineering design: Comparing fuzzy and probability calculus. *Res Eng Des* 1990;1:187–203. doi:10.1007/BF01581211.
- [71] Wood KL, Antonsson EK. Computations with imprecise parameters in engineering design: background and theory. *J Mech Transm Autom Des* 1989;111:616–25.
- [72] Schubel PJ. Cost modelling in polymer composite applications: Case study – Analysis of existing and automated manufacturing processes for a large wind turbine blade. *Compos Part B Eng* 2012;43:953–60. doi:10.1016/j.compositesb.2011.11.036.

- [73] Chattopadhyay A, McCarthy TR. Multidisciplinary optimization and design variable sensitivity of helicopter rotor blades using a composite box beam model. *Compos Eng* 1993;3:585–99. doi:10.1016/0961-9526(93)90084-W.
- [74] Zarouchas DS, Makris AA, Sayer F, Van Hemelrijck D, Van Wingerde AM. Investigations on the mechanical behavior of a wind rotor blade subcomponent. *Compos PART B-ENGINEERING* 2012;43:647–54. doi:10.1016/j.compositesb.2011.10.009.
- [75] Lee Y-J, Jhan Y-T, Chung C-H. Fluid–structure interaction of FRP wind turbine blades under aerodynamic effect. *Compos Part B Eng* 2012;43:2180–91. doi:10.1016/j.compositesb.2012.02.026.
- [76] Cairns D, Mastbergen D. Process Modeling and Validation of Resin Infusion Type Manufacturing of Composite Wind Turbine Blades. 44th AIAA Aerosp. Sci. Meet. Exhib., 2006, p. 1201.
- [77] Song F, Ni Y, Tan Z. Optimization design, modeling and dynamic analysis for composite wind turbine blade. *Procedia Eng* 2011;16:369–75.
- [78] Bechly ME, Clausen PD. Structural design of a composite wind turbine blade using finite element analysis. *Comput Struct* 1997;63:639–46. doi:10.1016/S0045-7949(96)00387-2.
- [79] Grujicic M, Arakere G, Pandurangan B, Sellappan V, Vallejo A, Ozen M. Multidisciplinary design optimization for glass-fiber epoxy-matrix composite 5 MW horizontal-axis wind-turbine blades. *J Mater Eng Perform* 2010;19:1116–27.
- [80] Schubel PJ, Crossley RJ. Wind Turbine Blade Design. *ENERGIES* 2012;5:3425–49. doi:10.3390/en5093425.
- [81] Jang H-K, Choi W-H, Kim C-G, Kim J-B, Lim D-W. Manufacture and characterization of stealth wind turbine blade with periodic pattern surface for reducing radar interference. *Compos Part B Eng* 2014;56:178–83. doi:10.1016/j.compositesb.2013.08.043.

## **Appendix A**

### **LIQUID INJECTION MOLDING SIMULATION (LIMS)**

#### **A.1 Introduction**

Liquid Injection Molding Simulation (LIMS) is a well-defined and versatile software package that simulates the mold filling stage of Liquid Composite Molding (LCM) processes by modeling flow through porous media by Finite Element Method. It provides a simple and cost-effective way to verify and optimize filling process design by providing a “virtual” mold filling process. This allows one to avoid or reduce the actual physical trial and error process which tends to be resource-intensive.

LIMS has been successfully used to design and simulate intelligent or adaptive filling process that utilizes sensors mounted on the part and controllable injection hardware, either as a stand-alone program or as a simulation engine for other programs. Because of the scripting capability, various LCM process variants were successfully modeled.

LIMS can be started using powerful and versatile scripting language which is called “LBASIC” to load mesh file, specify processing parameters, set material properties and generate difference simulation scenarios. Also, a graphic user interface (GUI) is also developed which is called LIMSUI. This provides the user a more explicit way to interact with meshed geometry and material and other processing parameters’ specification. LBASIC will be automatically generated once the user submits the simulation request and LIMS engine is called to kick off the simulation

and results are returned back to the user. Detailed manual can be found at the LIMS website at “<http://sites.udel.edu/lims/>”, from where the author strongly encourages the reader to download a trial version of both LIMS and LIMSUI and follow the steps to run some simulations using given example meshes. Due to the length of this dissertation, a few features of LIMS that are related to this work is introduced in this section.

## **A.2 Processing Parameters specification**

In LIMSUI, apart from all the necessary processing parameters such as injection gate location in RTM, infusion lines in VARTM and RTM-Light processes (Figure A-1(a)(b)), pressure condition and material permeability, the user can also introduce the high permeable distribution media and racetracking channels into the mesh (Figure A\_1(c)(d)). As shown in Figure A-1, point resin inlet is specified using a single node assigned with either a constant pressure or constant flow rate. Infusion lines are represented using a series of 1d elements whose permeability is automatically calculated provided with infusion line diameter. Distribution media is applied on top of the mesh by modifying the element properties (Figure A-1(c)), and the user can easily change its shape and location. More importantly, the user can easily specify the location of racetracking channels which can introduce flow disturbances during mold filling stage (Figure A-1(d)), and the racetracking strength can be calculated by the same means when calculating the permeability of infusion lines.

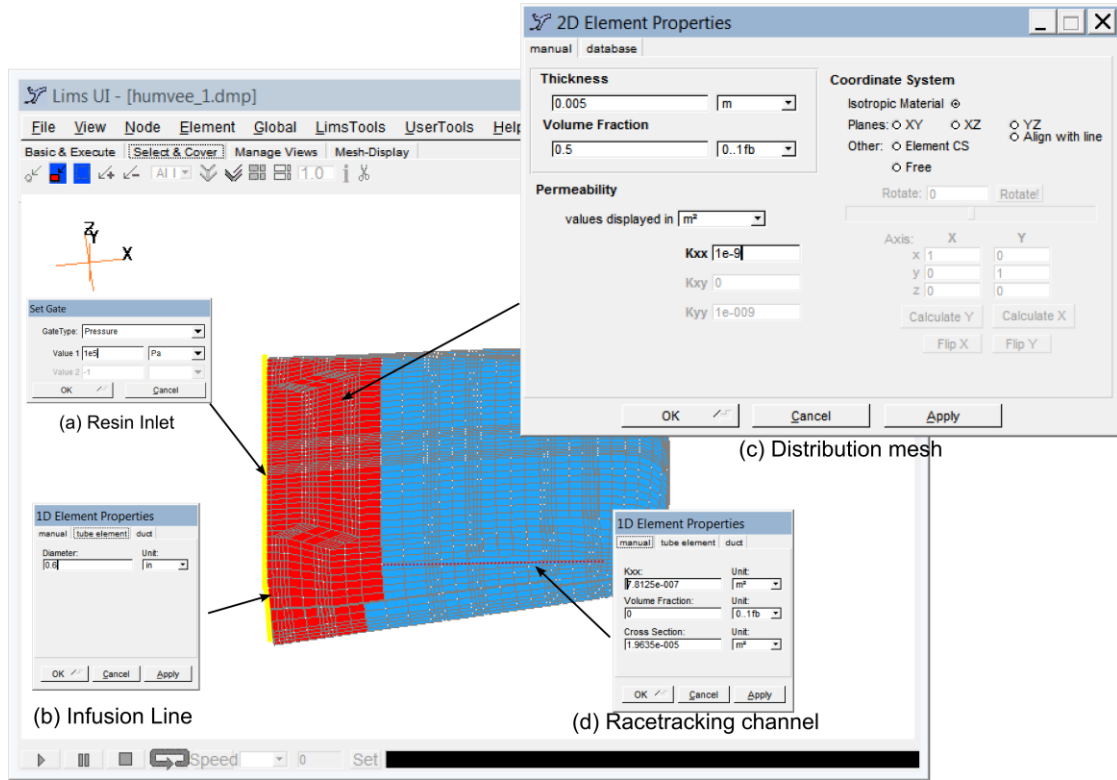


Figure A-1: Important processing parameters' specification in LIMSUI: (a) single node as resin inlet (b) 1d elements connected with resin inlet node as infusion line (c) high permeable 2d elements as distribution mesh (d) 1d elements to represent racetracking channel

### A.3 Package API

Apart from the LIMSUI that allows the user to manipulate the calculation engine in a straightforward way, LIMS can also be easily integrated within various commercial software packages thanks to the versatile built in scripting language LBASIC. Matlab and C++ wrappers have been developed so that LIMS can be instantiated within user's self-defined work flows, or hooked with commercial CAD software packages as introduced in previous chapters. These wrappers can easily

interpret multiple widely used mesh format such as Bulk Data Format (BDF) file that can be exported by most commercial CAD software, and MSH format that is written by open source software GNU MESH. Simulation execution details are included in the LB file that is also generated by the wrapper.

## **Appendix B**

### **REPRINT PERMISSION LETTERS**

#### **B.1 “Use Of Centroidal Voronoi Diagram To Find Optimal Gate Locations To Minimize Mold Filling Time In Resin Transfer Molding”**

**ELSEVIER LICENSE  
TERMS AND CONDITIONS**

Apr 11, 2017

This Agreement between Jiayin Wang ("You") and Elsevier ("Elsevier") consists of your license details and the terms and conditions provided by Elsevier and Copyright Clearance Center.

License Number	4085721207102
License date	Apr 11, 2017
Licensed Content Publisher	Elsevier
Licensed Content Publication	Composites Part A: Applied Science and Manufacturing
Licensed Content Title	Use of Centroidal Voronoi Diagram to find optimal gate locations to minimize mold filling time in resin transfer molding
Licensed Content Author	J. Wang,P. Simacek,S.G. Advani
Licensed Content Date	August 2016
Licensed Content Volume	87
Licensed Content Issue	n/a
Licensed Content Pages	13
Start Page	243
End Page	255
Type of Use	reuse in a thesis/dissertation
Portion	full article
Format	both print and electronic
Are you the author of this Elsevier article?	Yes
Will you be translating?	No
Order reference number	
Title of your thesis/dissertation	INTEGRATION OF COMPOSITE PART DESIGN AND PROCESSING SIMULATION IN LIQUID COMPOSITE MOLDING
Expected completion date	May 2017
Estimated size (number of pages)	200
Elsevier VAT number	GB 494 6272 12
Requestor Location	Jiayin Wang 126 Spencer Lab University of Delaware  NEWARK, DE 19716 United States Attn: Jiayin Wang
Publisher Tax ID	98-0397604
Total	0.00 USD
Terms and Conditions	

**INTRODUCTION**

1. The publisher for this copyrighted material is Elsevier. By clicking "accept" in connection with completing this licensing transaction, you agree that the following terms and conditions apply to this transaction (along with the Billing and Payment terms and conditions established by Copyright Clearance Center, Inc. ("CCC"), at the time that you opened your Rightslink account and that are available at any time at <http://myaccount.copyright.com>).

#### GENERAL TERMS

2. Elsevier hereby grants you permission to reproduce the aforementioned material subject to the terms and conditions indicated.

3. Acknowledgement: If any part of the material to be used (for example, figures) has appeared in our publication with credit or acknowledgement to another source, permission must also be sought from that source. If such permission is not obtained then that material may not be included in your publication/copies. Suitable acknowledgement to the source must be made, either as a footnote or in a reference list at the end of your publication, as follows:

"Reprinted from Publication title, Vol /edition number, Author(s), Title of article / title of chapter, Pages No., Copyright (Year), with permission from Elsevier [OR APPLICABLE SOCIETY COPYRIGHT OWNER]." Also Lancet special credit - "Reprinted from The Lancet, Vol. number, Author(s), Title of article, Pages No., Copyright (Year), with permission from Elsevier."

4. Reproduction of this material is confined to the purpose and/or media for which permission is hereby given.

5. Altering/Modifying Material: Not Permitted. However figures and illustrations may be altered/adapted minimally to serve your work. Any other abbreviations, additions, deletions and/or any other alterations shall be made only with prior written authorization of Elsevier Ltd. (Please contact Elsevier at [permissions@elsevier.com](mailto:permissions@elsevier.com)). No modifications can be made to any Lancet figures/tables and they must be reproduced in full.

6. If the permission fee for the requested use of our material is waived in this instance, please be advised that your future requests for Elsevier materials may attract a fee.

7. Reservation of Rights: Publisher reserves all rights not specifically granted in the combination of (i) the license details provided by you and accepted in the course of this licensing transaction, (ii) these terms and conditions and (iii) CCC's Billing and Payment terms and conditions.

8. License Contingent Upon Payment: While you may exercise the rights licensed immediately upon issuance of the license at the end of the licensing process for the transaction, provided that you have disclosed complete and accurate details of your proposed use, no license is finally effective unless and until full payment is received from you (either by publisher or by CCC) as provided in CCC's Billing and Payment terms and conditions. If full payment is not received on a timely basis, then any license preliminarily granted shall be deemed automatically revoked and shall be void as if never granted. Further, in the event that you breach any of these terms and conditions or any of CCC's Billing and Payment terms and conditions, the license is automatically revoked and shall be void as if never granted. Use of materials as described in a revoked license, as well as any use of the materials beyond the scope of an unrevoked license, may constitute copyright infringement and publisher reserves the right to take any and all action to protect its copyright in the materials.

9. Warranties: Publisher makes no representations or warranties with respect to the licensed material.

10. Indemnity: You hereby indemnify and agree to hold harmless publisher and CCC, and their respective officers, directors, employees and agents, from and against any and all claims arising out of your use of the licensed material other than as specifically authorized pursuant to this license.

11. No Transfer of License: This license is personal to you and may not be sublicensed, assigned, or transferred by you to any other person without publisher's written permission.

12. **No Amendment Except in Writing:** This license may not be amended except in a writing signed by both parties (or, in the case of publisher, by CCC on publisher's behalf).

13. **Objection to Contrary Terms:** Publisher hereby objects to any terms contained in any purchase order, acknowledgment, check endorsement or other writing prepared by you, which terms are inconsistent with these terms and conditions or CCC's Billing and Payment terms and conditions. These terms and conditions, together with CCC's Billing and Payment terms and conditions (which are incorporated herein), comprise the entire agreement between you and publisher (and CCC) concerning this licensing transaction. In the event of any conflict between your obligations established by these terms and conditions and those established by CCC's Billing and Payment terms and conditions, these terms and conditions shall control.

14. **Revocation:** Elsevier or Copyright Clearance Center may deny the permissions described in this License at their sole discretion, for any reason or no reason, with a full refund payable to you. Notice of such denial will be made using the contact information provided by you. Failure to receive such notice will not alter or invalidate the denial. In no event will Elsevier or Copyright Clearance Center be responsible or liable for any costs, expenses or damage incurred by you as a result of a denial of your permission request, other than a refund of the amount(s) paid by you to Elsevier and/or Copyright Clearance Center for denied permissions.

#### LIMITED LICENSE

The following terms and conditions apply only to specific license types:

15. **Translation:** This permission is granted for non-exclusive world **English** rights only unless your license was granted for translation rights. If you licensed translation rights you may only translate this content into the languages you requested. A professional translator must perform all translations and reproduce the content word for word preserving the integrity of the article.

16. **Posting licensed content on any Website:** The following terms and conditions apply as follows: Licensing material from an Elsevier journal: All content posted to the web site must maintain the copyright information line on the bottom of each image; A hyper-text must be included to the Homepage of the journal from which you are licensing at <http://www.sciencedirect.com/science/journal/xxxxx> or the Elsevier homepage for books at <http://www.elsevier.com>; Central Storage: This license does not include permission for a scanned version of the material to be stored in a central repository such as that provided by Heron/XanEdu.

Licensing material from an Elsevier book: A hyper-text link must be included to the Elsevier homepage at <http://www.elsevier.com>. All content posted to the web site must maintain the copyright information line on the bottom of each image.

**Posting licensed content on Electronic reserve:** In addition to the above the following clauses are applicable: The web site must be password-protected and made available only to bona fide students registered on a relevant course. This permission is granted for 1 year only. You may obtain a new license for future website posting.

17. **For journal authors:** the following clauses are applicable in addition to the above:

#### Preprints:

A preprint is an author's own write-up of research results and analysis, it has not been peer-reviewed, nor has it had any other value added to it by a publisher (such as formatting, copyright, technical enhancement etc.).

Authors can share their preprints anywhere at any time. Preprints should not be added to or enhanced in any way in order to appear more like, or to substitute for, the final versions of articles however authors can update their preprints on arXiv or RePEc with their Accepted Author Manuscript (see below).

If accepted for publication, we encourage authors to link from the preprint to their formal publication via its DOI. Millions of researchers have access to the formal publications on ScienceDirect, and so links will help users to find, access, cite and use the best available

version. Please note that Cell Press, The Lancet and some society-owned have different preprint policies. Information on these policies is available on the journal homepage.

**Accepted Author Manuscripts:** An accepted author manuscript is the manuscript of an article that has been accepted for publication and which typically includes author-incorporated changes suggested during submission, peer review and editor-author communications.

Authors can share their accepted author manuscript:

- immediately
  - via their non-commercial person homepage or blog
  - by updating a preprint in arXiv or RePEc with the accepted manuscript
  - via their research institute or institutional repository for internal institutional uses or as part of an invitation-only research collaboration work-group
  - directly by providing copies to their students or to research collaborators for their personal use
  - for private scholarly sharing as part of an invitation-only work group on commercial sites with which Elsevier has an agreement
- After the embargo period
  - via non-commercial hosting platforms such as their institutional repository
  - via commercial sites with which Elsevier has an agreement

In all cases accepted manuscripts should:

- link to the formal publication via its DOI
- bear a CC-BY-NC-ND license - this is easy to do
- if aggregated with other manuscripts, for example in a repository or other site, be shared in alignment with our hosting policy not be added to or enhanced in any way to appear more like, or to substitute for, the published journal article.

**Published journal article (JPA):** A published journal article (PJA) is the definitive final record of published research that appears or will appear in the journal and embodies all value-adding publishing activities including peer review co-ordination, copy-editing, formatting, (if relevant) pagination and online enrichment.

Policies for sharing publishing journal articles differ for subscription and gold open access articles:

**Subscription Articles:** If you are an author, please share a link to your article rather than the full-text. Millions of researchers have access to the formal publications on ScienceDirect, and so links will help your users to find, access, cite, and use the best available version. Theses and dissertations which contain embedded PJAs as part of the formal submission can be posted publicly by the awarding institution with DOI links back to the formal publications on ScienceDirect.

If you are affiliated with a library that subscribes to ScienceDirect you have additional private sharing rights for others' research accessed under that agreement. This includes use for classroom teaching and internal training at the institution (including use in course packs and courseware programs), and inclusion of the article for grant funding purposes.

**Gold Open Access Articles:** May be shared according to the author-selected end-user license and should contain a [CrossMark logo](#), the end user license, and a DOI link to the formal publication on ScienceDirect.

Please refer to Elsevier's [posting policy](#) for further information.

18. **For book authors** the following clauses are applicable in addition to the above:

Authors are permitted to place a brief summary of their work online only. You are not allowed to download and post the published electronic version of your chapter, nor may you scan the printed edition to create an electronic version. **Posting to a repository:** Authors are permitted to post a summary of their chapter only in their institution's repository.

19. **Thesis/Dissertation:** If your license is for use in a thesis/dissertation your thesis may be submitted to your institution in either print or electronic form. Should your thesis be published commercially, please reapply for permission. These requirements include permission for the Library and Archives of Canada to supply single copies, on demand, of the complete thesis and include permission for Proquest/UMI to supply single copies, on demand, of the complete thesis. Should your thesis be published commercially, please reapply for permission. Theses and dissertations which contain embedded PJAs as part of the formal submission can be posted publicly by the awarding institution with DOI links back to the formal publications on ScienceDirect.

#### **Elsevier Open Access Terms and Conditions**

You can publish open access with Elsevier in hundreds of open access journals or in nearly 2000 established subscription journals that support open access publishing. Permitted third party re-use of these open access articles is defined by the author's choice of Creative Commons user license. See our [open access license policy](#) for more information.

#### **Terms & Conditions applicable to all Open Access articles published with Elsevier:**

Any reuse of the article must not represent the author as endorsing the adaptation of the article nor should the article be modified in such a way as to damage the author's honour or reputation. If any changes have been made, such changes must be clearly indicated.

The author(s) must be appropriately credited and we ask that you include the end user license and a DOI link to the formal publication on ScienceDirect.

If any part of the material to be used (for example, figures) has appeared in our publication with credit or acknowledgement to another source it is the responsibility of the user to ensure their reuse complies with the terms and conditions determined by the rights holder.

#### **Additional Terms & Conditions applicable to each Creative Commons user license:**

**CC BY:** The CC-BY license allows users to copy, to create extracts, abstracts and new works from the Article, to alter and revise the Article and to make commercial use of the Article (including reuse and/or resale of the Article by commercial entities), provided the user gives appropriate credit (with a link to the formal publication through the relevant DOI), provides a link to the license, indicates if changes were made and the licensor is not represented as endorsing the use made of the work. The full details of the license are available at <http://creativecommons.org/licenses/by/4.0>.

**CC BY NC SA:** The CC BY-NC-SA license allows users to copy, to create extracts, abstracts and new works from the Article, to alter and revise the Article, provided this is not done for commercial purposes, and that the user gives appropriate credit (with a link to the formal publication through the relevant DOI), provides a link to the license, indicates if changes were made and the licensor is not represented as endorsing the use made of the work. Further, any new works must be made available on the same conditions. The full details of the license are available at <http://creativecommons.org/licenses/by-nc-sa/4.0>.

**CC BY NC ND:** The CC BY-NC-ND license allows users to copy and distribute the Article, provided this is not done for commercial purposes and further does not permit distribution of the Article if it is changed or edited in any way, and provided the user gives appropriate credit (with a link to the formal publication through the relevant DOI), provides a link to the license, and that the licensor is not represented as endorsing the use made of the work. The full details of the license are available at <http://creativecommons.org/licenses/by-nc-nd/4.0>. Any commercial reuse of Open Access articles published with a CC BY NC SA or CC BY NC ND license requires permission from Elsevier and will be subject to a fee.

Commercial reuse includes:

- Associating advertising with the full text of the Article
- Charging fees for document delivery or access
- Article aggregation
- Systematic distribution via e-mail lists or share buttons

Posting or linking by commercial companies for use by customers of those companies.

**20. Other Conditions:**

v1.9

**Questions? [customercare@copyright.com](mailto:customercare@copyright.com) or +1-855-239-3415 (toll free in the US) or +1-978-646-2777.**

---

---

**B.2 “Use Of Medial Axis To Find Optimal Channel Designs To Reduce Mold Filling Time In Resin Transfer Molding”**

**ELSEVIER LICENSE  
TERMS AND CONDITIONS**

Apr 11, 2017

This Agreement between Jiayin Wang ("You") and Elsevier ("Elsevier") consists of your license details and the terms and conditions provided by Elsevier and Copyright Clearance Center.

License Number	4085721391163
License date	Apr 11, 2017
Licensed Content Publisher	Elsevier
Licensed Content Publication	Composites Part A: Applied Science and Manufacturing
Licensed Content Title	Use of medial axis to find optimal channel designs to reduce mold filling time in resin transfer molding
Licensed Content Author	J. Wang,P. Simacek,S.G. Advani
Licensed Content Date	April 2017
Licensed Content Volume	95
Licensed Content Issue	n/a
Licensed Content Pages	12
Start Page	161
End Page	172
Type of Use	reuse in a thesis/dissertation
Intended publisher of new work	other
Portion	full article
Format	both print and electronic
Are you the author of this Elsevier article?	Yes
Will you be translating?	No
Order reference number	
Title of your thesis/dissertation	INTEGRATION OF COMPOSITE PART DESIGN AND PROCESSING SIMULATION IN LIQUID COMPOSITE MOLDING
Expected completion date	May 2017
Estimated size (number of pages)	200
Elsevier VAT number	GB 494 6272 12
Requestor Location	Jiayin Wang 126 Spencer Lab University of Delaware  NEWARK, DE 19716 United States Attn: Jiayin Wang
Publisher Tax ID	98-0397604
Total	0.00 USD

**INTRODUCTION**

1. The publisher for this copyrighted material is Elsevier. By clicking "accept" in connection with completing this licensing transaction, you agree that the following terms and conditions apply to this transaction (along with the Billing and Payment terms and conditions established by Copyright Clearance Center, Inc. ("CCC"), at the time that you opened your Rightslink account and that are available at any time at <http://myaccount.copyright.com>).

**GENERAL TERMS**

2. Elsevier hereby grants you permission to reproduce the aforementioned material subject to the terms and conditions indicated.

3. Acknowledgement: If any part of the material to be used (for example, figures) has appeared in our publication with credit or acknowledgement to another source, permission must also be sought from that source. If such permission is not obtained then that material may not be included in your publication/copies. Suitable acknowledgement to the source must be made, either as a footnote or in a reference list at the end of your publication, as follows:

"Reprinted from Publication title, Vol /edition number, Author(s), Title of article / title of chapter, Pages No., Copyright (Year), with permission from Elsevier [OR APPLICABLE SOCIETY COPYRIGHT OWNER]." Also Lancet special credit - "Reprinted from The Lancet, Vol. number, Author(s), Title of article, Pages No., Copyright (Year), with permission from Elsevier."

4. Reproduction of this material is confined to the purpose and/or media for which permission is hereby given.

5. Altering/Modifying Material: Not Permitted. However figures and illustrations may be altered/adapted minimally to serve your work. Any other abbreviations, additions, deletions and/or any other alterations shall be made only with prior written authorization of Elsevier Ltd. (Please contact Elsevier at [permissions@elsevier.com](mailto:permissions@elsevier.com)). No modifications can be made to any Lancet figures/tables and they must be reproduced in full.

6. If the permission fee for the requested use of our material is waived in this instance, please be advised that your future requests for Elsevier materials may attract a fee.

7. Reservation of Rights: Publisher reserves all rights not specifically granted in the combination of (i) the license details provided by you and accepted in the course of this licensing transaction, (ii) these terms and conditions and (iii) CCC's Billing and Payment terms and conditions.

8. License Contingent Upon Payment: While you may exercise the rights licensed immediately upon issuance of the license at the end of the licensing process for the transaction, provided that you have disclosed complete and accurate details of your proposed use, no license is finally effective unless and until full payment is received from you (either by publisher or by CCC) as provided in CCC's Billing and Payment terms and conditions. If full payment is not received on a timely basis, then any license preliminarily granted shall be deemed automatically revoked and shall be void as if never granted. Further, in the event that you breach any of these terms and conditions or any of CCC's Billing and Payment terms and conditions, the license is automatically revoked and shall be void as if never granted. Use of materials as described in a revoked license, as well as any use of the materials beyond the scope of an unrevoked license, may constitute copyright infringement and publisher reserves the right to take any and all action to protect its copyright in the materials.

9. Warranties: Publisher makes no representations or warranties with respect to the licensed material.

10. Indemnity: You hereby indemnify and agree to hold harmless publisher and CCC, and their respective officers, directors, employees and agents, from and against any and all claims arising out of your use of the licensed material other than as specifically authorized pursuant to this license.

11. **No Transfer of License:** This license is personal to you and may not be sublicensed, assigned, or transferred by you to any other person without publisher's written permission.

12. **No Amendment Except in Writing:** This license may not be amended except in a writing signed by both parties (or, in the case of publisher, by CCC on publisher's behalf).

13. **Objection to Contrary Terms:** Publisher hereby objects to any terms contained in any purchase order, acknowledgment, check endorsement or other writing prepared by you, which terms are inconsistent with these terms and conditions or CCC's Billing and Payment terms and conditions. These terms and conditions, together with CCC's Billing and Payment terms and conditions (which are incorporated herein), comprise the entire agreement between you and publisher (and CCC) concerning this licensing transaction. In the event of any conflict between your obligations established by these terms and conditions and those established by CCC's Billing and Payment terms and conditions, these terms and conditions shall control.

14. **Revocation:** Elsevier or Copyright Clearance Center may deny the permissions described in this License at their sole discretion, for any reason or no reason, with a full refund payable to you. Notice of such denial will be made using the contact information provided by you. Failure to receive such notice will not alter or invalidate the denial. In no event will Elsevier or Copyright Clearance Center be responsible or liable for any costs, expenses or damage incurred by you as a result of a denial of your permission request, other than a refund of the amount(s) paid by you to Elsevier and/or Copyright Clearance Center for denied permissions.

#### LIMITED LICENSE

The following terms and conditions apply only to specific license types:

15. **Translation:** This permission is granted for non-exclusive world **English** rights only unless your license was granted for translation rights. If you licensed translation rights you may only translate this content into the languages you requested. A professional translator must perform all translations and reproduce the content word for word preserving the integrity of the article.

16. **Posting licensed content on any Website:** The following terms and conditions apply as follows: Licensing material from an Elsevier journal: All content posted to the web site must maintain the copyright information line on the bottom of each image; A hyper-text must be included to the Homepage of the journal from which you are licensing at <http://www.sciencedirect.com/science/journal/xxxxx> or the Elsevier homepage for books at <http://www.elsevier.com>; Central Storage: This license does not include permission for a scanned version of the material to be stored in a central repository such as that provided by Heron/XanEdu.

Licensing material from an Elsevier book: A hyper-text link must be included to the Elsevier homepage at <http://www.elsevier.com>. All content posted to the web site must maintain the copyright information line on the bottom of each image.

**Posting licensed content on Electronic reserve:** In addition to the above the following clauses are applicable: The web site must be password-protected and made available only to bona fide students registered on a relevant course. This permission is granted for 1 year only. You may obtain a new license for future website posting.

17. **For journal authors:** the following clauses are applicable in addition to the above:

#### Preprints:

A preprint is an author's own write-up of research results and analysis, it has not been peer-reviewed, nor has it had any other value added to it by a publisher (such as formatting, copyright, technical enhancement etc.).

Authors can share their preprints anywhere at any time. Preprints should not be added to or enhanced in any way in order to appear more like, or to substitute for, the final versions of articles however authors can update their preprints on arXiv or RePEc with their Accepted Author Manuscript (see below).

If accepted for publication, we encourage authors to link from the preprint to their formal publication via its DOI. Millions of researchers have access to the formal publications on ScienceDirect, and so links will help users to find, access, cite and use the best available version. Please note that Cell Press, The Lancet and some society-owned have different preprint policies. Information on these policies is available on the journal homepage.

**Accepted Author Manuscripts:** An accepted author manuscript is the manuscript of an article that has been accepted for publication and which typically includes author-incorporated changes suggested during submission, peer review and editor-author communications.

Authors can share their accepted author manuscript:

- immediately
  - via their non-commercial person homepage or blog
  - by updating a preprint in arXiv or RePEc with the accepted manuscript
  - via their research institute or institutional repository for internal institutional uses or as part of an invitation-only research collaboration work-group
  - directly by providing copies to their students or to research collaborators for their personal use
  - for private scholarly sharing as part of an invitation-only work group on commercial sites with which Elsevier has an agreement
- After the embargo period
  - via non-commercial hosting platforms such as their institutional repository
  - via commercial sites with which Elsevier has an agreement

In all cases accepted manuscripts should:

- link to the formal publication via its DOI
- bear a CC-BY-NC-ND license - this is easy to do
- if aggregated with other manuscripts, for example in a repository or other site, be shared in alignment with our hosting policy not be added to or enhanced in any way to appear more like, or to substitute for, the published journal article.

**Published journal article (JPA):** A published journal article (PJA) is the definitive final record of published research that appears or will appear in the journal and embodies all value-adding publishing activities including peer review co-ordination, copy-editing, formatting, (if relevant) pagination and online enrichment.

Policies for sharing publishing journal articles differ for subscription and gold open access articles:

**Subscription Articles:** If you are an author, please share a link to your article rather than the full-text. Millions of researchers have access to the formal publications on ScienceDirect, and so links will help your users to find, access, cite, and use the best available version. Theses and dissertations which contain embedded PJAs as part of the formal submission can be posted publicly by the awarding institution with DOI links back to the formal publications on ScienceDirect.

If you are affiliated with a library that subscribes to ScienceDirect you have additional private sharing rights for others' research accessed under that agreement. This includes use for classroom teaching and internal training at the institution (including use in course packs and courseware programs), and inclusion of the article for grant funding purposes.

**Gold Open Access Articles:** May be shared according to the author-selected end-user license and should contain a [CrossMark logo](#), the end user license, and a DOI link to the formal publication on ScienceDirect.

Please refer to Elsevier's [posting policy](#) for further information.

18. **For book authors** the following clauses are applicable in addition to the above:

Authors are permitted to place a brief summary of their work online only. You are not

allowed to download and post the published electronic version of your chapter, nor may you scan the printed edition to create an electronic version. **Posting to a repository:** Authors are permitted to post a summary of their chapter only in their institution's repository.

**19. Thesis/Dissertation:** If your license is for use in a thesis/dissertation your thesis may be submitted to your institution in either print or electronic form. Should your thesis be published commercially, please reapply for permission. These requirements include permission for the Library and Archives of Canada to supply single copies, on demand, of the complete thesis and include permission for Proquest/UMI to supply single copies, on demand, of the complete thesis. Should your thesis be published commercially, please reapply for permission. Theses and dissertations which contain embedded PJAs as part of the formal submission can be posted publicly by the awarding institution with DOI links back to the formal publications on ScienceDirect.

#### **Elsevier Open Access Terms and Conditions**

You can publish open access with Elsevier in hundreds of open access journals or in nearly 2000 established subscription journals that support open access publishing. Permitted third party re-use of these open access articles is defined by the author's choice of Creative Commons user license. See our [open access license policy](#) for more information.

#### **Terms & Conditions applicable to all Open Access articles published with Elsevier:**

Any reuse of the article must not represent the author as endorsing the adaptation of the article nor should the article be modified in such a way as to damage the author's honour or reputation. If any changes have been made, such changes must be clearly indicated.

The author(s) must be appropriately credited and we ask that you include the end user license and a DOI link to the formal publication on ScienceDirect.

If any part of the material to be used (for example, figures) has appeared in our publication with credit or acknowledgement to another source it is the responsibility of the user to ensure their reuse complies with the terms and conditions determined by the rights holder.

#### **Additional Terms & Conditions applicable to each Creative Commons user license:**

**CC BY:** The CC-BY license allows users to copy, to create extracts, abstracts and new works from the Article, to alter and revise the Article and to make commercial use of the Article (including reuse and/or resale of the Article by commercial entities), provided the user gives appropriate credit (with a link to the formal publication through the relevant DOI), provides a link to the license, indicates if changes were made and the licensor is not represented as endorsing the use made of the work. The full details of the license are available at <http://creativecommons.org/licenses/by/4.0>.

**CC BY NC SA:** The CC BY-NC-SA license allows users to copy, to create extracts, abstracts and new works from the Article, to alter and revise the Article, provided this is not done for commercial purposes, and that the user gives appropriate credit (with a link to the formal publication through the relevant DOI), provides a link to the license, indicates if changes were made and the licensor is not represented as endorsing the use made of the work. Further, any new works must be made available on the same conditions. The full details of the license are available at <http://creativecommons.org/licenses/by-nc-sa/4.0>.

**CC BY NC ND:** The CC BY-NC-ND license allows users to copy and distribute the Article, provided this is not done for commercial purposes and further does not permit distribution of the Article if it is changed or edited in any way, and provided the user gives appropriate credit (with a link to the formal publication through the relevant DOI), provides a link to the license, and that the licensor is not represented as endorsing the use made of the work. The full details of the license are available at <http://creativecommons.org/licenses/by-nc-nd/4.0>. Any commercial reuse of Open Access articles published with a CC BY NC SA or CC BY NC ND license requires permission from Elsevier and will be subject to a fee.

Commercial reuse includes:

- Associating advertising with the full text of the Article
- Charging fees for document delivery or access

- Article aggregation
- Systematic distribution via e-mail lists or share buttons

Posting or linking by commercial companies for use by customers of those companies.

**20. Other Conditions:**

v1.9

**Questions? [customer@copyright.com](mailto:customer@copyright.com) or +1-855-239-3415 (toll free in the US) or +1-978-646-2777.**

